

**ÇUKUROVA UNIVERSITY
INSTITUTE OF NATURAL AND APPLIED SCIENCES**

M.Sc. THESIS

Mehmet Can PEKTAŞ

AERODYNAMICS OF PITCHING DELTA WING WITH YAW ANGLE

DEPARTMENT OF MECHANICAL ENGINEERING

ADANA-2017

ÇUKUROVA UNIVERSITY
INSTITUTE OF NATURAL AND APPLIED SCIENCES


AERODYNAMICS OF PITCHING DELTA WING
WITH YAW ANGLE

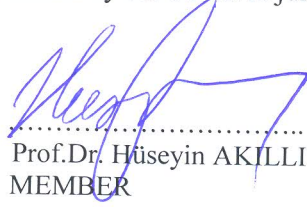
Mehmet Can PEKTAŞ

MSc THESIS

DEPARTMENT OF MECHANICAL ENGINEERING

We certify that the thesis titled above was reviewed and approved for the award of degree of the Master of Science by the board of jury on 16/01/2017.


.....
Prof. Dr. Beşir ŞAHİN
SUPERVISOR


.....
Prof. Dr. Hüseyin AKILLI
MEMBER


.....
Prof. Dr. Hüseyin YAPICI
MEMBER

This MSc Thesis is written at the Department of Institute of Natural and Applied Sciences of Çukurova University.

Registration Number:

Prof. Dr. Mustafa GÖK
Director
Institute of Natural and Applied Sciences

This thesis was supported by Scientific and Technological Research Council of Turkey under contract no: 114M497. Additional financial support was also received from the Scientific Research Project Office of Çukurova University under contract no: FYL-2016-6283.

Note: The usage of the presented specific declaration's, tables, figures, and photographs either in this thesis or in any other reference without citation is subject to "The law of Arts and Intellectual Products" number of 5846 of Turkish Republic.

ABSTRACT

MSc. THESIS

AERODYNAMICS OF PITCHING DELTA WING WITH YAW ANGLE

Mehmet Can PEKTAŞ

ÇUKUROVA UNIVERSITY
INSTITUTE OF NATURAL AND APPLIED SCIENCES
DEPARTMENT OF MECHANICAL ENGINEERING

Supervisor : Prof. Dr. Beşir ŞAHİN
Year: 2017, Pages: 103
Jury : Prof. Dr. Beşir ŞAHİN
: Prof. Dr. Hüseyin AKILLI
: Prof. Dr. Hüseyin YAPICI

In this study, a slender delta wing with 70° sweep angle, Λ was oscillated about its mid-cord in a vertical plane according to the equation $\alpha(t)=\alpha_m+\alpha_o\sin(\omega_e t)$. The values of mean angle of attack, α_m were taken as 25° , 30° and 35° . The yaw angle, β was varied over the range of $0^\circ \leq \beta \leq 16^\circ$. The delta wing was sinusoidally pitched within the range of period of time, $T_e=2\pi/\omega_e$, $5s \leq T_e \leq 60s$ and the reduced frequencies were set as $K=0.16, 0.25, 0.49, 1.96$ and lastly amplitude of pitching motions was varied within the range of $\pm 5^\circ \leq \alpha_o \leq \pm 10^\circ$.

The main aim of this study is to observe the effect of pitching motion of delta wing on the formation of vortex breakdown and structures of vortical flow downstream of vortex breakdown under yaw angle, β using a dye visualization and the particle image velocimetry (PIV) technique.

Leading edge vortex breakdown position on the windward side moves towards the apex of the delta wing and vorticity concentrations spread over the most part of the delta wing. But the other leading edge vortex on the other side moves in free-stream flow direction without bursting at different yaw angles, β .

Key Words: Angle of attack, delta wing, dimensionless reduced frequency, pitching, vortex breakdown, yaw angle

ÖZ

YÜKSEK LİSANS TEZİ

YÜKSEK GENLİKTE SALINIM YAPAN DELTA KANAT AERODİNAMİĞİNİN SAPMA AÇISI İLE DEĞİŞİMİ

Mehmet Can PEKTAŞ

ÇUKUROVA ÜNİVERSİTESİ
FEN BİLİMLERİ ENSTİTÜSÜ
MAKİNE MÜHENDİSLİĞİ ANABİLİM DALI

Danışman : Prof. Dr. Beşir ŞAHİN
Yıl: 2017, Sayfa: 103
Jüri : Prof. Dr. Beşir ŞAHİN
: Prof. Dr. Hüseyin AKILLI
: Prof. Dr. Hüseyin YAPICI

Bu çalışmada, 70 derece süpürme açısına sahip narin delta kanat, kanadın orta noktasından dikey düzlemde, $\alpha(t)=\alpha_m+\alpha_o\sin(\omega_e t)$ denklemine göre salınım hareketi verilmiştir. Ortalama hücum açısı, α_m değerleri 25°, 30° ve 35° olarak alınmıştır. Sapma açısı, β , $0^\circ \leq \beta \leq 16^\circ$ aralığında değişmiştir. Delta kanada sinüzoidal olarak $5s \leq T_e \leq 60s$ zaman periyodu, T_e aralığında yunuslama hareketi verilmiştir ve periyotlar, $T_e=2\pi/\omega_e$ eşitliği ile ifade edilmiştir. Boyutsuzlaştırılmış frekans katsayıları, K sırasıyla 0.16, 0.25, 0.49, 1.96 olarak düzenlenmiş ve son olarak salınımın genliği, α_o , $\pm 5^\circ \leq \alpha_o \leq \pm 10^\circ$ aralığında alınmıştır.

Çalışmanın asıl amacı, boya ile görselleştirme ve 2D PIV tekniklerini kullanarak, sapma açısı, β altında, yüksek genlikte ve düşük frekansta, kanadın yunuslama hareketinin girdap çökme noktası oluşumu üstündeki etkilerini ve girdap çökmelerinin akıntı yönündeki girdaplı akış yapısını gözlemlemektir.

Rüzgâra maruz kalan delta kanat hücum kenarı üzerindeki girdap çökme noktası, delta kanadın ucuna doğru hareket etmektedir ve girdap yığılmaları delta kanat yüzeyinin büyük bir kısmını kaplamıştır. Fakat rüzgâra maruz kalan delta kanat hücum kenarının tersi yöndeki girdap çökmeleri, sapma açısının, β etkisi ile herhangi bir çökme meydana gelmeden serbest akış doğrultusunda hareket ettiği gözlemlenmiştir.

Anahtar Kelimeler: Hücum açısı, delta kanat, boyutsuzlaştırılmış frekans katsayısı, yunuslama, girdap çökmesi, sapma açısı

EXPENDED ABSTRACT

Investigations of unsteady flow structures, onset of vortex breakdown and wing-vortex interaction in delta wing aerodynamics are substantially important to control vortex bursting and unstable vortical flows.

Position of vortex breakdown varies with respect to specific parameters such as sweep angle, Λ , angle of attack, α , yaw angle, β , roll angle, θ , Reynolds numbers, Re , wing geometry, etc. Vortex breakdown position moves towards apex of the wing, when sweep angle, Λ and angle of attack, α increase. Yaw angle, β has two types of effects on the delta wings aerodynamics. Position of vortex breakdown on the leeward side of the wing moves in the downstream direction, on the contrary, windward side of vortex bursting moves towards the wing apex.

Vortex breakdown decreases aerodynamic performance of air vehicles and severally unstable flow structures cause instability in the delta wing performance. For this reason flow control is substantially important. It necessary to study instability of flow structures over the delta wing in order to design effective flow control mechanisms. An extensive review of delta wing aerodynamics that has been done in the present work revealed that one of the parameter that effects the instability of flow structures over the delta wing is yaw angle, β . In the light of this idea, it was aimed to study effects of yaw angle, β on the aerodynamics of the delta wing in the present study. In general it is know that along the central axis of the leading edge vortex a stagnation point occurs resulting in vortex breakdown and severe vortical flow structure downstream of vortex breakdown. During the flight of air vehicles this flow phenomena happens and severity of unstable flow structures vary frequently. In the present study, effect of pitching motion of delta wing on onset of vortex breakdown and vortical flow structures under yaw angle, β were experimentally studied using a technique of dye visualization and PIV system in side-view planes. Comparison of static and dynamic delta wing cases are investigated. During dye visualization, delta wing was sinusoidally pitched at an

amplitude of α_0 of $\pm 5^\circ$ and $\pm 10^\circ$, at three different mean angles of attack, α_m of 25° , 30° and 35° . The yaw angle, β was varied over the range of $0^\circ \leq \beta \leq 16^\circ$. The delta wing was sinusoidally pitched within the range of period of time, $T_e = 2\pi/\omega_e$, $5 \text{ s} \leq T_e \leq 60 \text{ s}$ and the reduced frequencies were set as $K=0.16, 0.25, 0.49, 1.96$ and lastly amplitude of pitching motions was arranged to be varied within the range of $\pm 5^\circ \leq \alpha_0 \leq \pm 10^\circ$.

The delta wing is made of Plexiglas having cord, C length of 250 mm, and 180 mm during PIV experiments, thickness of 6 mm, and sweep angle, Λ 70° for the experiments of dye visualizations. The leading edges of delta wing had chamfer of 45° . Small holes were placed in close region of the apex on both sides of the central axis of the wing to eject the Rhodamine dye. The depth of water in water channel was kept as 53 cm and free-stream velocity is maintained as 80 mm/s. The Reynolds number was kept constant at a value of $Re=2.10^4$ based on the cord length of delta wing. Effects of pitching motion on the windward side leading edge vortex are presented quantitatively by capturing instantaneous velocities over side-view planes by The PIV technique. A few selected figures related to the quantitative measurement were included in the present study.

Hysteresis loops of vortex breakdowns of the perturbing delta wing are established using dye observations and the results are compared with the results of the stationary delta wing. In additions, effects of angle of attack, α , amplitude of pitching motion, α_0 and period of oscillation, T_e on the historical record of vortex breakdown and vortical flow characteristics were also examined.

Breakdown position of leading edge vortex on the windward side moves towards to the apex of the delta wing and vorticity concentrations spreads over majority of the delta wing surface, with increasing yaw angle, β of the wing, conversely, leading edge vortex of leeward side slides sideway away from the central axis of the delta wing. Dye visualizations show that with increasing angle of attack, α and the yaw angle, β strong Kelvin-Helmholtz instabilities are developed

and interactions between vortical flow and the delta wing surface increase which may lead to an unsteady flow loading such as buffeting.

Flow separation is more propagated towards apex of the delta wing, when amplitude of pitching motion, α_0 increases from $+5^\circ$ to $+10^\circ$. Location of vortex breakdown moves downstream of the wing with increasing amplitude of pitching motion, α_0 from -5° to -10° . Because of the difference of the angular speed of the wing, vortex bursting positions are different for values of $\alpha_0 \pm 5^\circ$ and $\pm 10^\circ$.

As the delta wing is oscillated, hysteresis loops occur with respect to upstroke or downstroke motion. There is a time lag between movement of location of vortex breakdown and oscillation of delta wing during period of cycle. This period of time lag gets shorter by increasing oscillation period, T_e or decreasing reduced frequency, K . Generally speaking, the effect of large amplitude, low frequency motion of a wing on the buffet loading of a downstream aerodynamic surface has not been pursued yet for slender delta wing. Complex maneuvers of an actual aircraft typically occur at relatively low dimensionless frequencies, in comparison with dimensionless frequencies of either vortex breakdown or a shear layer instability from the leading-edge of the wing.

Breakdown position of leading edge vortex on the windward side moves towards to the apex of the delta wing and vorticity concentrations spreads over majority of the delta wing surface. But the other side of leading edge vortex moves in forward direction without bursting underneath the delta wing for a higher yaw angle, β . Dye visualizations show that with increasing angle of attack, α and yaw angle, β , a strong Kelvin-Helmholtz instabilities form and leading edge vortices breakdown earlier causing a large scale vorticity concentrations and these vorticity concentrations interact with the surface of the delta wing leading to unsteady loading or buffeting the delta wing surface on the windward side of the wing.

ACKNOWLEDGEMENTS

First of all, I would like to express my gratitude to my advisor, Prof. Dr. Beşir ŞAHİN for his guidance, support and encouragement during my studies. I sincerely thank Prof. Dr. Hüseyin AKILLI, Head of Mechanical Engineering Department, for his valuable advises during my studies. I appreciate Assist. Prof. Dr. İlyas KARASU and M.Sc. student and research assistant, Mehmet Oğuz TAŞCI for their support and teaching the method of dye visualization and the PIV technique to me.

I am very grateful to Research Asistant Tahir DURHASAN, Asist. Prof. Dr. Engin PINAR and Asist. Prof. Dr. Göktürk Memduh ÖZKAN, Sedat DOĞRU, Ferdi BESNİ, Yusuf BAKIR, Sefa MERAL and Enver Can DORAN for their help during my experiments. I would also like to thank the Scientific and Technological Research Council of Turkey (TÜBİTAK) and Çukurova University Scientific Research Unit (BAP) for their financial supports.

I would sincerely like to thank my dearest family for their great patience and support during my studies. I would also like to express my gratitude to my mother and father and all family members who have great trust and support up to now.

CONTENTS	PAGE
ABSTRACT.....	I
ÖZ	II
EXPENDED ABSTRACT.....	III
ACKNOWLEDGEMENTS	VI
CONTENTS.....	VII
LIST OF FIGURES	IX
NOMENCLATURE	XXI
1. INTRODUCTION	1
2. PRELIMINARY WORKS.....	5
2.1. Structure of Vortex Breakdown over Delta Wings.....	5
2.2. Response of Vortex Breakdown in the Case of Pitching Delta Wing.....	13
3. MATERIAL AND METHOD	23
3.1. Water Channel System.....	23
3.2. Experimental Apparatuses	24
3.3. Experiments Conducted by Dye Visualization and Particle Image Velocimetry (PIV).....	25
3.3.1. Dye Visualization Experiments	25
3.3.2. Experiments Performed by PIV	25
3.4. Experimental System of Dye Visualization.....	27
3.4.1. Dimensions of Delta Wing and Related Information.....	27
4. RESULTS AND DISCUSSION.....	33
4.1. Experimental Results of Pitching Delta Wing.....	33
4.1.1. Flow Control Techniques.....	33
4.2. Dye Experiments.....	34
4.2.1. Visual Observations of Vortical Flow Using Dye	34

4.2.2. Observation of Delta Wing Aerodynamics under Pitching Motion with High Rate of Amplitude and Oscillating Period Using Dye Visualization.....	34
4.2.3. Vortex Breakdown Hysteresis of Delta Wing.....	52
4.3. Instantaneous Velocity Measurements Using PIV.....	89
4.3.1. Time-Averaged and Instantaneous Vectors, Streamline and Vorticity Patterns	89
5. CONCLUSION AND FUTURE STUDIES	93
REFERENCES	97
CIRRICULUM VITAE	103

LIST OF FIGURES**PAGE**

Figure 1.1. Different types of delta wings a) Saab 210 Draken (Dorr, 1985) b) The F-16XL's double delta wing (NASA, 2015) c) Canard Saab AJS-37 Viggen (Wikipedia, 2016) d) Jet-powered tailless delta wing (Wikipedia, 2016).....	1
Figure 1.2. Schematic representation of vortices on wing of the plane (Pakistan defence, 2012)	2
Figure 2.1. Types of vortex breakdown a) Bubble type vortex breakdown b) Spiral type vortex breakdown (NASA, 2016) c) Double helix vortex breakdown (Sarpkaya, 1971).....	5
Figure 2.2. The representation of vortex formations and primary, secondary vortices (Anderson, 2001)	6
Figure 2.3. Patterns of instantaneous ω , $\langle\omega\rangle$, and ω_{rms} in comparison with $\langle V \rangle$ at $\alpha=32^\circ$. Minimum and incremental values of instantaneous ω are 1 and 0.75 s^{-1} , of $\langle\omega\rangle$ are 1 and 0.75 s^{-1} and of $\omega_{rms}= 0.5$ and 0.5 s^{-1} . For contours of $\langle V \rangle$, units of numerical values designated on contour lines are mm/s and incremental value between contours is 2.5 mm/s (Ozgoren et al., 2002)	7
Figure 2.4. Effect of angle of attack on patterns of instantaneous, ω . Minimum and incremental values of ω for all cases are 1 and 0.75 s^{-1} (Ozgoren et al., 2002)	8
Figure 2.5. Dye visualizations in side-view plane of same delta wing representing effect of yaw angle, β , on flow structures at angles of attack, $\alpha= 25^\circ, 30^\circ$ and 35° (Karasu, 2015)	12
Figure 2.6. Overview of delta wing and wire arrangement (Akilli et al., 2001)...	13
Figure 2.7. Chord wise location of vortex breakdown and hysteresis with different reduced frequencies, K, (LeMay et al., 1988)	14

Figure 2.8. Variations of the instantaneous vortex breakdown positions for different sweep, Λ in the pitch up motion, pitch center located at $\frac{1}{2}$ chord length: a) With 59° sweep angle, Λ , at $Re = 9 \times 10^3$, $K = 0, 0.01, 0.02,$ and 0.04 ; b) With 63.4° sweep angle, at $Re = 9 \times 10^3$, $K = 0, 0.02, 0.03,$ and 0.04 ; c) With 67° sweep, Λ , at $Re = 11 \times 10^3$, $K = 0, 0.03, 0.038, 0.047,$ and 0.072 ; and d) With 70° sweep angle, Λ , at $Re = 11 \times 10^3$, $K = 0, 0.02, 0.031, 0.056, 0.064,$ and 0.073 (Miau et al., 1992)	16
Figure 2.9. Comparison of static and dynamic hysteresis loops of onset of vortex breakdown versus attack angle, α . Oscillating period, $T_e = 22.54$ s and reduced frequency, $K = 0.74$ and amplitude of pitching motion, $\alpha_0 = 10^\circ$ (Ozgoren and Sahin, 2002)	19
Figure 2.10. Schematic representation of stationary and pitching delta wing	20
Figure 2.11. Patterns of time-averaged vorticity, $\langle \omega \rangle$ and contours of transverse velocity components, $\langle V/U \rangle$ of the delta wing under stationary and perturbed conditions with the mean angle of attack, $\alpha = 10^\circ$ (Canpolat et al., 2015).....	21
Figure 3.1. Schematic of closed circle of water channel	23
Figure 3.2. Representation of special apparatus (angle apparatus).....	24
Figure 3.3. Servo motor and its control unit	25
Figure 3.4. Measurement of PIV Principle (Dantec Dynamics, 2013)	26
Figure 3.5. Dimensions of the delta wing	28
Figure 3.6. Schematic representation of water channel during dye experiment in side view plane	29
Figure 3.7. Print screen of Sony Play Memories Software	30
Figure 3.8. Schematic representation of pitching motion of the delta wing and experimental set up for dye experiment.....	31

Figure 3.9. Schematic representation of varying yaw angle, $\beta=0^\circ, 4^\circ, 8^\circ, 12^\circ$ and 16° and changing location of vortex breakdown in side and plan view planes	32
Figure 4.1. Formation of onset of vortex breakdown in the cases of stationary and oscillating delta wings under variation of yaw angle, β within the range of $0^\circ \leq \beta \leq 16^\circ$, period of oscillation, T_e ranging from 5s to 60s at mean angle of attack, α_m of 25° , amplitude of delta wing pitching motion, α_o of $+5^\circ$ (upstroke) and dynamic angles of attack, $\alpha(t)$ vary between 20° and 30° . All images are taken at angle of attack, $\alpha=30^\circ$	37
Figure 4.2. Formation of onset of vortex breakdown in the cases of stationary and oscillating delta wings under variation of yaw angle, β within the range of $0^\circ \leq \beta \leq 16^\circ$, period of oscillation, T_e ranging from 5s to 60s at mean angle of attack, α_m of 30° , amplitude of delta wing pitching motion, α_o of $+5^\circ$ (upstroke) and dynamic angles of attack, $\alpha(t)$ vary between 25° and 35° . All images are taken at angle of attack, $\alpha=35^\circ$	38
Figure 4.3. Formation of onset of vortex breakdown in the cases of stationary and oscillating delta wings under variation of yaw angle, β within the range of $0^\circ \leq \beta \leq 16^\circ$, period of oscillation, T_e ranging from 5s to 60s at mean angle of attack, α_m of 35° , amplitude of delta wing pitching motion, α_o of $+5^\circ$ (upstroke) and dynamic angles of attack, $\alpha(t)$ vary between 30° and 40° . All images are taken at angle of attack, $\alpha=40^\circ$	39
Figure 4.4. Formation of onset of vortex breakdown in the cases of stationary and oscillating delta wings under variation of yaw angle, β within the range of $0^\circ \leq \beta \leq 16^\circ$, period of oscillation, T_e ranging from 5s to 60s at mean angle of attack, α_m of 25° , amplitude of delta wing pitching motion, α_o of -5° (downstroke) and dynamic angles of	

	attack, $\alpha(t)$ vary between 20° and 30° . All images are taken at angle of attack, $\alpha=20^\circ$	43
Figure 4.5.	Formation of onset of vortex breakdown in the cases of stationary and oscillating delta wings under variation of yaw angle, β within the range of $0^\circ \leq \beta \leq 16^\circ$, period of oscillation, T_e ranging from 5s to 60s at mean angle of attack, α_m of 30° , amplitude of delta wing pitching motion, α_o of -5° (downstroke) and dynamic angles of attack, $\alpha(t)$ vary between 25° and 35° . All images are taken at angle of attack, $\alpha=25^\circ$	44
Figure 4.6.	Formation of onset of vortex breakdown in the cases of stationary and oscillating delta wings under variation of yaw angle, β within the range of $0^\circ \leq \beta \leq 16^\circ$, period of oscillation, T_e ranging from 5s to 60s at mean angle of attack, α_m of 35° , amplitude of delta wing pitching motion, α_o of -5° (downstroke) and dynamic angles of attack, $\alpha(t)$ vary between 30° and 40° . All images are taken at angle of attack, $\alpha=30^\circ$	45
Figure 4.7.	Formation of onset of vortex breakdown in the cases of stationary and oscillating delta wings under variation of yaw angle, β within the range of $0^\circ \leq \beta \leq 16^\circ$, period of oscillation, T_e ranging from 5s to 60s at mean angle of attack, α_m of 25° , amplitude of delta wing pitching motion, α_o of $+10^\circ$ (upstroke) and dynamic angles of attack, $\alpha(t)$ vary between 15° and 35° . All images are taken at angle of attack, $\alpha=35^\circ$	46
Figure 4.8.	Formation of onset of vortex breakdown in the cases of stationary and oscillating delta wings under variation of yaw angle, β within the range of $0^\circ \leq \beta \leq 16^\circ$, period of oscillation, T_e ranging from 5s to 60s at mean angle of attack, α_m of 30° , amplitude of delta wing pitching motion, α_o of $+10^\circ$ (upstroke)	

	and dynamic angles of attack, $\alpha(t)$ vary between 20° and 40° . All images are taken at angle of attack, $\alpha=40^\circ$	47
Figure 4.9.	Formation of onset of vortex breakdown in the cases of stationary and oscillating delta wings under variation of yaw angle, β within the range of $0^\circ \leq \beta \leq 16^\circ$, period of oscillation, T_e ranging from 5s to 60s at mean angle of attack, α_m of 35° , amplitude of delta wing pitching motion, α_o of $+10^\circ$ (upstroke) and dynamic angles of attack, $\alpha(t)$ vary between 25° and 45° . All images are taken at angle of attack, $\alpha=45^\circ$	48
Figure 4.10.	Formation of onset of vortex breakdown in the cases of stationary and oscillating delta wings under variation of yaw angle, β within the range of $0^\circ \leq \beta \leq 16^\circ$, period of oscillation, T_e ranging from 5s to 60s at mean angle of attack, α_m of 25° , amplitude of delta wing pitching motion, α_o of -10° (downstroke) and dynamic angles of attack, $\alpha(t)$ vary between 15° and 35° . All images are taken at angle of attack, $\alpha=15^\circ$	49
Figure 4.11.	Formation of onset of vortex breakdown in the cases of stationary and oscillating delta wings under variation of yaw angle, β within the range of $0^\circ \leq \beta \leq 16^\circ$, period of oscillation, T_e ranging from 5s to 60s at mean angle of attack, α_m of 30° , amplitude of delta wing pitching motion, α_o of -10° (downstroke) and dynamic angles of attack, $\alpha(t)$ vary between 20° and 40° . All images are taken at angle of attack, $\alpha=20^\circ$	50
Figure 4.12.	Formation of onset of vortex breakdown in the cases of stationary and oscillating delta wings under variation of yaw angle, β within the range of $0^\circ \leq \beta \leq 16^\circ$, period of oscillation, T_e ranging from 5s to 60s at mean angle of attack, α_m of 35° , amplitude of delta wing pitching motion, α_o of -10° (downstroke)	

and dynamic angles of attack, $\alpha(t)$ vary between 25° and 45° . All images are taken at angle of attack, $\alpha=25^\circ$	51
Figure 4.13. Comparisons of static and dynamic loops of vortex breakdown as a function of angle of attack, α . Mean angle of attack is $\alpha_m=25^\circ$, amplitude of pitching motion is $\alpha_o=\pm 5^\circ$, yaw angle is $\beta=0^\circ$, period of oscillation is $T_e=5s, 20s, 40s, 60s$ and reduced frequency is $K=0.16, 0.25, 0.49, 1.96$	57
Figure 4.14. Comparisons of static and dynamic loops of vortex breakdown as a function of angle of attack, α . Mean angle of attack is $\alpha_m=25^\circ$, amplitude of pitching motion is $\alpha_o=\pm 5^\circ$, yaw angle is $\beta=4^\circ$, period of oscillation is $T_e=5s, 20s, 40s, 60s$ and reduced frequency is $K=0.16, 0.25, 0.49, 1.96$	58
Figure 4.15. Comparisons of static and dynamic loops of vortex breakdown as a function of angle of attack, α . Mean angle of attack is $\alpha_m=25^\circ$, amplitude of pitching motion is $\alpha_o=\pm 5^\circ$, yaw angle is $\beta=8^\circ$, period of oscillation is $T_e=5s, 20s, 40s, 60s$ and reduced frequency is $K=0.16, 0.25, 0.49, 1.96$	59
Figure 4.16. Comparisons of static and dynamic loops of vortex breakdown as a function of angle of attack, α . Mean angle of attack is $\alpha_m=25^\circ$, amplitude of pitching motion is $\alpha_o=\pm 5^\circ$, yaw angle is $\beta=12^\circ$, period of oscillation is $T_e=5s, 20s, 40s, 60s$ and reduced frequency is $K=0.16, 0.25, 0.49, 1.96$	60
Figure 4.17. Comparisons of static and dynamic loops of vortex breakdown as a function of angle of attack, α . Mean angle of attack is $\alpha_m=25^\circ$, amplitude of pitching motion is $\alpha_o=\pm 5^\circ$, yaw angle is $\beta=16^\circ$, period of oscillation is $T_e=5s, 20s, 40s, 60s$ and reduced frequency is $K=0.16, 0.25, 0.49, 1.96$	61
Figure 4.18. Comparisons of static and dynamic loops of vortex breakdown as a function of angle of attack, α . Mean angle of attack is $\alpha_m=30^\circ$,	

amplitude of pitching motion is $\alpha_o=\pm 5^\circ$, yaw angle is $\beta=0^\circ$, period of oscillation is $T_e=5s, 20s, 40s, 60s$ and reduced frequency is $K=0.16, 0.25, 0.49, 1.96$ 62

Figure 4.19. Comparisons of static and dynamic loops of vortex breakdown as a function of angle of attack, α . Mean angle of attack is $\alpha_m=30^\circ$, amplitude of pitching motion is $\alpha_o=\pm 5^\circ$, yaw angle is $\beta=4^\circ$, period of oscillation is $T_e=5s, 20s, 40s, 60s$ and reduced frequency is $K=0.16, 0.25, 0.49, 1.96$ 63

Figure 4.20. Comparisons of static and dynamic loops of vortex breakdown as a function of angle of attack, α . Mean angle of attack is $\alpha_m=30^\circ$, amplitude of pitching motion is $\alpha_o=\pm 5^\circ$, yaw angle is $\beta=8^\circ$, period of oscillation is $T_e=5s, 20s, 40s, 60s$ and reduced frequency is $K=0.16, 0.25, 0.49, 1.96$ 64

Figure 4.21. Comparisons of static and dynamic loops of vortex breakdown as a function of angle of attack, α . Mean angle of attack is $\alpha_m=30^\circ$, amplitude of pitching motion is $\alpha_o=\pm 5^\circ$, yaw angle is $\beta=12^\circ$, period of oscillation is $T_e=5s, 20s, 40s, 60s$ and reduced frequency is $K=0.16, 0.25, 0.49, 1.96$ 65

Figure 4.22. Comparisons of static and dynamic loops of vortex breakdown as a function of angle of attack, α . Mean angle of attack is $\alpha_m=30^\circ$, amplitude of pitching motion is $\alpha_o=\pm 5^\circ$, yaw angle is $\beta=16^\circ$, period of oscillation is $T_e=5s, 20s, 40s, 60s$ and reduced frequency is $K=0.16, 0.25, 0.49, 1.96$ 66

Figure 4.23. Comparisons of static and dynamic loops of vortex breakdown as a function of angle of attack, α . Mean angle of attack is $\alpha_m=35^\circ$, amplitude of pitching motion is $\alpha_o=\pm 5^\circ$, yaw angle is $\beta=0^\circ$, period of oscillation is $T_e=5s, 20s, 40s, 60s$ and reduced frequency is $K=0.16, 0.25, 0.49, 1.96$ 67

Figure 4.24. Comparisons of static and dynamic loops of vortex breakdown as a function of angle of attack, α . Mean angle of attack is $\alpha_m=35^\circ$, amplitude of pitching motion is $\alpha_o=\pm 5^\circ$, yaw angle is $\beta=4^\circ$, period of oscillation is $T_e=5s, 20s, 40s, 60s$ and reduced frequency is $K=0.16, 0.25, 0.49, 1.96$	68
Figure 4.25. Comparisons of static and dynamic loops of vortex breakdown as a function of angle of attack, α . Mean angle of attack is $\alpha_m=35^\circ$, amplitude of pitching motion is $\alpha_o=\pm 5^\circ$, yaw angle is $\beta=8^\circ$, period of oscillation is $T_e=5s, 20s, 40s, 60s$ and reduced frequency is $K=0.16, 0.25, 0.49, 1.96$	69
Figure 4.26. Comparisons of static and dynamic loops of vortex breakdown as a function of angle of attack, α . Mean angle of attack is $\alpha_m=35^\circ$, amplitude of pitching motion is $\alpha_o=\pm 5^\circ$, yaw angle is $\beta=12^\circ$, period of oscillation is $T_e=5s, 20s, 40s, 60s$ and reduced frequency is $K=0.16, 0.25, 0.49, 1.96$	70
Figure 4.27. Comparisons of static and dynamic loops of vortex breakdown as a function of angle of attack, α . Mean angle of attack is $\alpha_m=35^\circ$, amplitude of pitching motion is $\alpha_o=\pm 5^\circ$, yaw angle is $\beta=16^\circ$, period of oscillation is $T_e=5s, 20s, 40s, 60s$ and reduced frequency is $K=0.16, 0.25, 0.49, 1.96$	71
Figure 4.28. Comparisons of static and dynamic loops of vortex breakdown as a function of angle of attack, α . Mean angle of attack is $\alpha_m=25^\circ$, amplitude of pitching motion is $\alpha_o=\pm 10^\circ$, yaw angle is $\beta=0^\circ$, period of oscillation is $T_e=5s, 20s, 40s, 60s$ and reduced frequency is $K=0.16, 0.25, 0.49, 1.96$	72
Figure 4.29. Comparisons of static and dynamic loops of vortex breakdown as a function of angle of attack, α . Mean angle of attack is $\alpha_m=25^\circ$, amplitude of pitching motion is $\alpha_o=\pm 10^\circ$, yaw angle is $\beta=4^\circ$,	

period of oscillation is $T_e=5s, 20s, 40s, 60s$ and reduced frequency is $K= 0.16, 0.25, 0.49, 1.96$ 73

Figure 4.30. Comparisons of static and dynamic loops of vortex breakdown as a function of angle of attack, α . Mean angle of attack is $\alpha_m=25^\circ$, amplitude of pitching motion is $\alpha_o=\pm 10^\circ$, yaw angle is $\beta=8^\circ$, period of oscillation is $T_e=5s, 20s, 40s, 60s$ and reduced frequency is $K= 0.16, 0.25, 0.49, 1.96$ 74

Figure 4.31. Comparisons of static and dynamic loops of vortex breakdown as a function of angle of attack, α . Mean angle of attack is $\alpha_m=25^\circ$, amplitude of pitching motion is $\alpha_o=\pm 10^\circ$, yaw angle is $\beta=12^\circ$, period of oscillation is $T_e=5s, 20s, 40s, 60s$ and reduced frequency is $K= 0.16, 0.25, 0.49, 1.96$ 75

Figure 4.32. Comparisons of static and dynamic loops of vortex breakdown as a function of angle of attack, α . Mean angle of attack is $\alpha_m=25^\circ$, amplitude of pitching motion is $\alpha_o=\pm 10^\circ$, yaw angle is $\beta=16^\circ$, period of oscillation is $T_e=5s, 20s, 40s, 60s$ and reduced frequency is $K= 0.16, 0.25, 0.49, 1.96$ 76

Figure 4.33. Comparisons of static and dynamic loops of vortex breakdown as a function of angle of attack, α . Mean angle of attack is $\alpha_m=30^\circ$, amplitude of pitching motion is $\alpha_o=\pm 10^\circ$, yaw angle is $\beta=0^\circ$, period of oscillation is $T_e=5s, 20s, 40s, 60s$ and reduced frequency is $K= 0.16, 0.25, 0.49, 1.96$ 77

Figure 4.34. Comparisons of static and dynamic loops of vortex breakdown as a function of angle of attack, α . Mean angle of attack is $\alpha_m=30^\circ$, amplitude of pitching motion is $\alpha_o=\pm 10^\circ$, yaw angle is $\beta=4^\circ$, period of oscillation is $T_e=5s, 20s, 40s, 60s$ and reduced frequency is $K= 0.16, 0.25, 0.49, 1.96$ 78

Figure 4.35. Comparisons of static and dynamic loops of vortex breakdown as a function of angle of attack, α . Mean angle of attack is $\alpha_m=30^\circ$,

amplitude of pitching motion is $\alpha_o=\pm 10^\circ$, yaw angle is $\beta=8^\circ$, period of oscillation is $T_e=5s, 20s, 40s, 60s$ and reduced frequency is $K=0.16, 0.25, 0.49, 1.96$ 79

Figure 4.36. Comparisons of static and dynamic loops of vortex breakdown as a function of angle of attack, α . Mean angle of attack is $\alpha_m=30^\circ$, amplitude of pitching motion is $\alpha_o=\pm 10^\circ$, yaw angle is $\beta=12^\circ$, period of oscillation is $T_e=5s, 20s, 40s, 60s$ and reduced frequency is $K=0.16, 0.25, 0.49, 1.96$ 80

Figure 4.37. Comparisons of static and dynamic loops of vortex breakdown as a function of angle of attack, α . Mean angle of attack is $\alpha_m=30^\circ$, amplitude of pitching motion is $\alpha_o=\pm 10^\circ$, yaw angle is $\beta=16^\circ$, period of oscillation is $T_e=5s, 20s, 40s, 60s$ and reduced frequency is $K=0.16, 0.25, 0.49, 1.96$ 81

Figure 4.38. Comparisons of static and dynamic loops of vortex breakdown as a function of angle of attack, α . Mean angle of attack is $\alpha_m=35^\circ$, amplitude of pitching motion is $\alpha_o=\pm 10^\circ$, yaw angle is $\beta=0^\circ$, period of oscillation is $T_e=5s, 20s, 40s, 60s$ and reduced frequency is $K=0.16, 0.25, 0.49, 1.96$ 82

Figure 4.39. Comparisons of static and dynamic loops of vortex breakdown as a function of angle of attack, α . Mean angle of attack is $\alpha_m=35^\circ$, amplitude of pitching motion is $\alpha_o=\pm 10^\circ$, yaw angle is $\beta=4^\circ$, period of oscillation is $T_e=5s, 20s, 40s, 60s$ and reduced frequency is $K=0.16, 0.25, 0.49, 1.96$ 83

Figure 4.40. Comparisons of static and dynamic loops of vortex breakdown as a function of angle of attack, α . Mean angle of attack is $\alpha_m=35^\circ$, amplitude of pitching motion is $\alpha_o=\pm 10^\circ$, yaw angle is $\beta=8^\circ$, period of oscillation is $T_e=5s, 20s, 40s, 60s$ and reduced frequency is $K=0.16, 0.25, 0.49, 1.96$ 84

Figure 4.41. Comparisons of static and dynamic loops of vortex breakdown as a function of angle of attack, α . Mean angle of attack is $\alpha_m=35^\circ$, amplitude of pitching motion is $\alpha_o=\pm 10^\circ$, yaw angle is $\beta=12^\circ$, period of oscillation is $T_e=5s, 20s, 40s, 60s$ and reduced frequency is $K=0.16, 0.25, 0.49, 1.96$	85
Figure 4.42. Comparisons of static and dynamic loops of vortex breakdown as a function of angle of attack, α . Mean angle of attack is $\alpha_m=35^\circ$, amplitude of pitching motion is $\alpha_o=\pm 10^\circ$, yaw angle is $\beta=16^\circ$, period of oscillation is $T_e=5s, 20s, 40s, 60s$ and reduced frequency is $K=0.16, 0.25, 0.49, 1.96$	86
Figure 4.43. Comparisons of static and dynamic cases of vortex breakdown as a function of yaw angle, β . Amplitude of pitching motion is $\alpha_o=+5^\circ$ (upstroke), reduced frequency is $K=0.16, 0.25, 0.49, 1.96$...	87
Figure 4.44. Comparisons of static and dynamic cases of vortex breakdown as a function of yaw angle, β . Amplitude of pitching motion is $\alpha_o=+10^\circ$ (upstroke), reduced frequency is $K=0.16, 0.25, 0.49, 1.96$	88
Figure 4.45. Patterns of time-averaged velocity vectors, $\langle V \rangle$ and instantaneous velocity vectors, V for the stationary and oscillating wing under yaw angle, β of 0° , period of oscillation, T_e ranging from 5s to 40s at mean angle of attack, α_m of 30° , amplitude of delta wing pitching motion, α_o of $\pm 10^\circ$ and dynamic angles of attack, $\alpha(t)$ of 40° in side view plane	90
Figure 4.46. Patterns of time-averaged streamline, $\langle \psi \rangle$ and instantaneous streamline, ψ for the stationary and oscillating wing under yaw angle, β of 0° , period of oscillation, T_e ranging from 5s to 40s at mean angle of attack, α_m of 30° , amplitude of delta wing pitching motion, α_o of $\pm 10^\circ$ and dynamic angles of attack, $\alpha(t)$ of 40° in side view plane	91

Figure 4.47. Patterns of time-averaged vorticity, $\langle\omega\rangle$ and instantaneous vorticity, ω for the stationary and oscillating wing under yaw angle, β of 0° , period of oscillation, T_e ranging from 5s to 40s at mean angle of attack, α_m of 30° , amplitude of delta wing pitching motion, α_o of $\pm 10^\circ$ and dynamic angles of attack, $\alpha(t)$ of 40° in side view plane. Minimum and incremental values of vorticity, ω are $\omega_{\min}=\pm 0.5 \text{ sec}^{-1}$ and $\Delta\omega=0.5 \text{ sec}^{-1}$ 92

NOMENCLATURE

C	: Chord of the delta wing (mm)
D_w	: Vortex diameter prior to vortex breakdown
f_e	: Oscillation frequency (Hz), $f_e=1/T_e$
f_s	: Shedding frequency
F_L	: Lift force (N)
K	: Dimensionless reduced frequency, $K=\pi f_e C/U_{ref}$
max	: Maximum
min	: Minimum
x, y, z	: Streamwise, transverse and vertical coordinate directions
Re	: Reynolds number, $Re= \rho U_\infty C/\mu$
s	: Span of the delta wing (mm)
t	: Time (sec)
T_e	: Period of oscillation (sec)
Tu	: Turbulence intensity
U_{ref}	: Free-stream velocity (mm/sec)
V	: Instantaneous total velocity (mm/sec)
$\langle V \rangle$: Averaged total velocity (mm/sec)
$\langle V/U \rangle$: Contours of transverse velocity components
X_{vb}	: Vortex breakdown position from the apex of the delta wing (mm)
X_w	: Location of wire from the apex of the delta wing (mm)

Abbreviations

CCD	: Charge Coupled Device
Nd:YAG	: Neodymium-doped Yttrium Aluminum Garnet
PIV	: Particle Image Velocimetry
RMS	: Root-Mean-Square

Greek symbols

α	: Angle of attack ($^{\circ}$)
α_m	: Mean angle of attack ($^{\circ}$)
α_o	: Amplitude of pitching motion ($^{\circ}$)
$\alpha(t)$: Dynamic angle of attack ($^{\circ}$)
β	: Yaw angle ($^{\circ}$)
Λ	: Sweep angle ($^{\circ}$)
Γ	: Circulation of the vorticity concentration (mm^2/sec)
Δ	: Difference in the value of a physical quantity
θ	: Roll angle ($^{\circ}$)
ρ	: Density of fluid (kg/m^3)
ω	: Instantaneous vorticity ($1/\text{sec}$)
$\langle\omega\rangle$: Averaged vorticity ($1/\text{sec}$)
ω_e	: Angular frequency (Hz), $2\pi f_e$
ω_{rms}	: Root-mean-square vorticity fluctuation ($1/\text{sec}^2$)

1. INTRODUCTION

As a result of past researches, delta wings are main element of combat aircrafts. The control of vortex dynamics, unsteady flow characteristic and physics are also considerably important to improve the maneuverability of air vehicles (Heron and Myose, 2004).

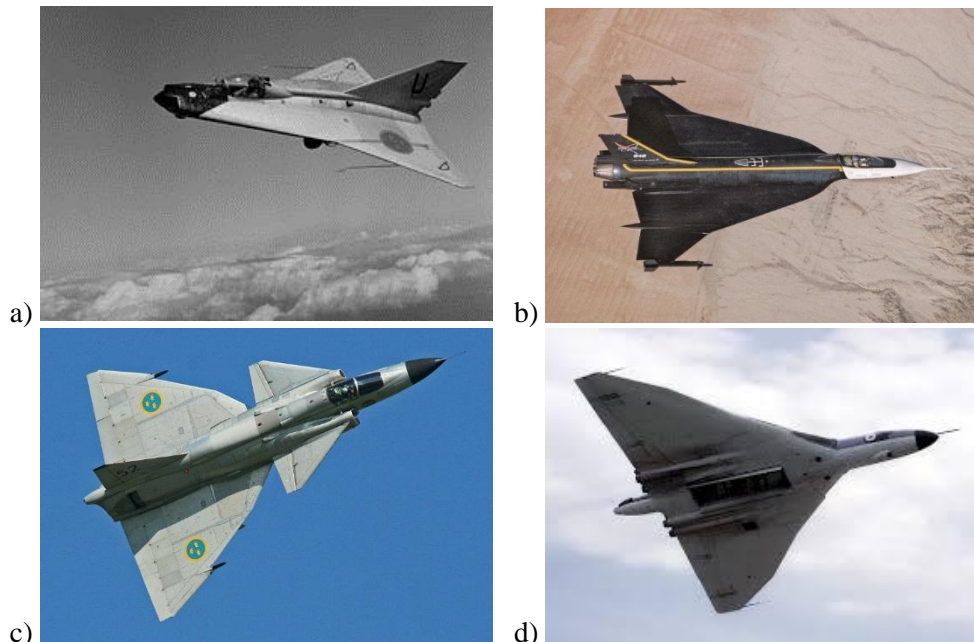


Figure 1.1. Different types of delta wings a) Saab 210 Draken (Dorr, 1985) b) The F-16XL's double delta wing (NASA, 2015) c) Canard Saab AJS-37 Viggen (Wikipedia, 2016) d) Jet-powered tailless delta wing (Wikipedia, 2016)

Figure 1.1 shows different types of delta wing aircrafts. Saab 210 Draken (a) is a first ever double delta wing (Dorr,1985), F-16 XL (b) is unusual curved double delta wing platform (NASA, 2015), Canard Saab AJS-37 Viggen (c) is an aeronautical arrangement wherein a small forewing or foreplane is placed in the forward face of the main wing of a fixed-wing aircraft (Clancy, 1975), Avro

Vulcan bomber (d) is a jet-powered tailless delta wing high-altitude strategic bomber (Wikipedia, 2016).

Vortex breakdown can be described as a vortex with a bursting point located between apex and trailing edge of the delta wing (Su et al., 1990). Also, vortex breakdown can be defined as; sudden deceleration of flow along the central axis of leading edge vortex due to the reduction in axial velocity magnitude, formation of a small size circulatory flow regions, a declining of circumferential velocity and expansion of vortex in size and finally bursting of the vortex (Payne and Nelson, 1986).

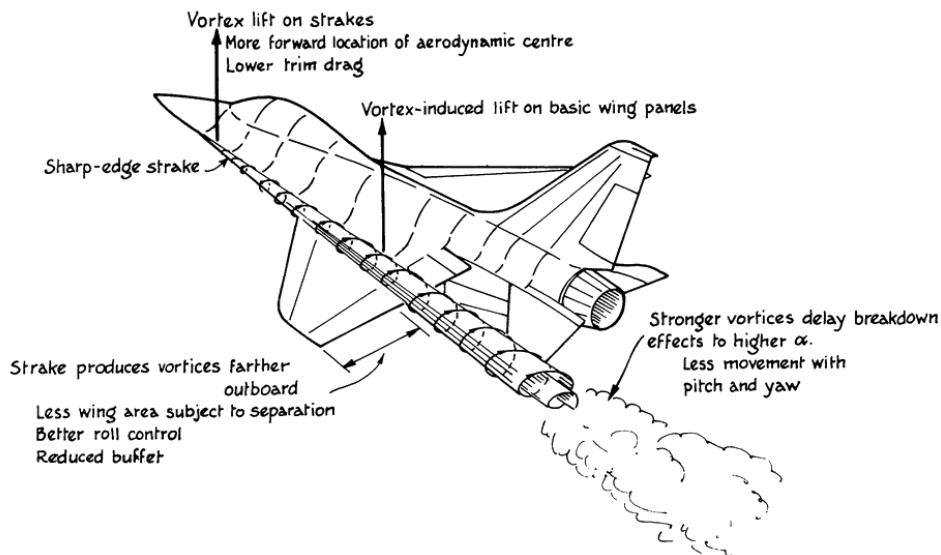


Figure 1.2. Schematic representation of vortices on the wing of the plane (Pakistan defence, 2012)

Position and structure of vortex breakdown alters over delta wings according to the numbers of geometrical factors. For example:

Sweep angle, Λ of the wing: If sweep angle, Λ of the wing decreases, vortex breakdown position moves towards the wing apex.

Angle of attack, α of the wing: Similar, vortex breakdown moves in the upstream direction towards the forward face of a wing with increasing angle of attack, α .

Yaw angle, β : The windward side of vortex bursting location slides upstream of the wing, on the other hand, the leeward side of vortex bursting location travels in the downstream direction as yaw angle, β rises. Also, vortex breakdown position changes according to roll angle θ , the certain level of Reynolds number Re , thickness of the wings t and shape of the wing etc. (Nelson and Pelletier, 2003).

Because occurrence of vortex breakdown near the apex leads decline in lift force, F_L , vortex breakdown causes changes in lateral and longitudinal forces, moments and stability of flow (Nelson and Pelletier, 2003). Also, vortex bursting causes decreasing of the lift and pitching moment, so that vortex breakdown is a limiting parameter of aerodynamic of the delta wing (Gursul et al., 2005).

Vortical flow contributes a high rate of aerodynamic forces on the delta wing. Therefore, there are many studies on vortex control to increase steady characteristic of flow structure of the delta wing.

For example;

i.) Flow-momentum control. Active method such as control of vortex breakdown, leading edge vortex and flow characteristics with blowing and suction on the apex and tail of the delta wing.

ii.) There are some vortex control methods. For instance; change of shape and geometry of the delta wing. Addition of flap on apex and tail, change of sweep angle, Λ and aspect ratio, C/s of the delta wing.

In the present study, the aerodynamics of oscillating delta wing is investigated that how the location of vortex breakdown and characteristic value of flow changes employing the dye visualization technique. In dye experiment, it was determined that the location of both vortex breakdowns move toward the wing apex or trailing edge during pitching motion either upstroke or downstroke

directions. As it is known, detecting of vortex breakdown with instantaneous velocity vectors measured near the surface of the delta wing to determine flow characteristics needs special attention for sensitive measurements. In additions, interactions between vorticity contrantrations and the delta wing which are formed after onset of vortex breakdown should also be examined.

Gad-el-Hak and Ho (1985) reported the existence of a time lag in the flow field during the pitching motion of delta wing. Maltby and Keating (1963) researched the existence of a phase lag of the motion of the vortex core, compared with the static case of the delta wing. Lambourne et al. (1969) investigated the behavior of the leading edge vortices over a delta wing following the termination of pitching maneuver. Gursul (2005) emphasized on the similarity between the spatial response of the vortex core and to that of a first-order dynamic system to a step function input, and thereby, a phase lag in the variation of the position of the vortex core was expected.

When the wing is sinusoidally oscillated, a hysteresis is observed in moving of vortex breakdown positions. Hysteresis loops improves in vortex breakdown position at the lowest value of reduced frequency, K . If the reduced frequency rises, hysteresis effect gets greater. Also, at lowest reduced frequency, an overshoot in the breakdown location past the static case is evident. This overshoot is slight and becomes at minimum attack angle. As reduced frequency becomes higher, overshoots do not occur (LeMay et al., 1988).

2. PRELIMINARY WORKS

2.1. Structure of Vortex Breakdown over Delta Wings

Vortex breakdown is one of the most important parameter on the delta wing surface. NASA (2016) showed that bubble and spiral type vortex breakdown and Sarpkaya (1971) also stated that double helix vortex breakdown can be visualized in a diverging cylindrical tube.

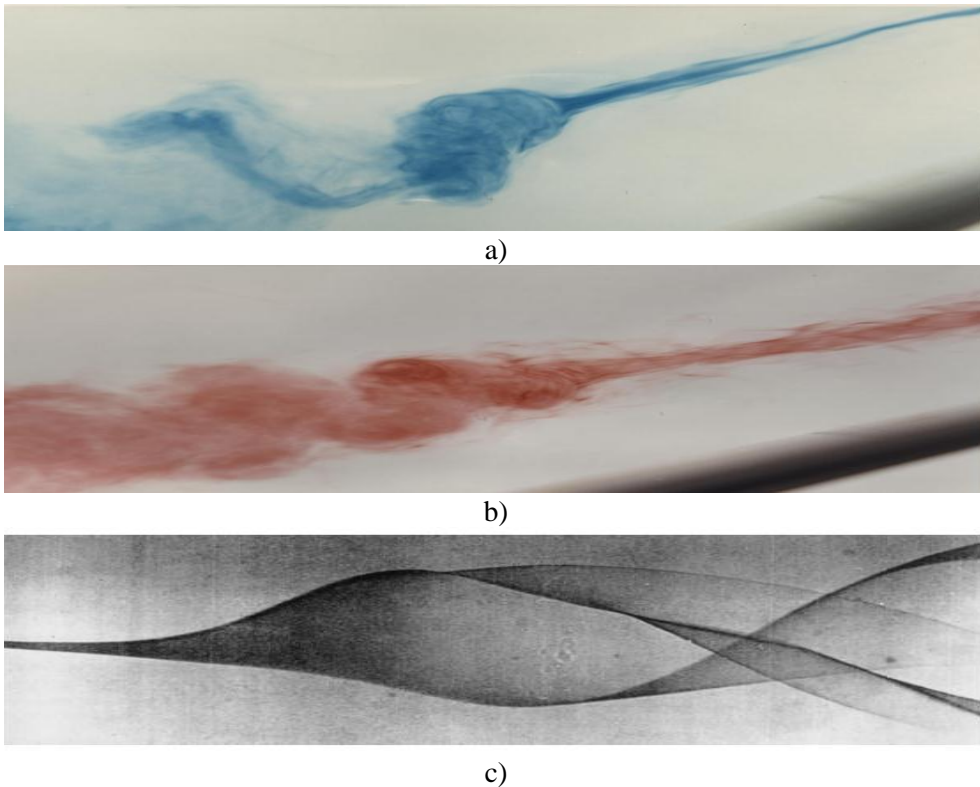


Figure 2.1. Types of vortex breakdown a) Bubble type vortex breakdown b) Spiral type vortex breakdown (NASA, 2016) c) Double helix vortex breakdown (Sarpkaya, 1971)

Nelson and Pelletier (2003) reported that the leading edge vortices caused by the flow moving in the spanwise direction originated from the upper surface of

the wing and later over the suction side of the delta wing the part of this flow detaches from the wing surface to develop a secondary vortex and takes place below the primary vortex as shown in Figure 2.2. In addition, Breitsamter (2008) examined that leading edge vortices cause further lift force and raise angle of attack, α in fully develop state and this situation provides increasing maneuver capabilities of aircraft.

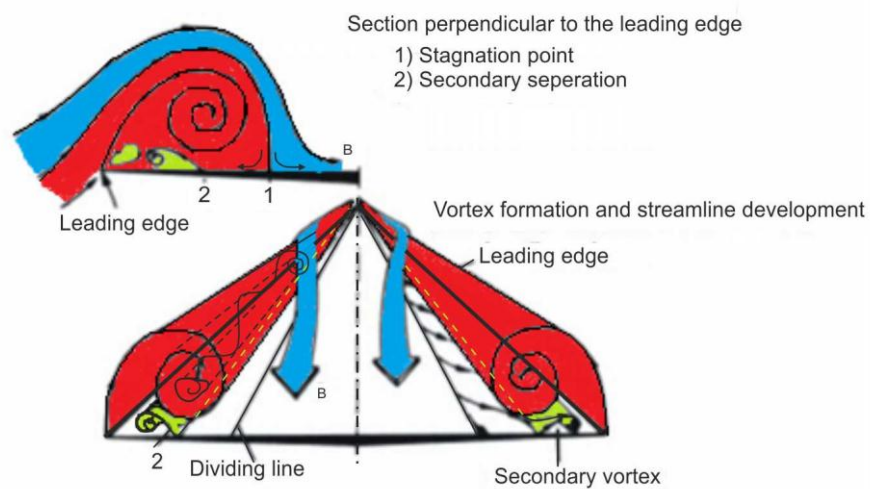


Figure 2.2. The representation of leading edge vortex formations and primary, secondary vortices (Anderson, 2001)

Ozgoren et al. (2002) experimentally determined that there were three different vorticity concentrations, Γ over the flow structure of delta wings with a higher sweep angle, $\Lambda=75^\circ$ at higher attack angles, $\alpha=24^\circ$, 30° and 32° using the PIV technique as seen in Figures 2.3 and 2.4. First of them was concentrations of azimuthal vorticity due to centrifugal instability of vortex having lower circulation and wave length value. Secondary vorticity concentration is developed due to the vortex breakdown and has a circulation with highest magnitude and wave length. Third circulation occurs with a higher wave length because of instability of leading

edge vortex. These structures are concerned to distributions of averaged and fluctuating vorticity and velocity.

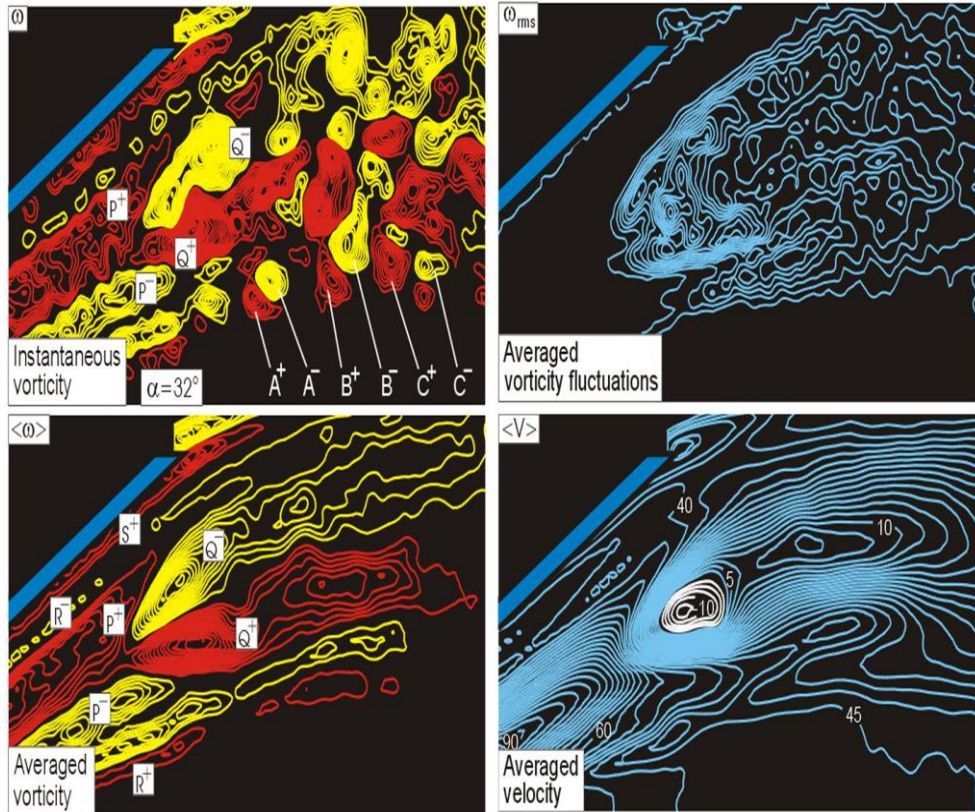


Figure 2.3. Patterns of instantaneous ω , $\langle\omega\rangle$, and ω_{rms} in comparison with $\langle V\rangle$ at $\alpha=32^\circ$. Minimum and incremental values of instantaneous ω are 1 and 0.75 s^{-1} , of $\langle\omega\rangle$ are 1 and 0.75 s^{-1} and of $\omega_{rms}= 0.5$ and 0.5 s^{-1} . For contours of $\langle V\rangle$, units of numerical values designated on contour lines are mm/s and incremental value between contours is 2.5 mm/s (Ozgoren et al., 2002)

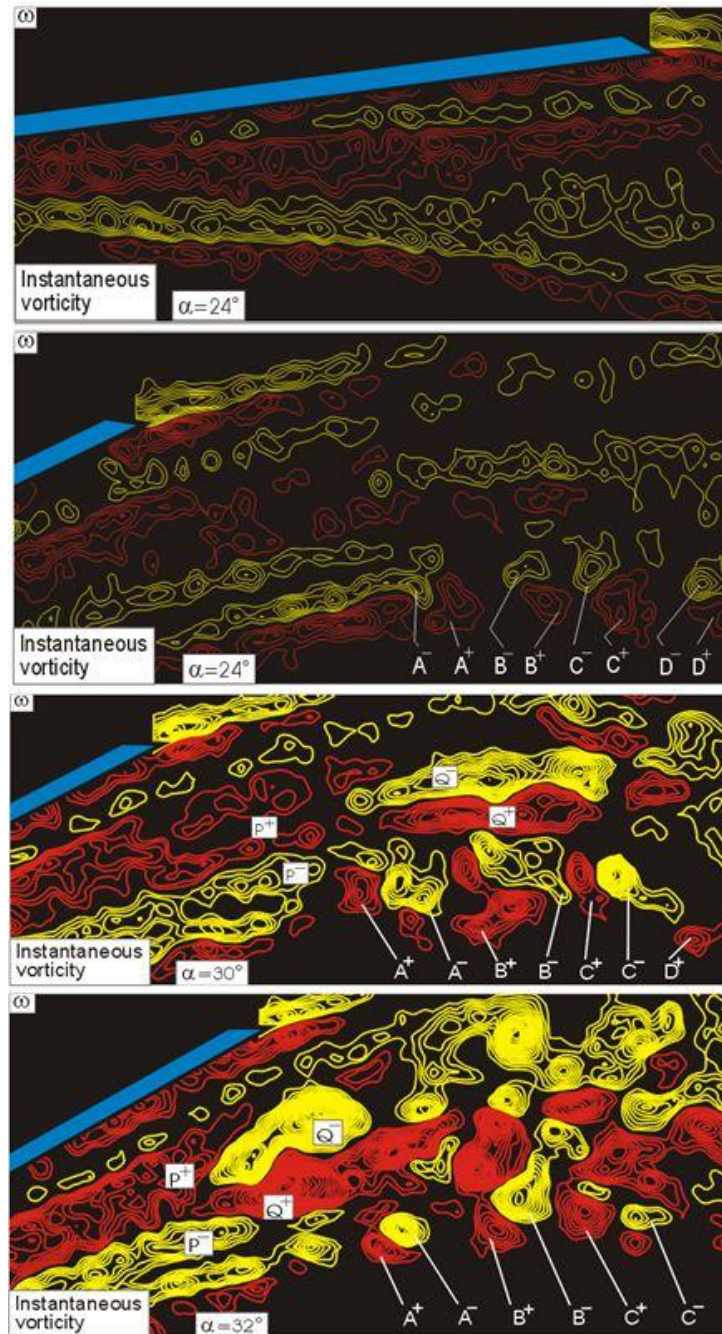


Figure 2.4. Effect of angle of attack on patterns of instantaneous, ω . Minimum and incremental values of ω for all cases are 1 and 0.75 s^{-1} (Ozgoren et al., 2002)

Gad el-Hak and Blackwelder (1985) reported experimental findings on the aerodynamics of delta wing with 45° sweep angle, Λ having NACA0012 flat profile and with 60° sweep angle, Λ . These findings can be summarized as follows; Shedding frequency, f_s near the leading edge is independent of leading edge shape and sweep angle, Λ at a constant free-stream velocity, U . If angle of attack, α is increased, shedding frequency, f_s decreases and at a constant angle of attack, α , shedding frequency, f_s is proportional to the square root of free-stream velocity, U .

Shih and Ding (1996) prepared an experimental survey at lower Reynolds numbers (9000 and 9800) via the PIV technique and dye visualization methods in the towing tank channel to demonstrate flow structures of over the delta wings with 75° and 60° sweep angles, Λ . They detected that delta wing-vortex interaction was higher for 60° sweep angle, Λ ; this interaction was not as higher as in the case of delta wings with 75° sweep angle, Λ .

Rediniotis et al. (1993) investigated the flow structures of delta wing with 76° sweep angle, Λ at Reynolds numbers varying within the range of $3.9 \times 10^4 < Re < 9.02 \times 10^5$ in wind tunnel and a higher angles of attack, α for example, the range of $30^\circ \leq \alpha \leq 90^\circ$. They observed that leading edge vortex breakdown became outside of delta wing until angle of attack, α of 35° , when angles of attack vary with the range of $35^\circ \leq \alpha \leq 70^\circ$, leading edge vortices changed simultaneously. Nevertheless, when attack angle, $\alpha > 70^\circ$, secondary vortex breakdown having moderate frequency of breakdown was observed. In addition, they showed that shedding frequency, f_s is dependent on angle of attack, α and there is nonlinear relationship between shedding frequency, f_s and angle of attacks, α . On the other hand, Ozgoren et al. (2002) examined the patterns of instantaneous vorticity of delta wing having 75° sweep angle, Λ , at higher angles of attack, α of 30° and 32° and at the value of Reynolds number of 1.07×10^4 in water channel. They found that when angle of attack, α of the wing is 30° , the location of vortex breakdown occurs outside of the delta wing, on the contrary, at angle of attack, α of 32° the onset of vortex breakdown relatively moves upstream of tailing edge of the wing. They also

showed that the pattern of ω_{rms} gets relatively higher vorticity level at the onset of vortex breakdown.

Canpolat et al. (2009) examined structures of flow on the surface of non-slender delta wing which has 40° sweep angle, Λ under angles of attack, $\alpha=7^\circ$, 10° , 13° and 17° at locations of $X/C=0.6$, 0.8 and 1.0 . They concluded that when the delta wing had even a moderate yaw angle, β , macro scale symmetrical flow structures have vanished. Vortex bursting occurs earlier on the windward side with respect to the leeward side of the non-slender delta wing. They also discovered that main vorticity concentrations in crossflow planes occurred inside of main vorticity concentration close to the central axis of the delta wing. In addition, analyzing all images in side-view plane reveals that a high-scale Kelvin-Helmholtz instabilities take place at the bottom of unstable flow region, particularly for angles of attack of $\alpha=13^\circ$ and 17° .

Flow structures close to the surface of non-slender diamond wing studied by (Yayla et al., 2009) using techniques such as dye visualization and the Stereo Particle Image Velocimetry technique. Flow compositions and vortex bursting transformation were examined by altering yaw angle, β in the limit of $0^\circ \leq \beta \leq 15^\circ$ for angle of attack of $\alpha=7^\circ$ and $Re=10^5$. They stated that when yaw angle, β increases, vortex bursting location on one side approaches to the wing apex, on the other side moves in the direction of free-stream flow towards the trailing edge. Also, Yayla et al. (2010) performed experimental studies on the aerodynamics of a non-slender diamond wing which has 40° sweep angle, Λ . They concluded that up to 4° of yaw angle, β there are no clear changes of vortex bursting locations, but at a higher yaw attack, β for example, after 4° , the point of vortex bursting moves towards the leading edge on the windward side, while this location travels further downstream on the leeward side of the delta wing. In additions, locations of asymmetrical vortex bursting are seen over the delta wing in plan-view planes.

Furthermore, Yayla et al. (2013) examined flow characteristics over the lambda wing under variation of angle of attack within the range of $7^\circ \leq \alpha \leq 17^\circ$ using

dye visualization and the stereo PIV technique. They proved that flow structure and development of vortex breakdown profoundly are affected by angle of attack, α . Sahin et al. (2012) demonstrated that structures of vortex bursting and vortical flow over a non-slender diamond wing are sensitively effected by yaw angle, β using dye visualization and the PIV technique and time averaged flow data over the wing surface changes profoundly increasing over the yaw angle, $\beta=6^\circ$.

Karasu (2015) studied structures of leading edge vortices in side view planes. As shown in Figure 2.5, he showed that yaw angle, β influences flow structures in side view plane substantially. When yaw angle, β is increased to a value of 20° , a well-defined Kelvin-Helmholtz (K-H) instabilities appear on both sides of leading edge vortex before and after onset of vortex breakdown clearly.

Gursul and Xie (2000) performed an experimental investigation over a delta wing with 75° sweep angle, Λ to examine core of vortex breakdown. It was reported that the rms values at origin of vortex breakdown decrease at lower Reynolds numbers. Because shear layer does not exhibit Kelvin-Helmholtz (K-H) instability. But, it is observed that after a critical Reynolds number, shear layer is dominated by a vortical flow structure because of Kelvin-Helmholtz (K-H) instability.

Despite the several years of study, effective vortex breakdown control method has not been developed for a long period. Sahin et al. (2001) examined that a delta wing with 75 degree sweep angle, Λ having angles of attack, α of 24° and 30° . It was found vortical flow structure moves towards the flat plate which was placed downstream of delta wing with a distance of 73 mm. Akilli et al. (2001) tried to control the location of vortex breakdown by inserting a very thin wire (0.1 mm) to the leading edge vortex axis as seen in Figure 2.6. Furthermore, same wire were placed along the axis of leading edge vortex by Akilli el al. (2003). In both experiment, effects of wire diameter, on the development of vortex breakdown were experimentally examined It is observed that in both cases, the location of

vortex breakdown moved in the opposite of flow direction towards the leading edge of the delta wing.

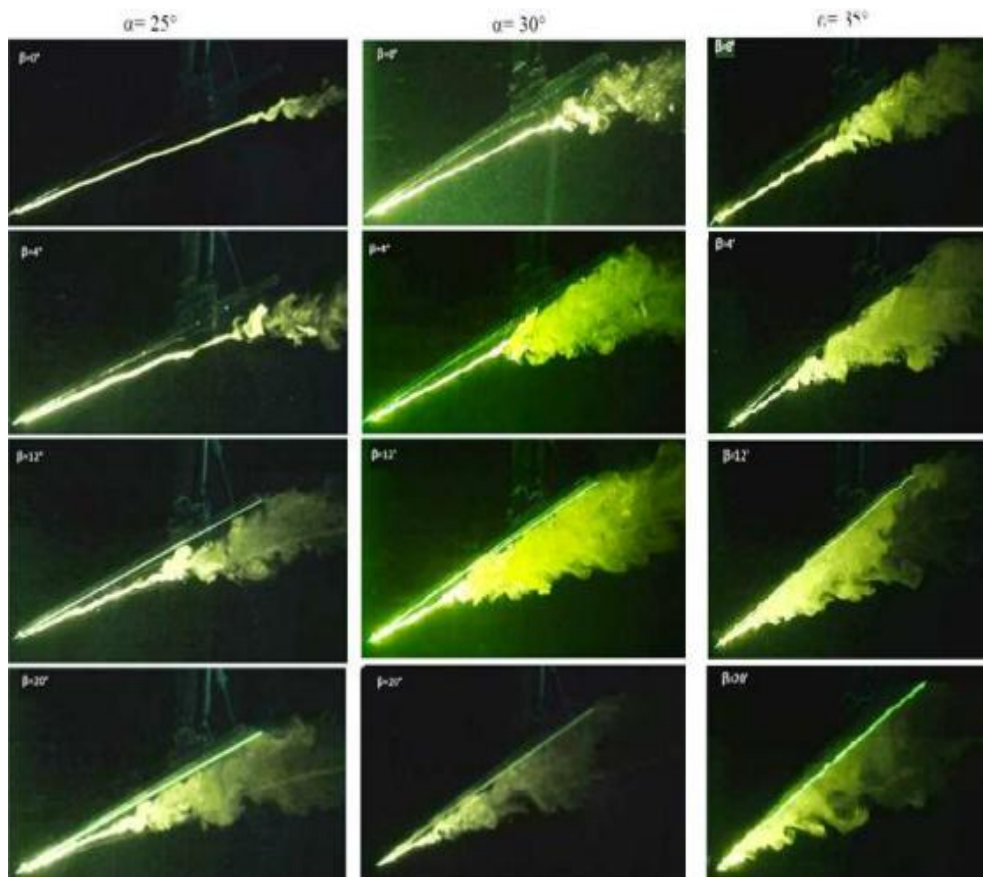


Figure 2.5. Dye visualizations in side-view plane of same delta wing representing effect of yaw angle, β , on flow structures at angles of attack, $\alpha = 25^\circ$, 30° and 35° (Karasu, 2015)

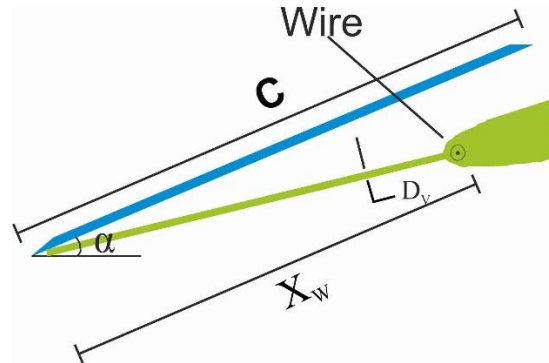


Figure 2.6. Overview of delta wing and wire arrangement (Akilli et al., 2001)

2.2. Response of Vortex Breakdown in the Case of Pitching Delta Wing

In recent years, the flow structure has been researched excessively, but studies on flow structures of an oscillating delta wing has been relatively taken less attention. Dynamic behavior of the leading edge vortices over a pitching delta wing having sweep angle, Λ of 70° were examined by LeMay et al., (1988). They defined the reduced frequency as $K=2\pi f_c C/U_{ref}$, where f is frequency of oscillation, C is the wing cord and U_{ref} is the free-stream velocity. In this study, the wing was sinusoidally pitched about its $1/2$ cord position (mid-cord) at Reynolds numbers between 9×10^4 and 35×10^4 based on the cord length at reduced frequencies, K varying from 0.05 to 0.30 and angles of attack, α ranges from 29° to 39° . As seen in Figure 2.7, they determined that when the wing was sinusoidally pitched, a hysteresis was observed. This hysteresis was increased with increasing reduced frequency, K . Also, they detected phase lag between model motion and location of leading edge vortex breakdown and compared the static delta wing case with the dynamic delta wing cases. Also, they detected % 2 difference over flow characteristics between stationary and oscillating delta wings.

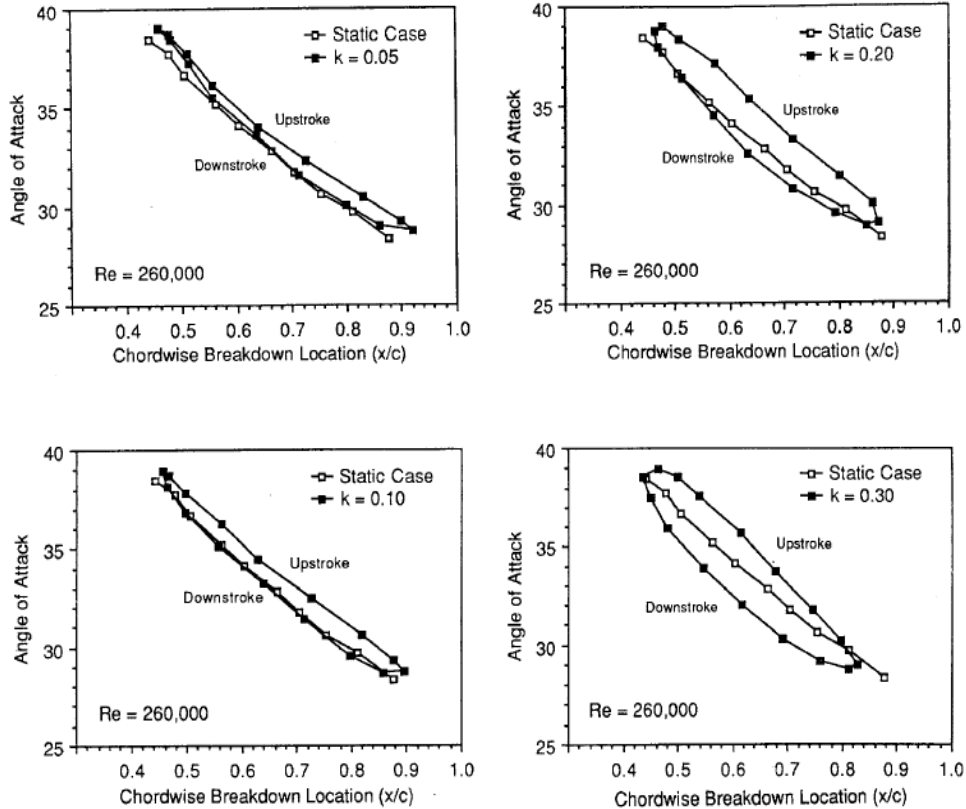


Figure 2.7. Chord wise location of vortex breakdown and hysteresis with different reduced frequencies, K , (LeMay et al., 1988)

Gad-el Hak and Ho (1985) sinusoidally pitched the delta wing with a 45° sweep angle, Λ at its the quarter chord position. Angle of attack, α ranging from 0° to 45° at reduced frequencies, K varying from 0.10 to 6.0. During the portion of the cycle in which the angle of attack, α expands in the upstroke direction, a flow separation firstly occurs in the vicinity of the trailing edge and later propagates towards the apex. The propagation velocity of vortex flow separation towards the leading edge is approximately equal to that of the free-stream velocity. During the downstroke direction, it is observed that there is no movement of the separation point from the wing surface towards the apex. They also found the existence of a hysteresis vortex breakdown locations of the delta wing with 45° sweep angle, Λ

which was sinusoidally perturbed between 10° and 20° for Reynolds numbers of 25×10^3 to 35×10^4 based on the cord length. The flow patterns at any particular dynamic angle of attack, $\alpha(t)$ are different in the case upstroke and downstroke motion of the delta wing. When the wing was oscillated at a reduced frequencies such as $K = 0.50, 1.0$ and 2.0 , the hysteresis was measured from development to weakening of the leading edge vortex.

Miau et al., (1992) observed occurrences of vortex breakdown positions under a pitching delta wing motion. In Figure 2.8, he specified that first delay of vortex breakdown was seen in all delta wings having sweep angles, Λ ranging from 59° to 70° in spite of pitching up or down motion. Second delay is defined as after this delay, slope of the curves does not follow same trend with respect to stationary wing. Occurrence of second delay is observed only during pitching up. He pointed out that this finding directly depends on the pitching motion and sweep angle, Λ of delta wing. When K increases and sweep angle, Λ of delta wing decreases, the occurrence of second delay cases become.

Rockwell et al. (1987) also reported that the existence of a substantial hysteresis in the vortex flow comparing to the static case. A 45° sweep delta wing, with a sharp leading edge, was sinusoidally pitched about its trailing edge from 5° to 20° at reduced frequencies of $K = 0.16$ to 10.68 . Reynolds numbers based on the cord length was ranging from 5.8×10^3 to 4.5×10^4 . When the position of vortex breakdown was determined as a function of instantaneous angle of attack, $\alpha(t)$, a hysteresis of vortex breakdowns became evident. They found hysteresis relative to the static delta wing case at a reduced frequency $K = 0.16$. The hysteretic behavior is generally the same for higher values of reduced frequency up to a value of $K = 1.75$. At $K = 1.75$ the hysteresis effect becomes negative. That is to say, having reduced frequencies of K , as 4.77 and higher, the behavior of the hysteresis is opposite to that of the $K < 1.75$ cases.

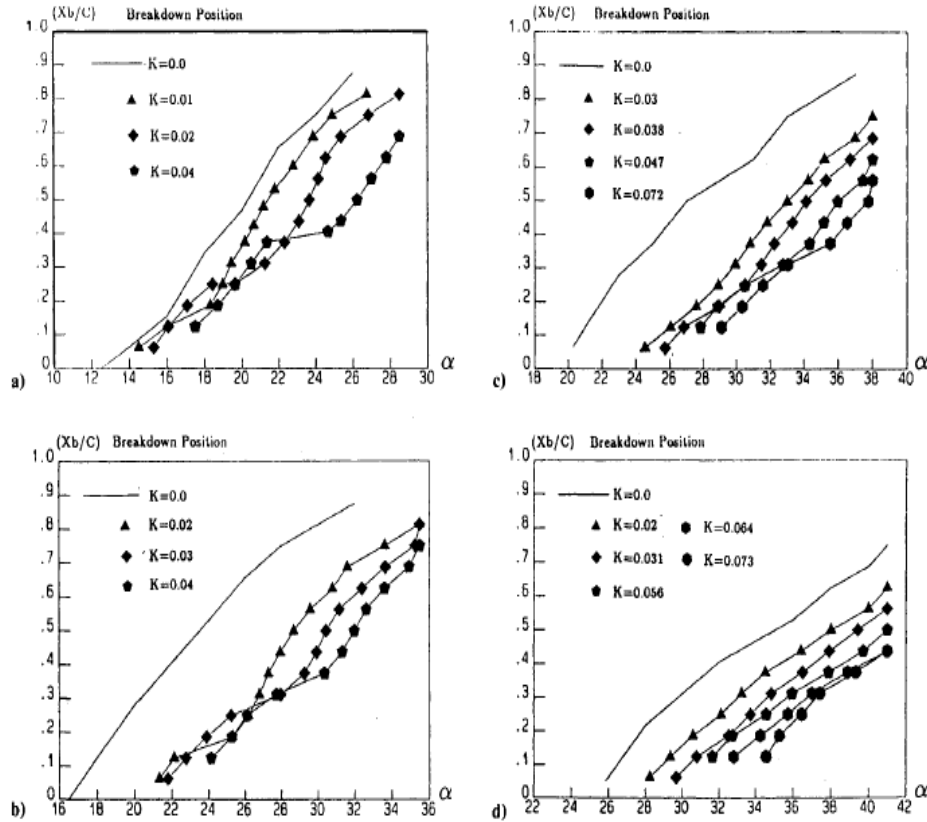


Figure 2.8. Variations of the instantaneous vortex breakdown positions for different sweep, Λ in the pitch up motion, pitch center located at $\frac{1}{2}$ chord length: a) With 59° sweep angle, Λ , at $Re = 9 \times 10^3$, $K = 0, 0.01, 0.02$, and 0.04 ; b) With 63.4° sweep angle, at $Re = 9 \times 10^3$, $K = 0, 0.02, 0.03$, and 0.04 ; c) With 67° sweep, Λ , at $Re = 11 \times 10^3$, $K = 0, 0.03, 0.038, 0.047$, and 0.072 ; and d) With 70° sweep angle, Λ , at $Re = 11 \times 10^3$, $K = 0, 0.02, 0.031, 0.056, 0.064$, and 0.073 (Miau et al., 1992)

Gilliam et al. (1987) perturbed the delta wing at a constant pitch rate from 0° to 60° . Flow field is described during the pitching motion by the vortical flow structures for a 30° sweep angle, Λ having a sharp leading edged delta wing. The unsteady flow field is generated near the leading edge when the angle of attack, α is increased. Also, the leading edge vortex remains more consistent and its diameter increases with increasing the pitch rate. No delay of vortex breakdown

was detected in the flow motion during the period of starting of the pitching motion.

A similar experiment was performed by (Reynolds and Abtahi, 1987). A delta wing of aspect ratio was pitched at a constant rate of $K= 0.06$. The wing was pitched in range of $30^{\circ} \leq \alpha \leq 51^{\circ}$ about its half of chord position at Reynolds numbers between 19,000 and 65,000. Large time delays were detected related with the vortex breakdown position comparing to the static case and a hysteresis was observed in the response of the vortex flow between the pitching-up and pitching-down cases.

Grismer and Nelson (1995) worked on the aerodynamic of double delta wing under yaw angle, β in order to investigate effect of oscillating motion. They found that the secondary wing vortex breaks down far away from the apex of wing during oscillations with increasing angle of attack, α comparing to angle of attack, α under pitch down motion. The discrepancy of vortex breakdown locations between upstroke and downstroke pitching motion of the delta wing can be altered further by increasing reduced frequency, K .

LeMay et al. (1990) investigated the effects of pitching motion on aerodynamics of diamond, cropped and double delta wing. Ericson (1999) reported the results of pitching motion at a higher angle of attack, α for a double delta wing.

Magness et al. (1993) investigated the unsteady flow structure during the transient pitching maneuvers. They provided a new topological structure over a delta wing with sweep angle, Λ of 70° undergoing transient pitching maneuvers at a high angle of attack, α . They observed instantaneous vorticity structure and streamline topology in a flow field, when a delta wing was subjected to unsteady pitching motion. The existence of critical topological features such as unstable foci at leading edge vortices and phase lag of vortex evolution were specified over a delta wing.

BOEING 1303 UCAV and SACCON configurations attracted the attention of researchers in recent years. Yilmaz and Rockwell (2012) investigated the effect

of oscillation with a lower amplitude on flow structures over the BOEING 1303 UCAV employing the PIV technique. In addition, flow structures over X-45 UCAV planform have also gain attention of researchers in recent years. Elkhoury and Rockwell (2004) performed dye visualization over this wing for different angles of attack, α and Reynolds numbers. Elkhoury et al. (2005) investigated time-mean unsteady flow structures near the surface of the wing for different angles of attack, α and Reynolds numbers. Woodiga et al. (2015) defined flow separation and integration on the surface of wing via numerical methods for the delta wings having sweep angles, Λ of 65° and $76^\circ/40^\circ$.

In the work of Ozgoren (2000) delta wing was sinusoidally pitched about its half cord position. He observed five different vorticity layers at a lower angle of attack, α before vortex bursting. He reported that structure of vortex core and vortex breakdown region depended on amplitude of angle of delta wing, α_o . Also, in his experimental surveys, he investigated effect of reduced frequency, K and time lag. He defined the reduced frequency as $K = \pi f_c C / U_{ref}$. Also, Ozgoren and Sahin (2002) investigated vortical flow structures over the pitching delta wing having 75° sweep angle, Λ using the PIV technique and comparing to vortical flow development of stationary and oscillating wing with and without the impingement plate as shown in Figure 2.9.

A similar experimental survey was performed by Ozgoren et al. (2002a, 2002b). They pitched the delta wing for three different values of angles of attack, such as $\alpha = 20^\circ, 24^\circ$ and 30° at an amplitude of perturbation, $\alpha_o = 10^\circ$, at a lower frequency. They observed that vortex breakdown, leading edge vortex and separation region severely influenced with a pitching delta wing and flow structures are changed as a function of oscillations. They searched the effect of characteristic of vortex bursting for a higher attack angle, α . Ozgoren et al. (2001a, 2002a and 2005c) performed experimental work on the vortical flow structures while they perturbed delta wing giving sinusoidal motion with amplitude of $\alpha_o = \pm 1^\circ$.

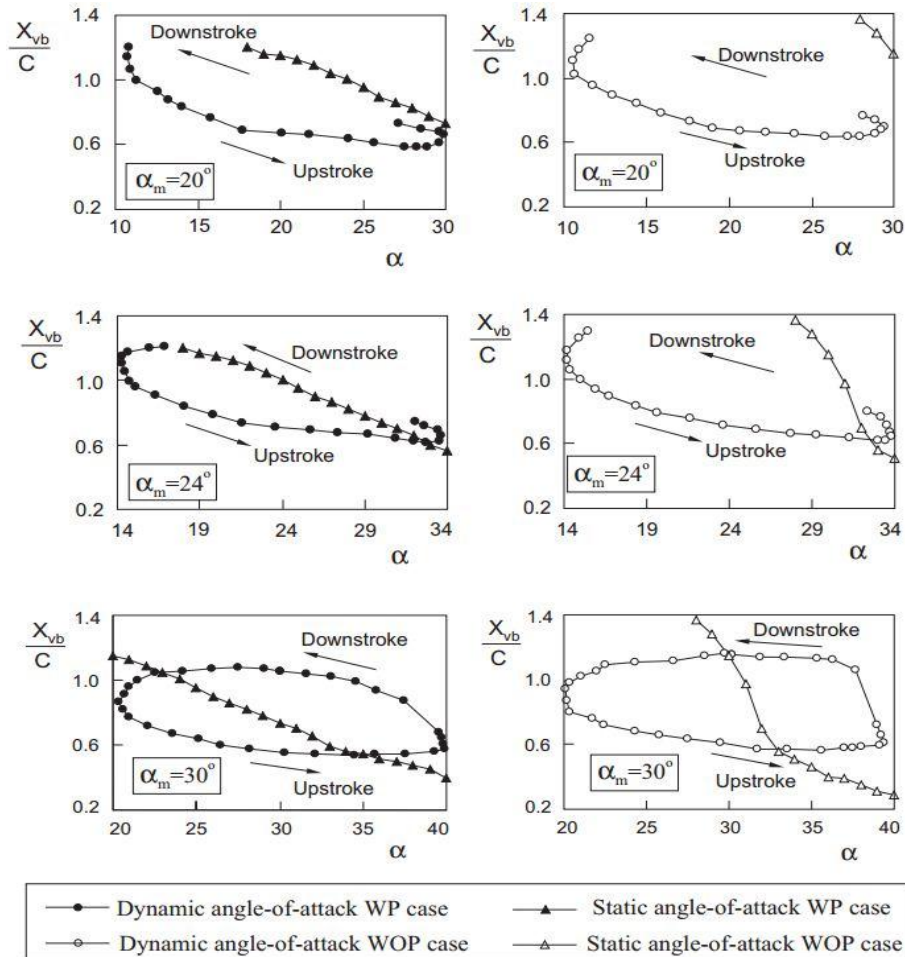


Figure 2.9. Comparison of static and dynamic hysteresis loops of onset of vortex breakdown versus attack angle, α . Oscillating period, $T_e=22.54$ s and reduced frequency, $K=0.74$ and amplitude of pitching motion, $\alpha_o=10^\circ$ (Ozgoren and Sahin, 2002)

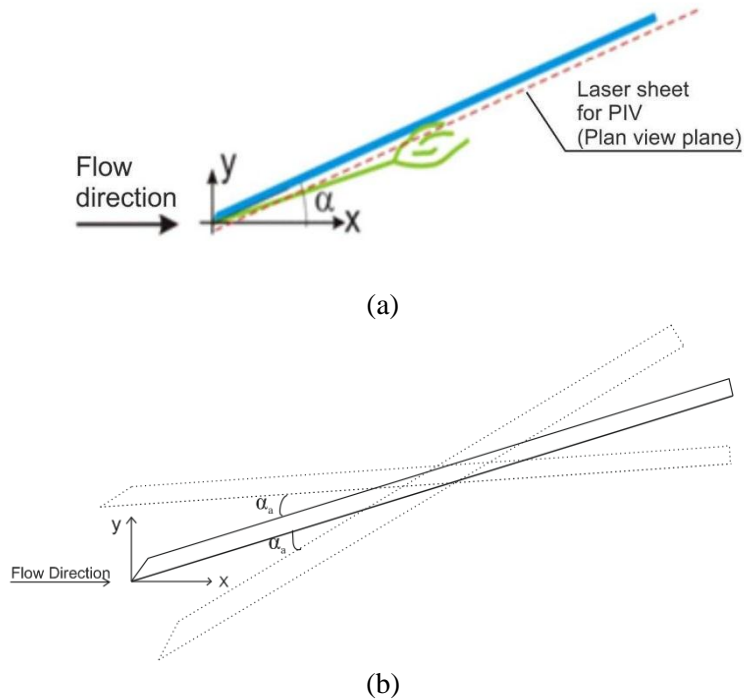


Figure 2.10. Schematic representation of stationary and pitching delta wing

Canpolat et al. (2015) experimentally investigated the flow structure and turbulence statistics of non-slender delta and diamond wings having sweep angle, of $\Lambda=40^\circ$. Wings are subjected to perturbation with the amplitude of $\alpha_0=\pm 0.5^\circ$ and oscillating period of $T_e=0.5$ s. They performed experiments using dye and the stereo PIV technique to observe vertical flow structures in plan-view plane by varying angles of attack, α at within the range of $7^\circ \leq \alpha \leq 17^\circ$. Patterns of time averaged vorticity and contours of transverse velocity components of the perturbed delta wing shown in Figure 2.11 are compared with the case of a stationary delta wing for angle of attack, α of 10° .

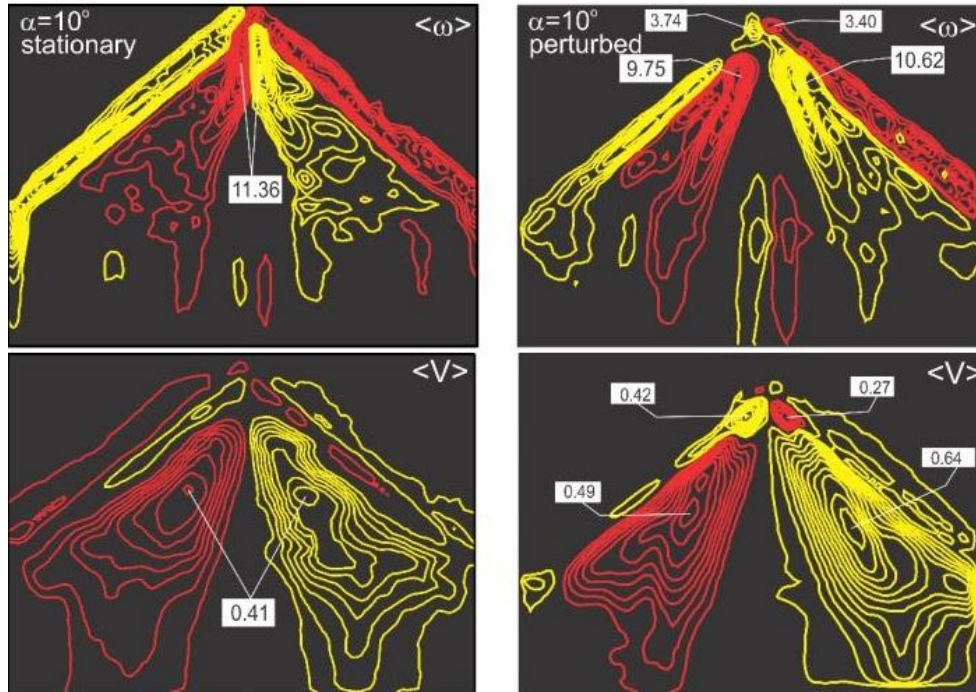


Figure 2.11. Patterns of time-averaged vorticity, $\langle \omega \rangle$ and contours of transverse velocity components, $\langle V/U \rangle$ of the delta wing under static and perturbed conditions having the mean angle of attack, $\alpha=10^\circ$ (Canpolat et al., 2015)

Yaniktepe and Rockwell (2004) reported the result of small amplitude of perturbations of delta wing, at a suitable frequency, which affects the time-averaged pattern of the separated shear layer near the wing surface. They revealed that when the wing is perturbed with a small amplitude, significant changings in the magnitude and distributions of instantaneous and time-averaged flow structures take place.

The reviewed studies were generally conducted to analyze and understand the physics of flow structures over the wings used for UCAV in recent years.

3. MATERIAL AND METHOD

3.1. Water Channel System

Experiments on the aerodynamics delta wings were performed in the free surface water channel having length of 8000 mm, width of 1000 mm and height of 750 mm. The channel was made from 15 mm thick Plexiglas.

Water channel system has 2 tanks; one of them is situated at inlet and the other one at outlet of the channel as shown in Figure 3.1. Two sets of honeycombs were placed in water channel before the test region where contraction of 2:1 is present to regulate the upstream flow. This design of channel with a double honeycombs provide turbulence intensity lower 0.5 %. Circulation of water was provided with a water pump having frequency control unit and power of 15 kW.

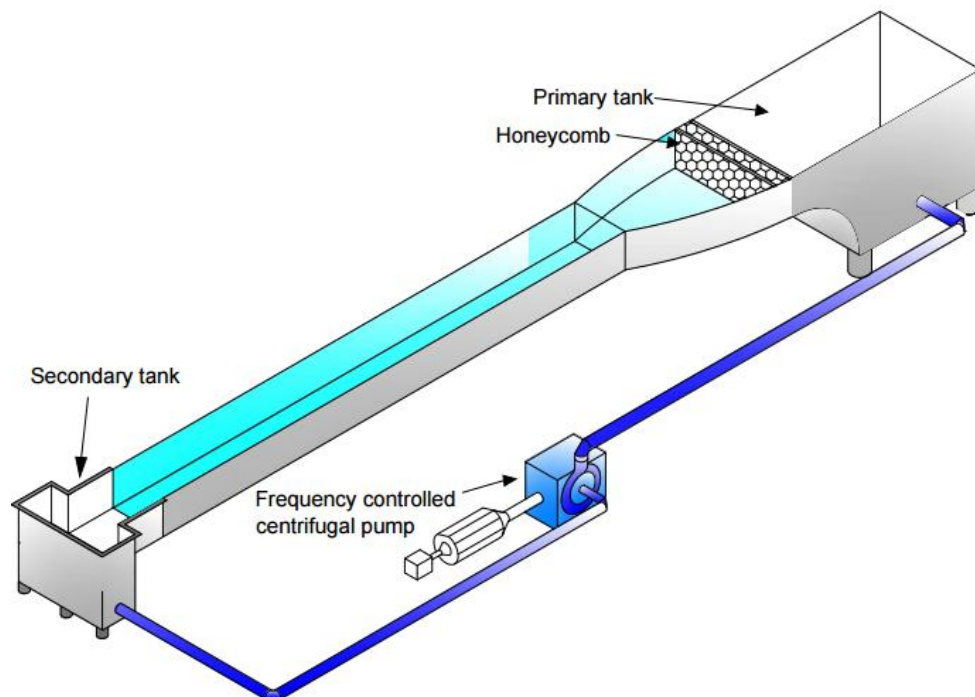


Figure 3.1. Schematic of closed circle water channel

3.2. Experimental Apparatuses

During the experiments, delta wing was placed in the water channel via special apparatus controlling yaw angle, β as shown in Figure 3.2. Servo motor was located on the angle apparatus to keep the wing stationary. Also, attack angle, α and period of oscillation, T_e was set by means of servo motor. Rotational part of servo motor was connected to the rod which exists on the angle apparatus and this rod was attached to the midcord of delta wing. Servo motor system includes servo motor and its control unit as seen in Figure 3.3. Servo motor's shaft angle can be adjusted in a right angular position according to the signal of control unit of servo motor. Angular location of output shaft can be altered by changing the signal code of control unit.

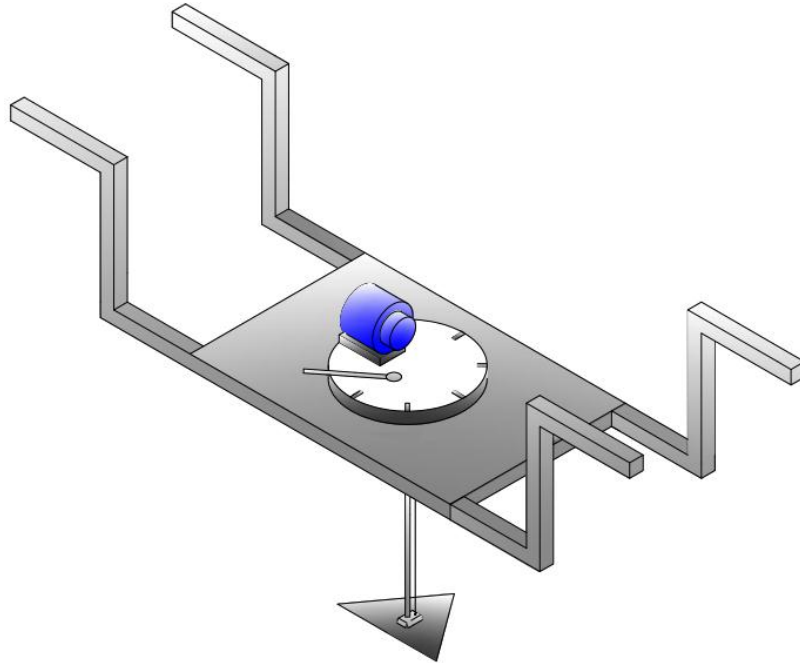


Figure 3.2. Representation of special apparatus (angle apparatus)



Figure 3.3. Servo motor and its control unit

3.3. Experiments Conducted by Dye Visualization and Particle Image Velocimetry (PIV)

3.3.1. Dye Visualization Experiments

The dye visualization technique is defined as the method which gives preliminary or qualitative information about flow structures over the delta wing. In the present study, dye experiments were performed by using fluorescent dye which changes color and shines under the laser sheet. Fluorescent dye is arranged by mixing powder of Rhodamine 6G with water. Dye was injected in the test region by taking the advantage of fluorescent dye reservoir height. Furthermore, continuous laser source was used during the dye observations.

3.3.2. Experiments Performed by PIV

Particle Image Velocimetry is an optical method which provides information about flow structures by measuring instantaneous velocity vectors over a certain flow field at the same time. Also, the procedure of capturing two images

by the PIV technique at a specified time interval is shown in Figure 3.4. Bright and coated silver particles which have 10 micron diameter are mixed with water for instantaneous flow data measurements. Although density of particles (1100 kg/m^3) is slightly higher than water density, they move at the same velocity with water to demonstrate particular movements of water flows. In the case of instantaneous velocity measurements since the distance between 2 pictures of the same particles in the flow field is known, instantaneous velocity vector is calculated with equation of $V = \frac{\Delta X}{\Delta t}$.

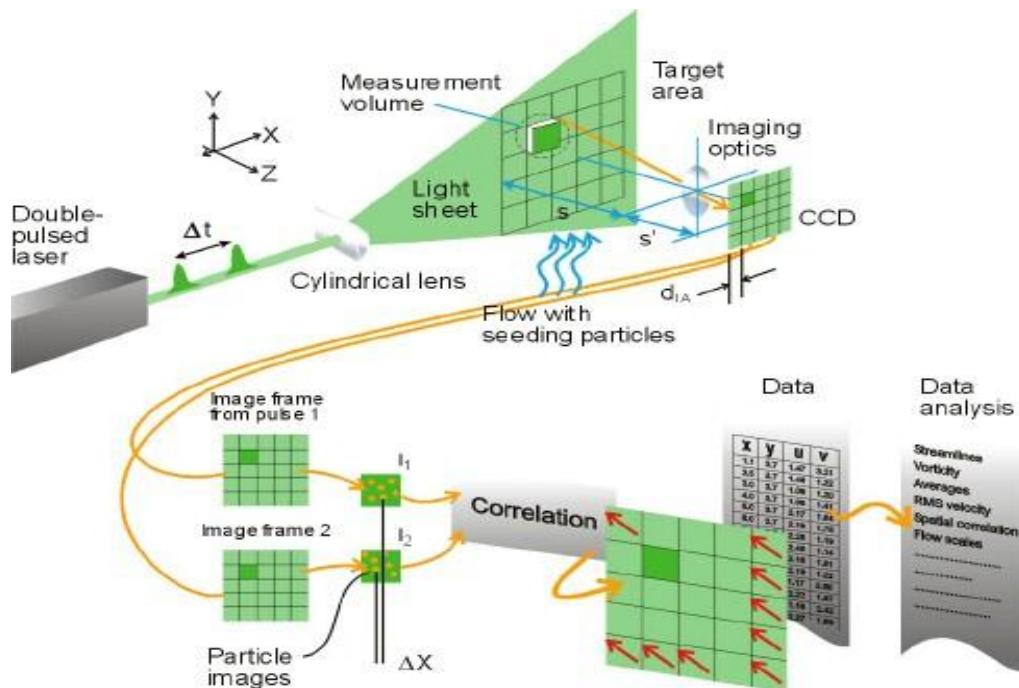


Figure 3.4. Measurement of PIV Principle (Dantec Dynamics, 2013)

Laser sheet which is created by double pulse laser source, Nd: YAG Laser (Neodymium-Doped Yttrium Aluminum Garnet) has a thickness of 1-2 mm with a width via optical devices. A double pulse laser source and camera must work simultaneously without time shift. Therefore, synchronizer controlled by a

computer unit exists on the PIV system. Laser source must provide a laser light to illuminate seeding particles in the test region.

CCD (Charged Couple Device) camera is used to capture images of observed flow field illuminated by a laser light. If the CCD camera works at a double frame mod, taking image 1 and image 2 which are used to determine instantaneous velocity vectors. According to instantaneous velocity, time averaged velocity vectors, patterns of streamlines, vorticity concentrations and turbulence statistics are calculated to provide physical characteristic flow structures.

Flow field or measuring plane is divided into partial areas and every area is called as “pixel”. Distribution of seeding particles is vitally important parameter to measure the instantaneous velocity results accurately. Otherwise, a nonhomogeneous distribution of seeding particles may cause higher errors in readings.

3.4. Experimental System of Dye Visualization

3.4.1. Dimensions of Delta Wing and Related Information

In the present work most part of the experiment were conducted using dye visualization to demonstrate flow structure qualitatively. The Delta wing is made of Plexiglas having cord, C length of 250 mm, and thickness of 6 mm, and sweep angle, Λ 70° for the experiments of dye visualizations as seen in Figure 3.5 schematically. The leading edges of delta wing had chamfer of 45°. Small holes were placed in close region of the apex on both sides of the central axis of wing to eject the Rodamine dye. The depth of water in water channel was kept as 53 cm and free-stream velocity is maintained as 80 mm/s. The Reynolds number was kept constant at a value of $Re=2.10^4$ based on the cord length of delta wing.

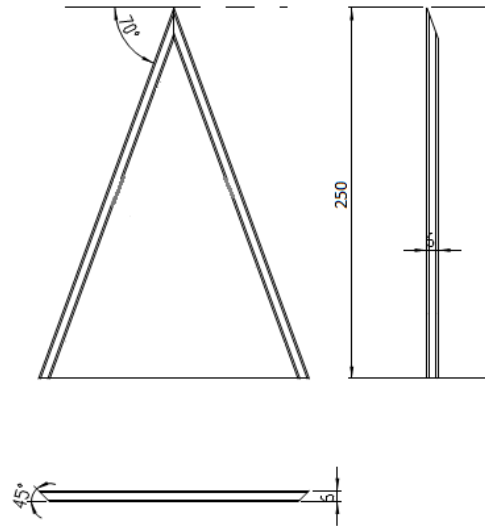


Figure 3.5. Dimensions of the delta wing

Dye experiments were carried out in side view plane as seen in Figure 3.6. Laser sheet was set by passing through the center of leading edge vortex and laser sheet is perpendicular to the plane of the delta wing. Flow structure was observed by ejecting Rhodamine 6G dye which was illuminated by laser sheet in the test region. A small size needle and plastic tube were used to eject dye. Images of hydrodynamic of flow structures were recorded with a SONY HD-SR1 video camera and Sony Play Memories Software was used to capture the picture of instantaneous flow data as shown in Figure 3.7.

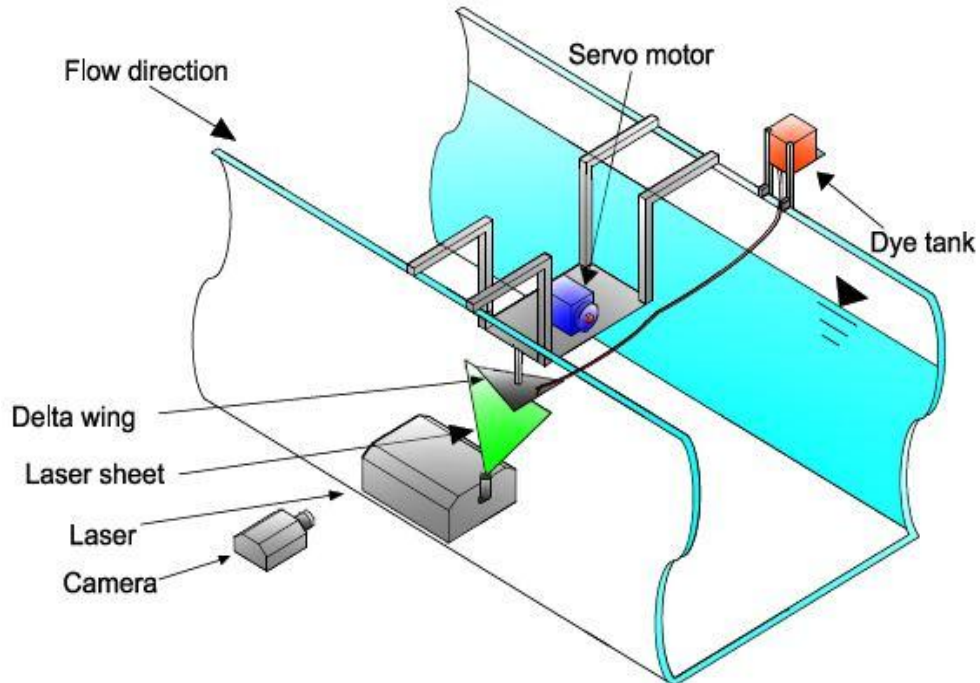


Figure 3.6. Schematic representation of water channel during dye experiment in side view plane

The delta wing was sinusoidally perturbed with the oscillation period, $T_e=2\pi/\omega_e$, of 5s, 20s, 40s and 60s and lastly amplitude of pitching, α_o was arranged in between ± 5 and $\pm 10^\circ$. Delta wing was oscillated according to the equation of $\alpha(t)=\alpha_m+\alpha_o\sin(\omega_e t)$ via servo motor during the experiment. Figure 3.8 shows pitch up, pitch down motion and location of laser sheet in side and plan-view planes schematically.

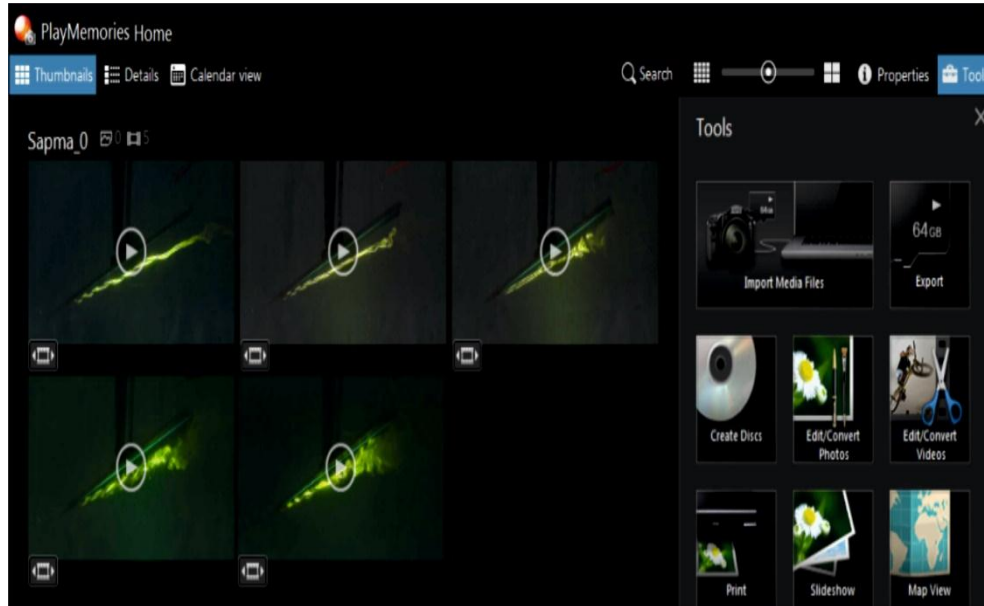


Figure 3.7. Print screen of Sony Play Memories Software

The values of mean angle of attack, α_m of the delta wing were taken as 25° , 30° and 35° . Yaw angle, β which was arranged manually by an angle operating apparatus considering the central axis of delta wing as a reference line which was 0° , 4° , 8° , 12° , and 16° . Figure 3.9 shows us yaw angle, β and its effect on the onset of vortex breakdown locations over five different plan-view planes of the delta wing.

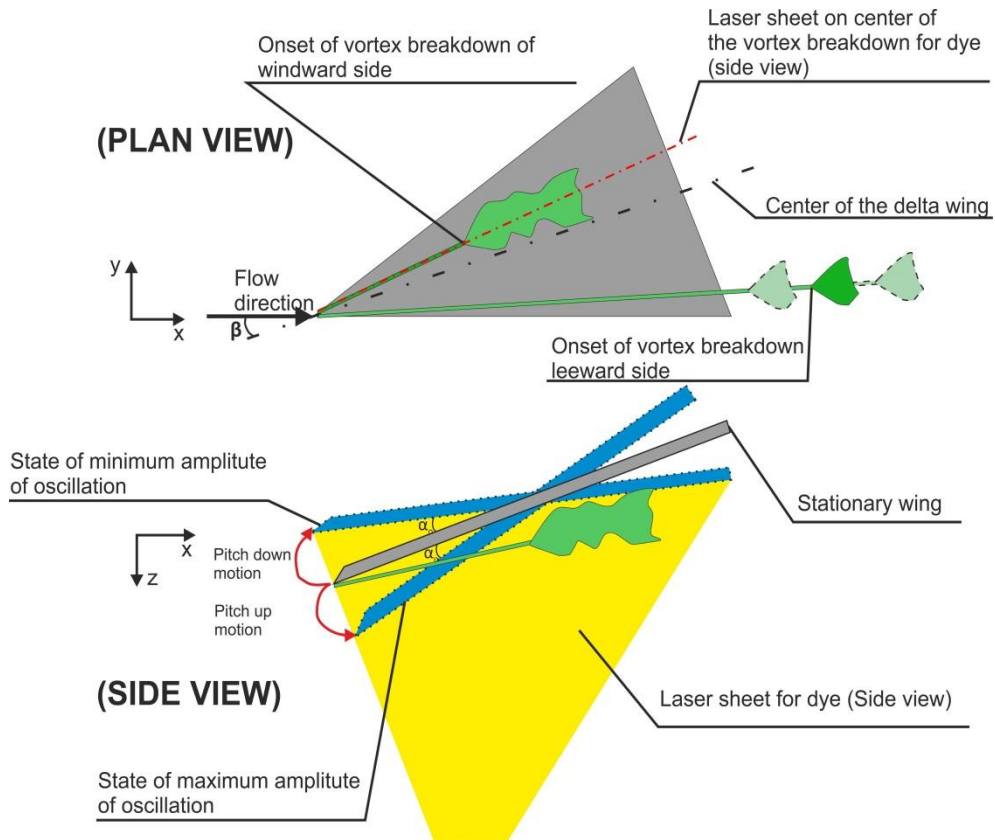


Figure 3.8. Schematic representation of pitching motion of the delta wing and experimental set up for dye experiment

All specified yaw angles, β , period of oscillations, T_e and amplitude of pitching, α_o were taken into account during the experiment for each mean angle of attack, α_m . Mean angle of attack, time period and amplitude of pitching were set by a servo motor and its control unit. Locations of vortex break down were investigated by a dye visualization technique. Lastly, obtained experimental results for static and dynamic cases of the delta wing were compared with each other.

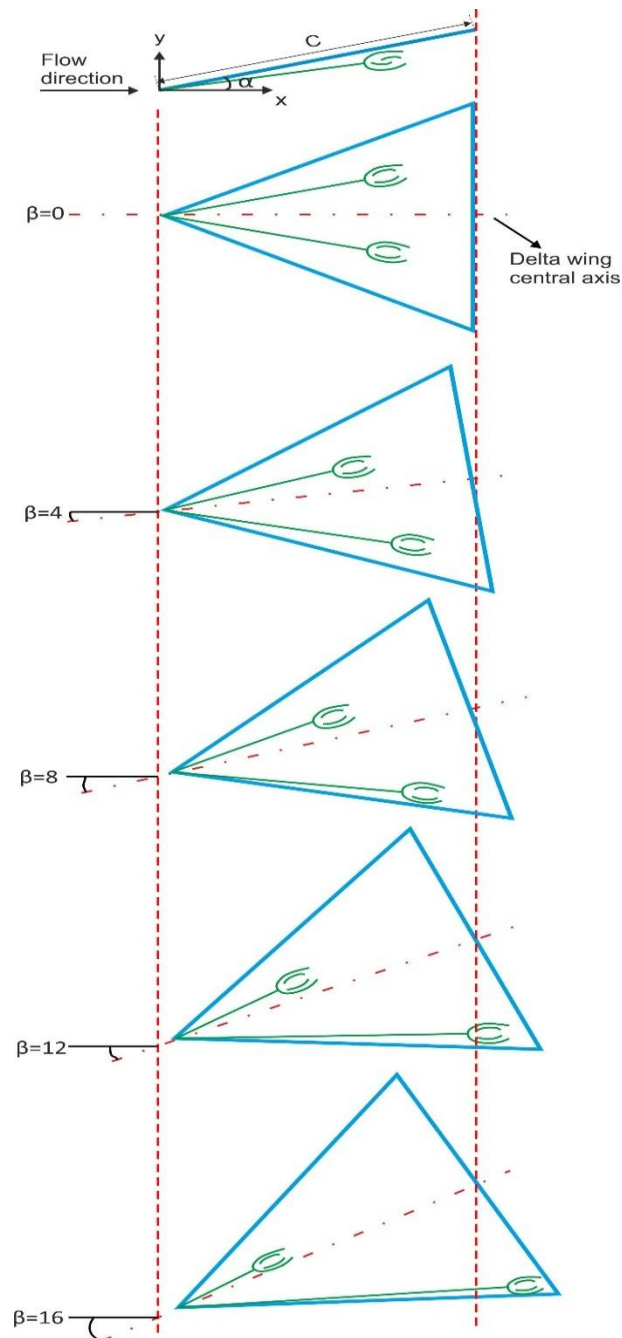


Figure 3.9. Schematic representation of varying yaw angle, $\beta=0^\circ, 4^\circ, 8^\circ, 12^\circ$ and 16° and changing location of vortex breakdown in side and plan view planes

4. RESULT AND DISCUSSION

4.1. Experimental Results of Pitching Delta Wing

4.1.1. Flow Control Techniques

Vortical flow on the delta wing causes a high rate of aerodynamic forces. There are many studies on vortex control to increase steady characteristic structure of the delta wing.

For example;

i.) Flow-momentum control. This is an active method to control vortex breakdown and flow characteristics with air blowing from the apex of delta wing or air suction from the trailing edge of delta wing.

ii.) There are also some vortex control techniques called passive control methods. For instance; alteration of the delta wing geometry, addition of flap on apex and tail, change of sweep angle and aspect ratio of delta wing.

In the present study, the aerodynamics of oscillating the delta wing is investigated to observe the location of vortex breakdown alterations and flow characteristics changes by employing the dye visualization technique. In dye visualization, it was demonstrated that the location of both vortex breakdowns move toward the wing apex during the upstroke pitching motion as observed by many other researchers. But the objective of the present study was to examine the effects of the pitching motion of delta wing under yaw angle, β . As it is known, detecting of vortex breakdown with instantaneous velocity vectors measured near the surface of the delta wing to determine flow characteristics needs special attention for a sensitive measurements. In additions, interactions between vortices as well delta wing which are formed after onset of vortex breakdown should be examined with special care.

4.2. Dye Experiments

4.2.1. Visual Observations of Vortical Flow Using Dye

The values of mean angles of attack, α_m was taken as 25° , 30° and 35° . The yaw angle, β was varied over the range of $0^\circ \leq \beta \leq 16^\circ$. The delta wing was sinusoidally pitched within the range of oscillation periods, $T_e = 2\pi/\omega_e$, of $5 \leq T_e \leq 60$ s and lastly amplitude of the pitching motion, α_o was arranged to be varied within the range of $\pm 5^\circ \leq \alpha_o \leq \pm 10^\circ$.

As it is known from the stationary delta wing, for the values of angles attack, $\alpha = 40^\circ$ and 45° , it is known that vortex breakdown starts from the apex of delta wing. As soon as the vortex breakdown occurs close to the apex of wing, the rate of flow unsteadiness dramatically increases. It was observed that dye completely covers the surface of wing, in the case of angle of attack, α , having 45° . It was seen that by pitching delta wing, flow structures on delta wing was noticeably dissimilar comparing to the static case of delta wing. When angle of attack, α is set up to 40° , oscillation of delta wing controls the flow characteristic. After a certain distance vortex breakdown occurs. When yaw angle, β is given to the delta wing, it is seen that flow characteristics in the pitching delta wing is more stable than in the case of stationary delta wing. Due to the non-symmetric vortex breakdowns on in each side of central cord axis of the delta wing, lateral forces and moment on the delta wing may be different (Lin, 1998).

4.2.2. Observation of Delta Wing Aerodynamics under Pitching Motion with High Rate of Amplitude and Oscillating Period Using Dye Visualization

In this part of experiment location of vortex breakdown was determined with the dye visualization technique. A distance between vortex breakdown position and apex of the delta wing was defined by the symbol X_{vb} . The chord length of delta wing was denoted by C . Vortex breakdown position was defined by a dimensionless number, X_{vb}/C .

It is understood that in dynamic cases, dynamic angle of attack, $\alpha(t)$ of the wing is calculated according to the equation of $\alpha(t)=\alpha_m+\alpha_o\sin(\omega_e t)$. Also, angle of attack, α of static delta wing in dye images is identified by adding values of amplitude of pitching motion, α_o and the mean angle of attack, α_m of the wing. As a result, static and dynamic cases are compared in the same angles of attack, α .

In dye visualization, the effect of yaw angle, β , period of oscillation, T_e , mean angle of attack, α_m , amplitude of the pitching motion, α_o and maximum-minimum positions of vortex breakdowns are clearly seen. Vortex breakdown locations with maximum and minimum lengths are defined as maximum-minimum distances which means that the location of vortex breakdown changes arbitrarily when delta wing is fixed at any angles of attack, α . These minimum and maximum lengths of pitching delta wing were also defined during the experiment. Figure 4.1 shows that vortex breakdown location in pitching delta wing motion for the maximum value of amplitude of the pitching motion, $\alpha_o=+5^\circ$ at a mean angle of attack, $\alpha_m=25^\circ$ does not proceed in accordance with pitching motion. Location of vortex breakdown moves towards the trailing edge of delta wing at the state of maximum dynamic angle of attack, $\alpha(t)=30^\circ$. On the other hand, dimensionless number, X_{vb}/C relatively increases in the case of pitching delta wing comparing to the stationary delta wing case. Onset of vortex break down occurs at about $X_{vb}=0,75C$ at a static delta wing case, for angle of attack of $\alpha=25^0+5^0=30^\circ$ and yaw angle of $\beta=0^\circ$ depending on the oscillation period, T_e .

The location of vortex breakdown moves towards downstream of trailing edge at $X_{vb} =1.1C$ at period of oscillation, $T_e=5$ s. On the contrary, enlarging the period of oscillation as $T_e=60$ s, variation of flow characteristics becomes similar to the static delta wing case for $\alpha_m=25^\circ$ and $\alpha_o=+5^\circ$. Application of 60 second oscillation period does not provide the delta wing to inforce fluid flow to restructure as a function of delta wing pitching motion.

It is clearly seen that onset of vortex breakdown moves towards apex of delta wing by providing yaw angle, β and increasing mean angle of attack, α_m from

25° to 30° and 35°, dimensionless number of cord length, X_{vb}/C regularly are decreased. Also, effect of oscillation period on the vortex breakdown location, X_{vb}/C is seen in figures. Thus, it is understood that varying yaw angle, β and period of oscillation, T_e effects the variation of vortex breakdown locations.

As seen in Figure 4.2, setting the mean angle of attack, α_m as 30° and yaw angle, β as 8°, onset of vortex breakdown appears at a location of $X_{vb}=0.2C$ for stationary delta wing case, on the other hand pitching the delta wing with a period of $T_e=5$ sec per cycle, flow separation starts at the middle of delta wing, $X_{vb}=0.55C$. But setting the oscillation period with $T_e=60$ s per cycle, location of vortex breakdown moves towards the apex of delta wing and hence onset of vortex breakdown occurs at a location of $X_{vb}=0.25C$. Because of decreasing angular velocity of oscillation, flow characteristics settle down gradually without having the effect of perturbing delta wing and hence vortical flow structures of perturbing delta wing having period of 60s become similar to the case of stationary delta wing.

As seen in Figure 4.3, for mean angle of $\alpha_m=35^\circ$ and yaw angle of $\beta=4^\circ$, the location of vortex breakdown take place at a location of $X_{vb}=0.18C$ for stationary delta wing, but this onset of vortex breakdown moves from mid-point towards the apex of delta wing, namely, from the location of $X_{vb}=0.4C$ to the location of 0.2C with the consequences of oscillation period upgrading from $T_e=5$ s to 60 s. Furthermore, there is time lag between movement of location of vortex breakdown and oscillation of wing during the pitching of delta wing cycle. This period of time lag gets shorter by increasing oscillation period, T_e . It is seen from experimental data that patterns of flow characteristics at $T_e=60$ s resemble closely with flow characteristics of the stationary delta wing case. Formation of vortex breakdown towards the wake region losses energy and also pressure decreases at the rare side of the delta wing.

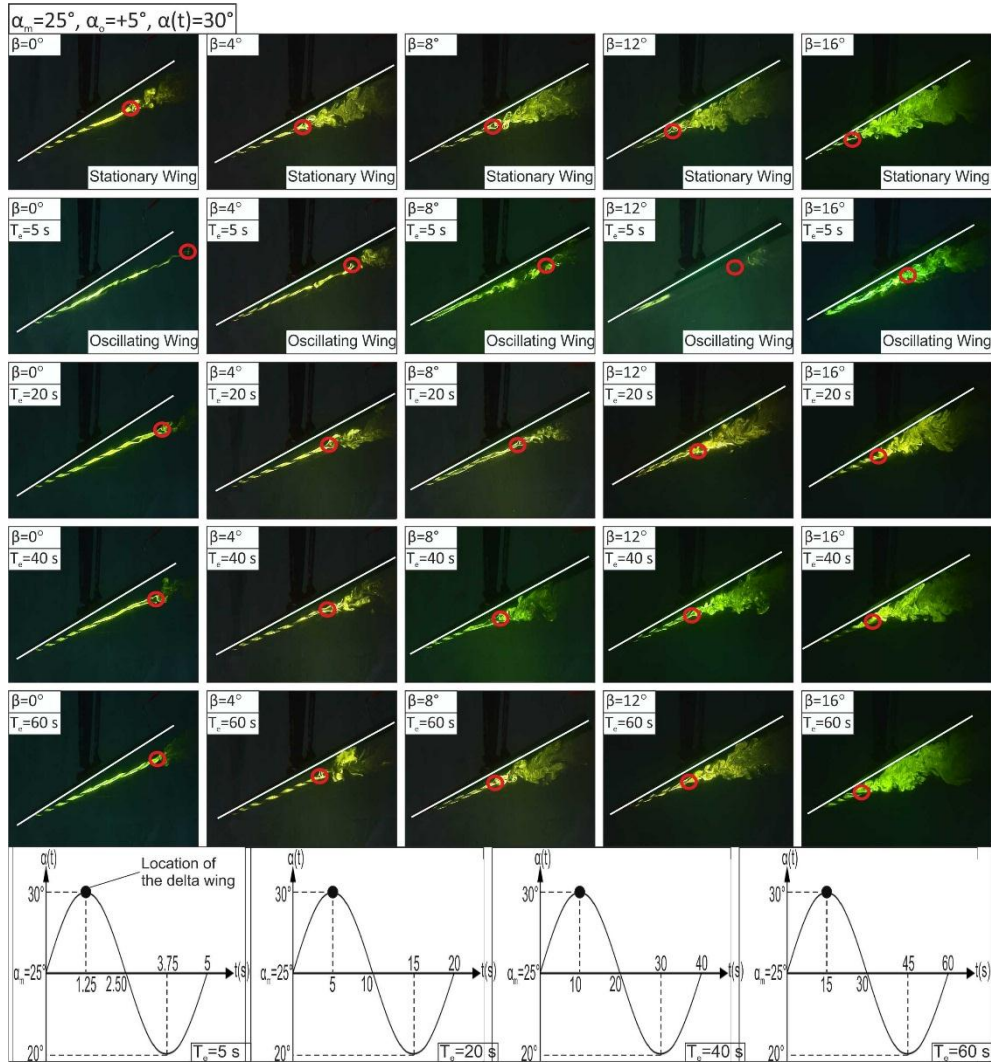


Figure 4.1. Formation of onset of vortex breakdown in the cases of stationary and oscillating delta wings under variation of yaw angle, β within the range of $0^\circ \leq \beta \leq 16^\circ$, period of oscillation, T_e ranging from 5s to 60s at mean angle of attack, α_m of 25° , amplitude of delta wing pitching motion, α_o of $+5^\circ$ (upstroke) and dynamic angles of attack, $\alpha(t)$ vary between 20° and 30° . All images are taken at angle of attack, $\alpha=30^\circ$

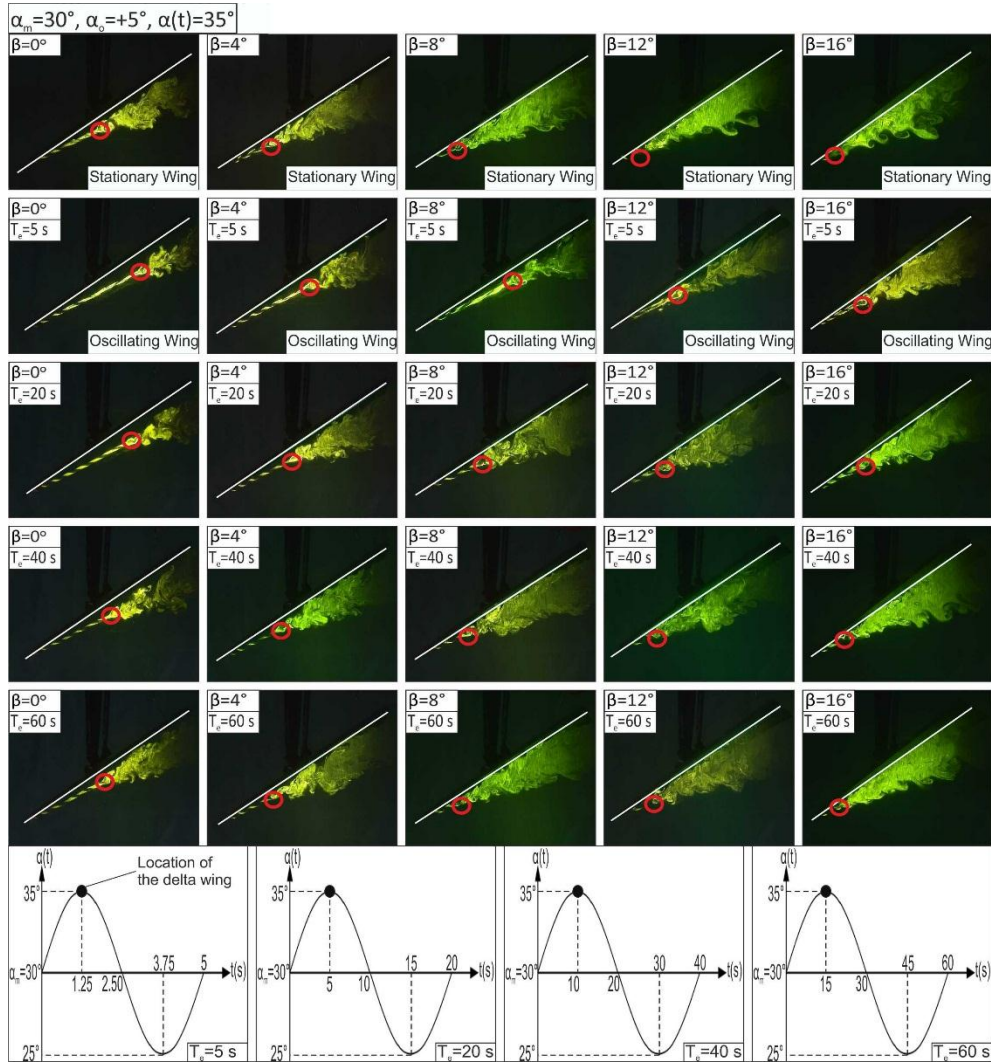


Figure 4.2. Formation of onset of vortex breakdown in the cases of stationary and oscillating delta wings under variation of yaw angle, β within the range of $0^\circ \leq \beta \leq 16^\circ$, period of oscillation, T_e ranging from 5s to 60s at mean angle of attack, α_m of 30° , amplitude of delta wing pitching motion, α_o of $+5^\circ$ (upstroke) and dynamic angles of attack, $\alpha(t)$ vary between 25° and 35° . All images are taken at angle of attack, $\alpha = 35^\circ$

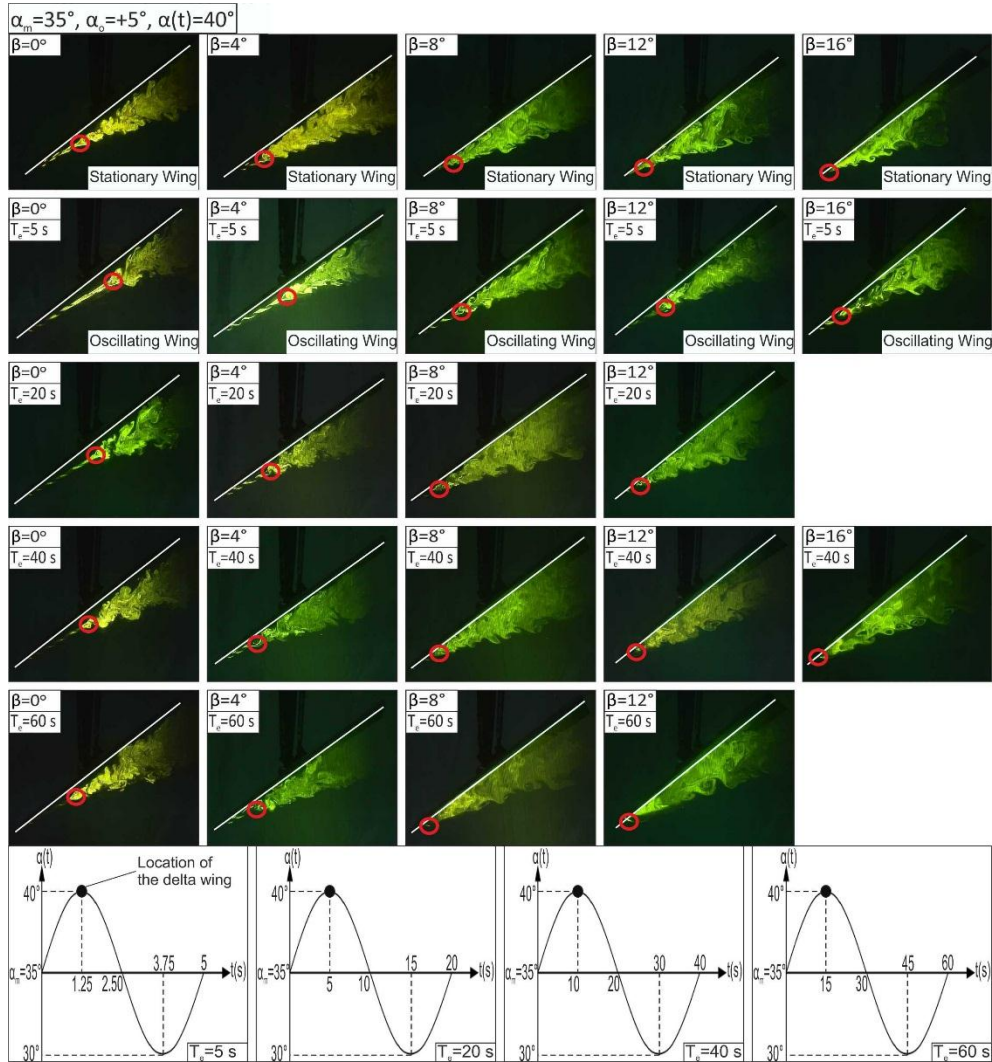


Figure 4.3. Formation of onset of vortex breakdown in the cases of stationary and oscillating delta wings under variation of yaw angle, β within the range of $0^\circ \leq \beta \leq 16^\circ$, period of oscillation, T_e ranging from 5s to 60s at mean angle of attack, α_m of 35° , amplitude of delta wing pitching motion, α_o of $+5^\circ$ (upstroke) and dynamic angles of attack, $\alpha(t)$ vary between 30° and 40° . All images are taken at angle of attack, $\alpha=40^\circ$

As specified in the above Figure 4.1, 4.2 and 4.3 location of vortex breakdown is shown for maximum value of amplitude of the pitching motion, $\alpha_o = +5^\circ$ or the end of the portion of cycle in which the angle of attack, α increases

which is stated as upstroke. In addition, it is seen that location of vortex breakdown, X_{vb}/C moves outside of the delta wing in minimum value of amplitude of the pitching motion, $\alpha_o = -5^\circ$ or the end of the portion of cycle in which the angle of attack, α decreases which is denoted as downstroke. To correctly compare stationary and dynamic cases of delta wing, the value of angle of attack, α for stationary delta wing cases in dye images is similar with the minimum value of dynamic angle of attack of pitching delta wing such as $\alpha(t) = 25^\circ - 5^\circ = 20^\circ$.

Figure 4.4 demonstrate the formations of onset of vortex breakdown in downstream region of trailing edge of stationary delta wing at angle of attack, α of 20° having yaw angles, β of 0° and 4° . But this onset of vortex breakdown is formed at a location of $X_{vb}/C = 1.0$ at yaw angle, β of 8° as seen in the first line of third images. Under yaw angle, β of 16° the location of this vortex breakdown moves towards mid-cord delta wing although angle of attack is quite small such as 25° on the windward side of the wing. As is mentioned before leeward side leading edge vortex does not break down over the surface of the suction side of delta wing. Namely, leading edge vortex of leeward side move further downstream in the core flow direction without bursting for the ranges of angles of attack, α and yaw angle, β considered in Figure 4.4.

Formation of onset of vortex breakdown in the cases of stationary and oscillating delta wings under variation of yaw angle, β within the range of $0^\circ \leq \beta \leq 16^\circ$, period of oscillation, T_e ranging from 5s to 60s at mean angle of attack, α_m of 25° , amplitude of delta wing pitching motion, α_o of $\pm 5^\circ$ are presented in Figures 4.3 and 4.4. Images of onset of vortex breakdown are presented for stationary delta wing for angle of attack, α of 25° under variation of yaw angle, β within the range of $0^\circ \leq \beta \leq 16^\circ$. But the rest of images presented in Figure 4.4 are visualized at a dynamic angle of attack, $\alpha(t)$ of 20° for periods of oscillation, T_e ranging from 5s to 60s. Images for oscillating delta wing at a dynamic angle of attack, $\alpha(t)$ of 20° (down-stroke) shown in the first column of Figure 4.4 indicate that excluding the results of zero yaw angle, β and 5s period onset of vortex

breakdown occurs over the surface of delta wing for $4^\circ \leq \beta \leq 16^\circ$ and $20s \leq T_e \leq 60s$. Examining all images for pitching delta wing reveals that the time lag between angles of attack, α of delta wing and onset of vortex breakdown is higher. But this period of phase shift get smaller for a high time period, for example for the case of 60s time period, the time lag between angles of attack, α of delta wing and onset of vortex breakdown becomes zero. This conclusion is derived from the comparisons of images presented in the first and last line of Figure 4.4.

Considering mean angle of attack, α_m and amplitude of the pitching motion, α_o for dynamic case vortex breakdown location moved away from the rear of the delta wing to the location of $X_{vb}=1.2C$. As dye experiments demonstrate in the cases of amplitude of the pitching motion, $\alpha_o=+5^\circ$ (upstroke) and $\alpha_o=-5^\circ$ (down stroke), it was determined that effect of yaw angle, β in the case of low period of oscillation, T_e in the motion of pitching delta wing in down stroke direction. Figures 4.4-5-6 show that the lower period of oscillation, T_e causes a high rate of phase differences. These flow behaviors also occur for mean angles of attack, α_m having $\alpha_m=30^\circ$ and 35° . But the level of phase shift gets smaller for a higher time period, T_e for example, in the case of 60s time period, the time lag between angles of attack, α of delta wing and onset of vortex breakdown becomes zero for $\alpha_m=25^\circ$, 30° and 35° .

Figures 4.7-12 demonstrate the results of dye visualization experiments for the value of amplitude of the pitching delta wing, such as $\alpha_o=\pm 10^\circ$. In general, these figures provide partially similar evidences that are optioned in the case of $\alpha_o=\pm 5^\circ$ for a smaller period of oscillation, T_e . Increasing angle of attack, α while delta wing pitches in upstroke direction, namely, at $\alpha=+25^\circ+10^\circ=35^\circ$ onset of vortex breakdown moves toward the leading edge of the delta wing. In other words, the region of flow separation expands in size towards the wing apex. Similarly, when the pitching motion of delta wing is in downstroke, say, at a value of $\alpha_o=-10^\circ$, the location of vortex breakdown moves further downstream from back side of the delta wing according to value of $\alpha_o=-5^\circ$. This is due to the angular

speed of the delta wing at a state of amplitude of the pitching motion, $\alpha_0 = \pm 10^\circ$ is higher than the state of $\alpha_0 = \pm 5^\circ$. To develop an appropriate and effective flow control technique, it is substantially important to comprehend unsteady flow phenomena, especially from a fundamental fluid dynamics aspect. Vortex breakdown control still attracts attentions of engineers since onset of vortex breakdown have a significant influence on the aerodynamics of delta wing. Sahin et al. (2001) pointed out that a considerable delay or delay of the onset of vortex breakdown results in attaining a growth of a large-scale concentration of vorticity when the impingement plate leading edge located downstream of vortex breakdown region is oscillated in accordance with at a frequency of vortex breakdown. Figures presenting the dye observations present locations of non-dimensional onset of vortex breakdown as a function of angles of attack, α under a pitching delta wing along with static delta wing data measured over the same range free-stream velocity, U_∞ and angles of attack, α . When the delta wing is subjected to a pitching motion with a sensible high reduced frequency, K a phase shift occurs between the delta wing motion and the onset of vortex breakdown. But, perturbing the delta wing with high period of time, T_e , for example, $T_e = 60s$ the position of vortex breakdown moves continuously with the motion of delta wing having same locations with the fixed delta wing case. It is worth to mention that the value of mean angle of attack, α_m is also a key parameter for the delta wing under pitching motions. That is to say, the period of time, T_e may be increased to avoid the phase shift between locations of vortex breakdown comparing to the case of stationary delta wing.

In figures, for some angle of attack, α and yaw angle, β locations of vortex breakdown cannot appear below the delta wing during upstroke or downstroke delta wing motions. In some images there were experimental difficulties to record the location of vortex breakdown using the dye visualization technique.

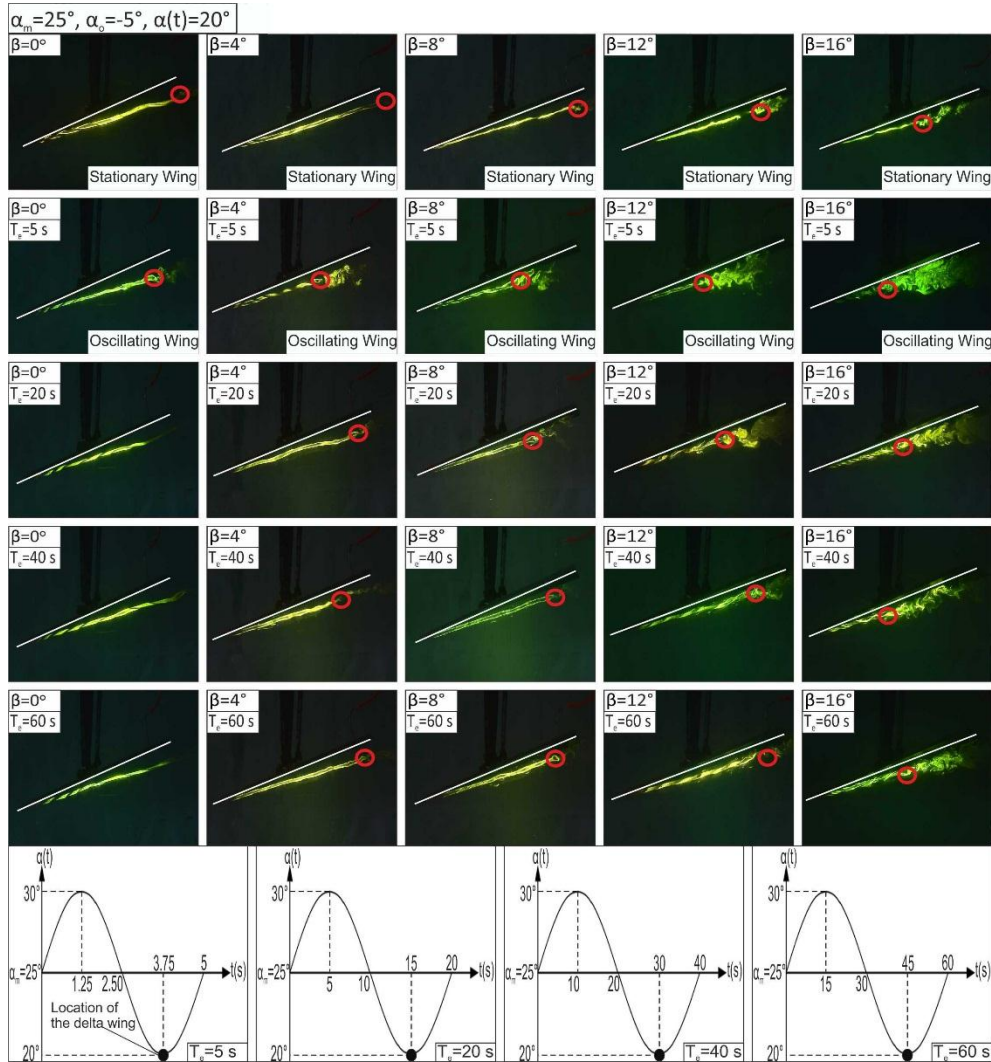


Figure 4.4. Formation of onset of vortex breakdown in the cases of stationary and oscillating delta wings under variation of yaw angle, β within the range of $0^\circ \leq \beta \leq 16^\circ$, period of oscillation, T_e ranging from 5s to 60s at mean angle of attack, α_m of 25° , amplitude of delta wing pitching motion, α_o of -5° (downstroke) and dynamic angles of attack, $\alpha(t)$ vary between 20° and 30° . All images are taken at angle of attack, $\alpha=20^\circ$

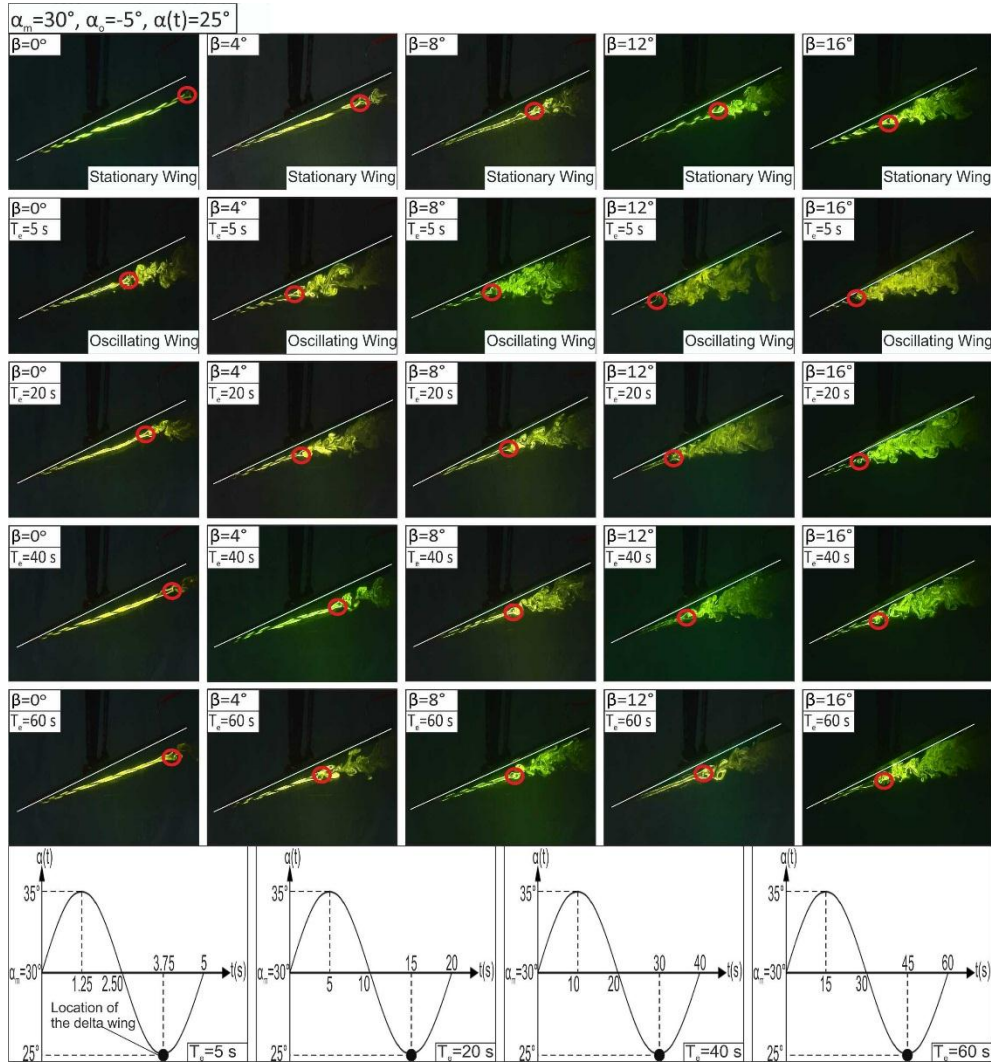


Figure 4.5. Formation of onset of vortex breakdown in the cases of stationary and oscillating delta wings under variation of yaw angle, β within the range of $0^\circ \leq \beta \leq 16^\circ$, period of oscillation, T_e ranging from 5s to 60s at mean angle of attack, α_m of 30° , amplitude of delta wing pitching motion, α_o of -5° (downstroke) and dynamic angles of attack, $\alpha(t)$ vary between 25° and 35° . All images are taken at angle of attack, $\alpha = 25^\circ$

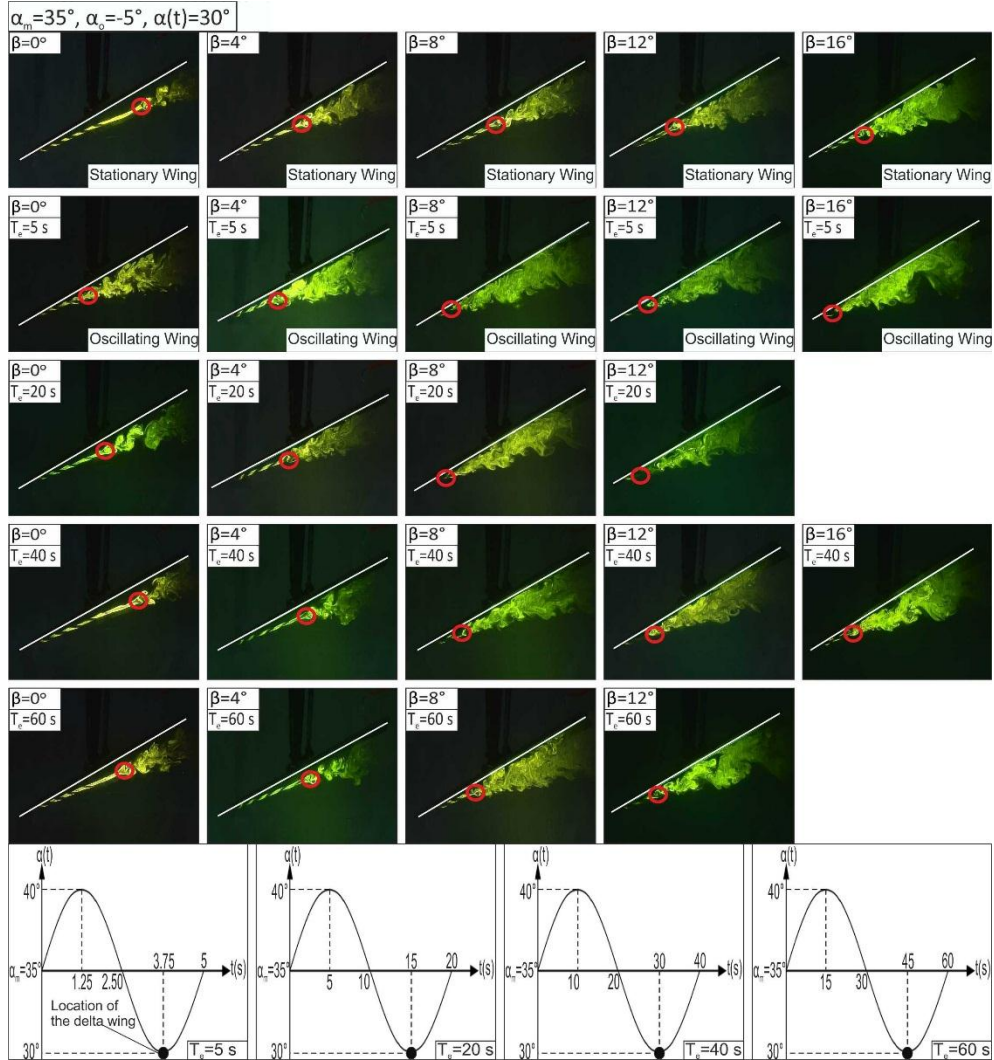


Figure 4.6. Formation of onset of vortex breakdown in the cases of stationary and oscillating delta wings under variation of yaw angle, β within the range of $0^\circ \leq \beta \leq 16^\circ$, period of oscillation, T_e ranging from 5s to 60s at mean angle of attack, α_m of 35° , amplitude of delta wing pitching motion, α_o of -5° (downstroke) and dynamic angles of attack, $\alpha(t)$ vary between 30° and 40° . All images are taken at angle of attack, $\alpha=30^\circ$

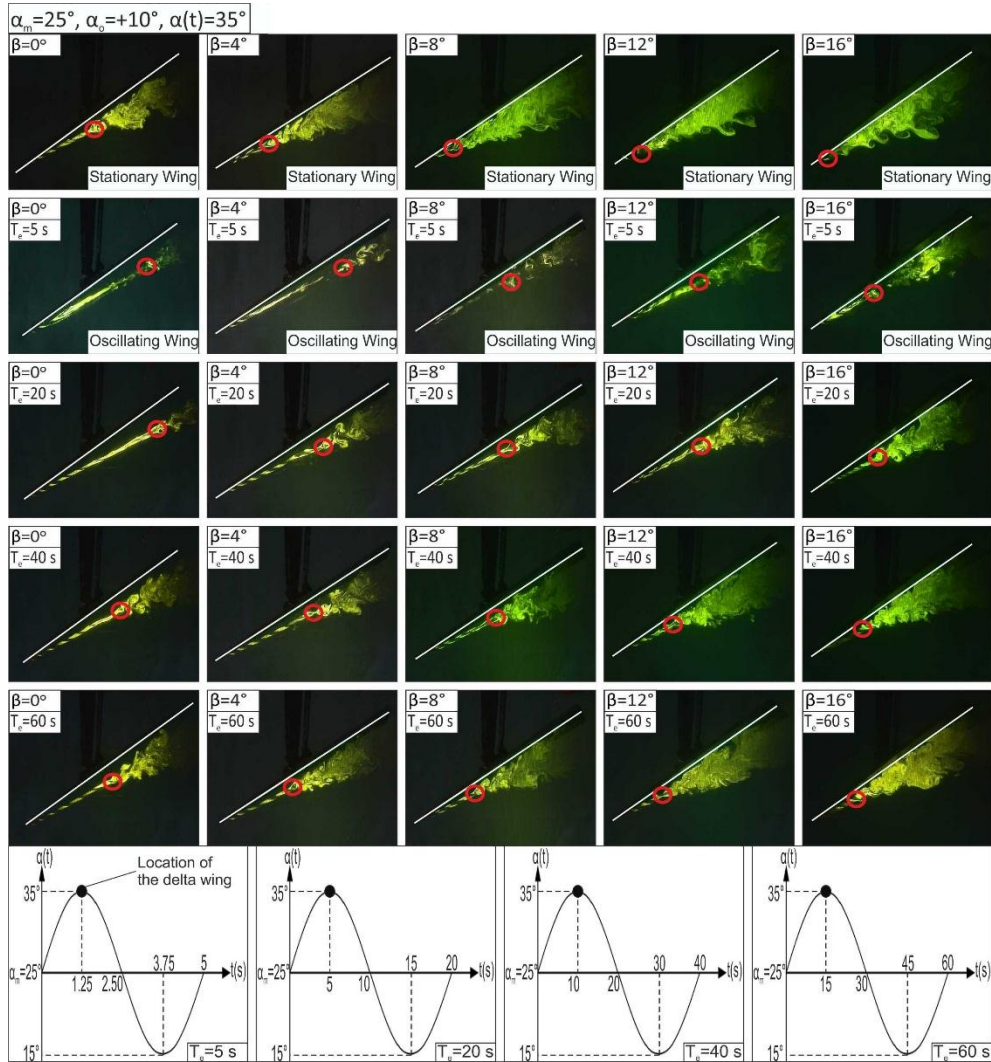


Figure 4.7. Formation of onset of vortex breakdown in the cases of stationary and oscillating delta wings under variation of yaw angle, β within the range of $0^\circ \leq \beta \leq 16^\circ$, period of oscillation, T_e ranging from 5s to 60s at mean angle of attack, α_m of 25° , amplitude of delta wing pitching motion, α_o of $+10^\circ$ (upstroke) and dynamic angles of attack, $\alpha(t)$ vary between 15° and 35° . All images are taken at angle of attack, $\alpha = 35^\circ$

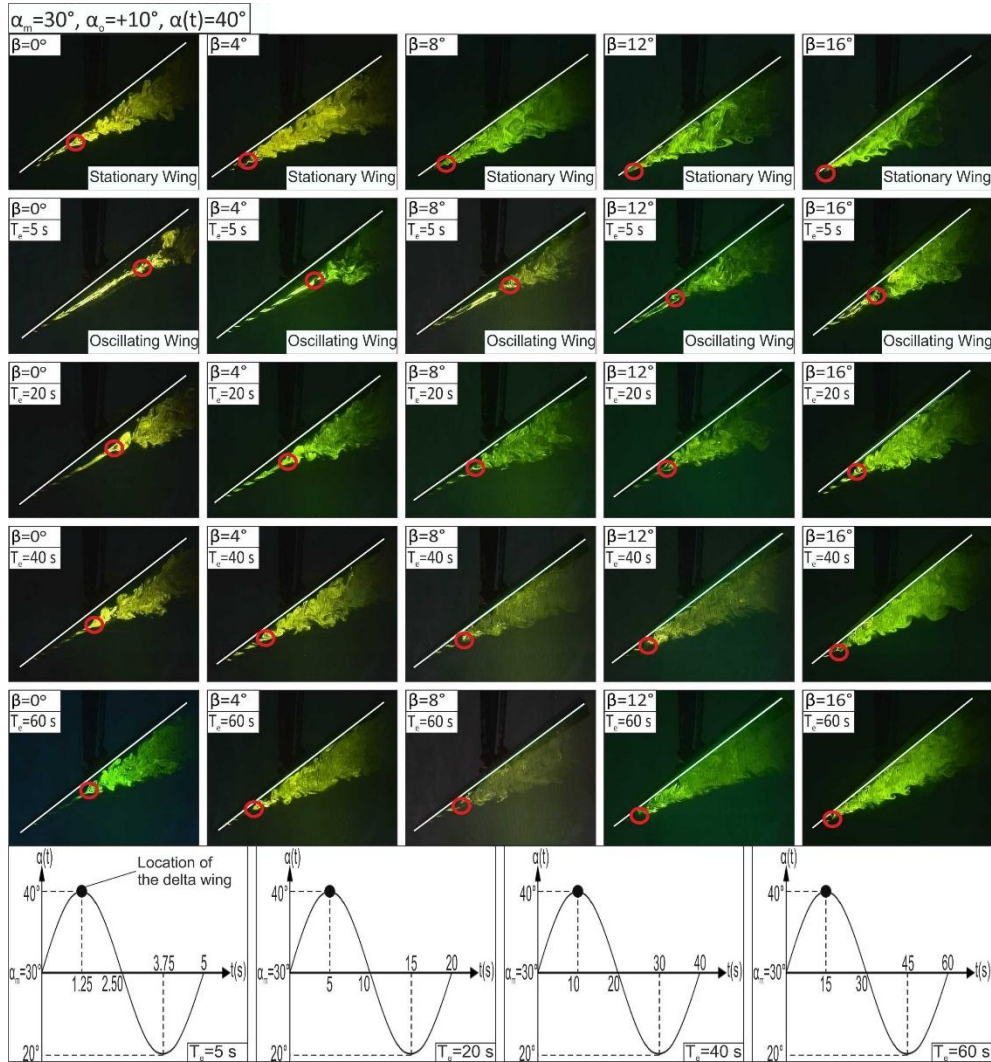


Figure 4.8. Formation of onset of vortex breakdown in the cases of stationary and oscillating delta wings under variation of yaw angle, β within the range of $0^\circ \leq \beta \leq 16^\circ$, period of oscillation, T_e ranging from 5s to 60s at mean angle of attack, α_m of 30° , amplitude of delta wing pitching motion, α_o of $+10^\circ$ (upstroke) and dynamic angles of attack, $\alpha(t)$ vary between 20° and 40° . All images are taken at angle of attack, $\alpha=40^\circ$

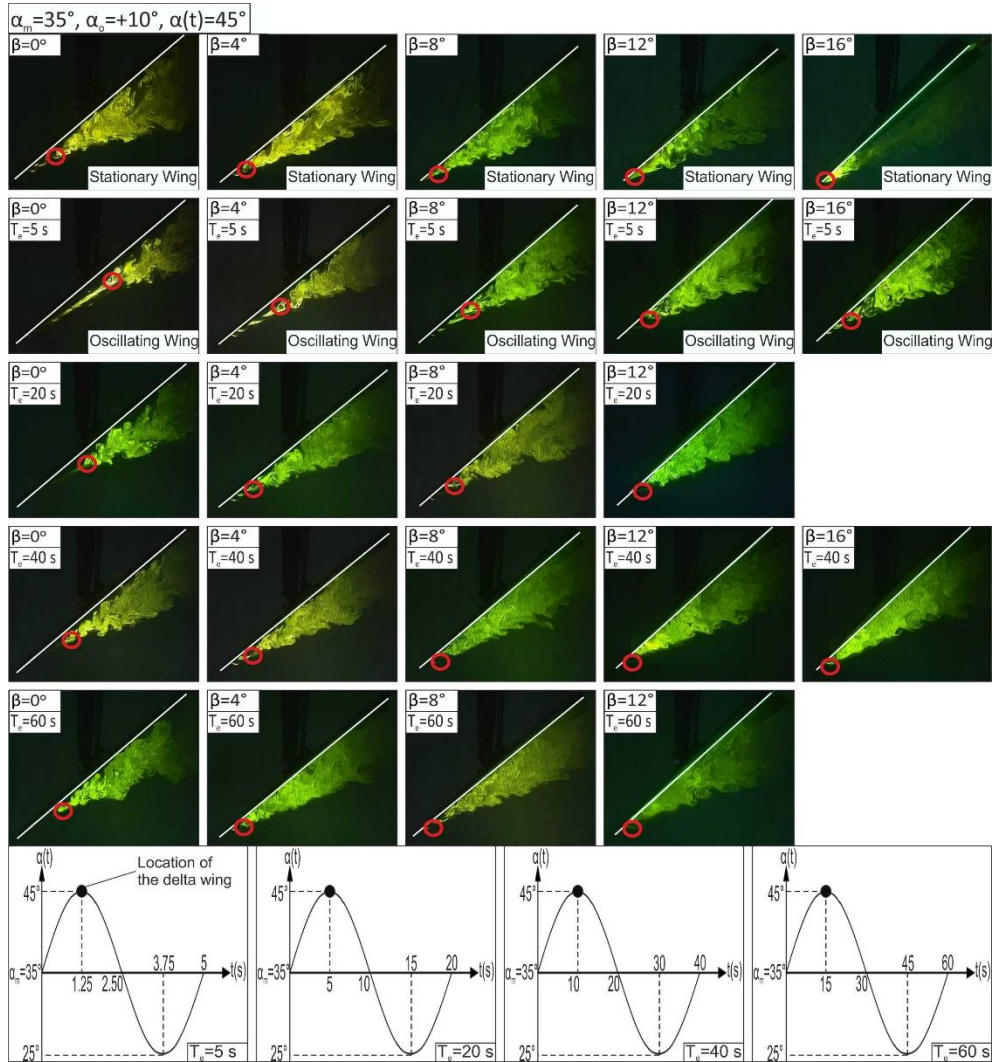


Figure 4.9. Formation of onset of vortex breakdown in the cases of stationary and oscillating delta wings under variation of yaw angle, β within the range of $0^\circ \leq \beta \leq 16^\circ$, period of oscillation, T_e ranging from 5s to 60s at mean angle of attack, α_m of 35° , amplitude of delta wing pitching motion, α_o of $+10^\circ$ (upstroke) and dynamic angles of attack, $\alpha(t)$ vary between 25° and 45° . All images are taken at angle of attack, $\alpha=45^\circ$

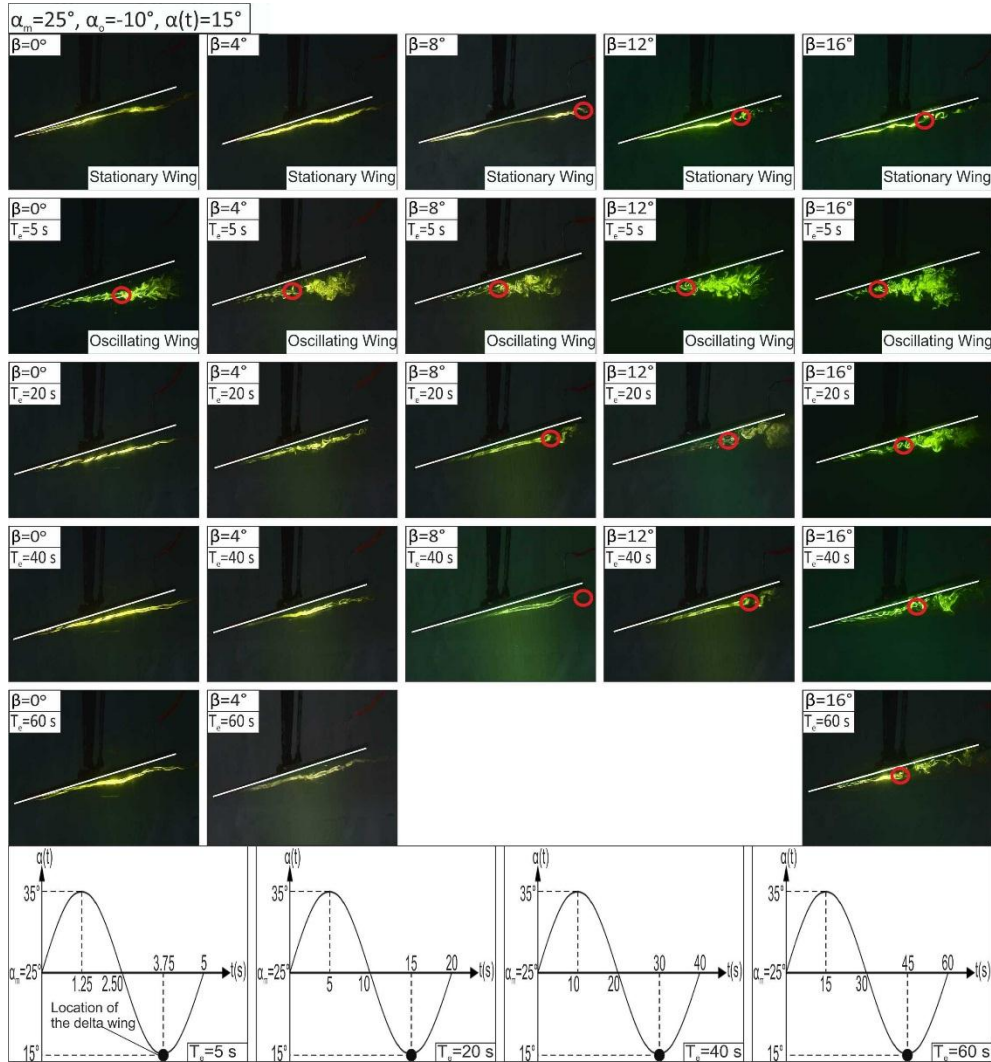


Figure 4.10. Formation of onset of vortex breakdown in the cases of stationary and oscillating delta wings under variation of yaw angle, β within the range of $0^\circ \leq \beta \leq 16^\circ$, period of oscillation, T_e ranging from 5s to 60s at mean angle of attack, α_m of 25° , amplitude of delta wing pitching motion, α_o of -10° (downstroke) and dynamic angles of attack, $\alpha(t)$ vary between 15° and 35° . All images are taken at angle of attack, $\alpha = 15^\circ$

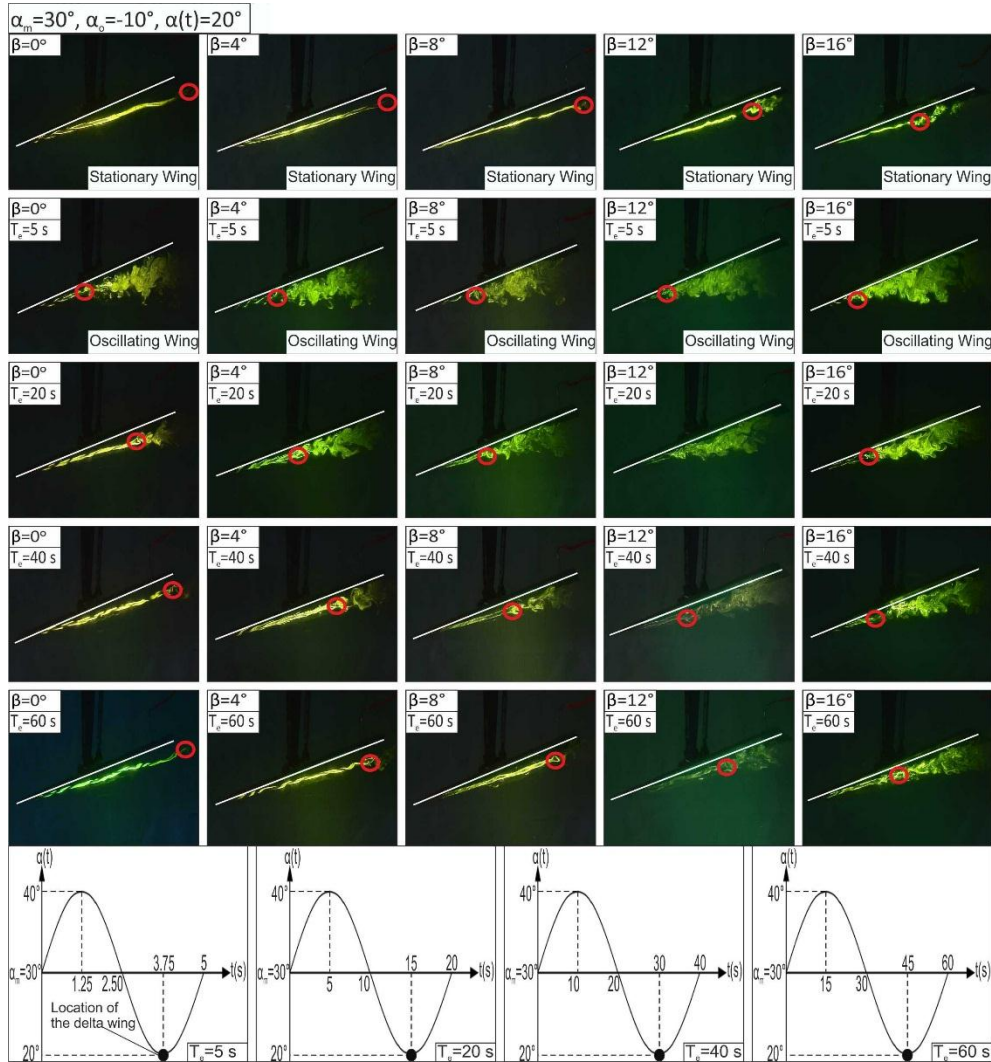


Figure 4.11. Formation of onset of vortex breakdown in the cases of stationary and oscillating delta wings under variation of yaw angle, β within the range of $0^\circ \leq \beta \leq 16^\circ$, period of oscillation, T_e ranging from 5s to 60s at mean angle of attack, α_m of 30° , amplitude of delta wing pitching motion, α_o of -10° (downstroke) and dynamic angles of attack, $\alpha(t)$ vary between 20° and 40° . All images are taken at angle of attack, $\alpha=20^\circ$

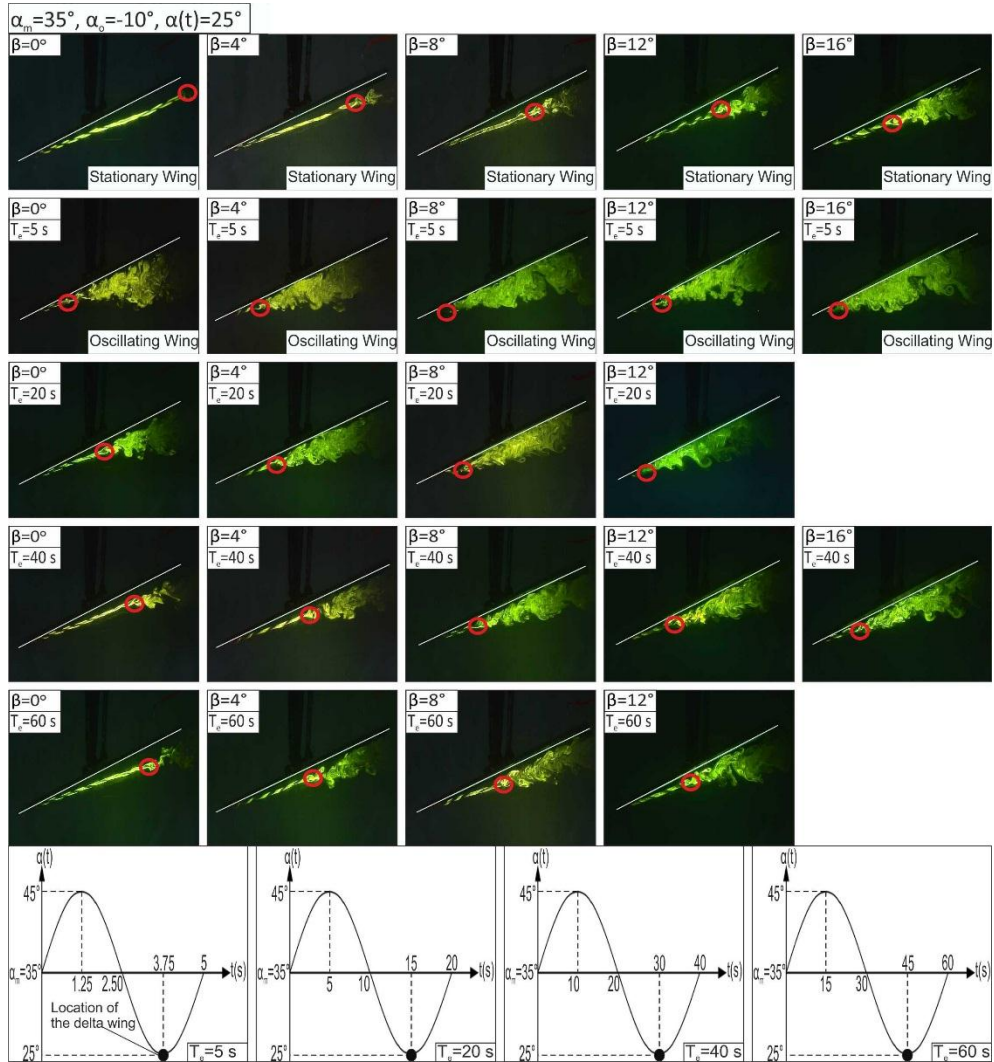


Figure 4.12. Formation of onset of vortex breakdown in the cases of stationary and oscillating delta wings under variation of yaw angle, β within the range of $0^\circ \leq \beta \leq 16^\circ$, period of oscillation, T_e ranging from 5s to 60s at mean angle of attack, α_m of 35° , amplitude of delta wing pitching motion, α_o of -10° (downstroke) and dynamic angles of attack, $\alpha(t)$ vary between 25° and 45° . All images are taken at angle of attack, $\alpha = 25^\circ$

4.2.3. Vortex Breakdown Hysteresis of Delta Wing

Aside from the dye pictures of pitching delta wing, it is shown that location of vortex breakdown, X_{vb}/C , changes as a function of angle of attack, α . The objective of this study was to determine the movement of the locations of vortex breakdown, X_{vb}/C , over a full period. For this purpose, consecutive locations of vortex breakdown are added in succession so the change of dynamic angle of attack, $\alpha(t)$, and movement of oscillation can be shown in the cyclic charts.

Figures presented in this section provide a graphical representation of how the location of vortex breakdown differs not only between the downstroke and upstroke of a given motion, but also how it diverts from the results of fixed delta wing for three different mean angle of attack values, α_m .

A study of the dynamic behavior of the leading edge vortices on a slender delta wing undergoing oscillatory pitching motion with a reduced frequency, K ranging from $K = 0.16$ to 1.96 was presented in the present work. An unsteady model of a vortex system was developed to simulate the phenomena of aerodynamic hysteresis of sinusoidally perturbed delta wings.

The detachment of the boundary layer on the wing surface considerably bounded up with the period of oscillation, T_e or the reduced frequency, K and direction of the pitching motion either upstroke or downstroke. In the present case as the wing pitches up, the detachment of boundary layer causing flow separation on the delta wing surface is suppressed because angles of attack, α gets smaller. On the other hand, as the wing pitches down, the detachment of boundary layer causing flow separation on the delta wing surface is facilitated, because, angle of attack, α gets higher. In both cases, there are phase shifts depending of oscillating period, T_e or the level of reduced frequency, K . In summary, Ozgoren and Sahin (2002) reported that the time delay that occurs in the flow field strongly depends on the dimensionless reduced frequency, K compared with the case of stationary delta wing. In the experiment of Ozgoren and Sahin (2002) inconsistency between the

results of static and dynamic (pitching) delta wing cases is considerably high because of the high-reduced frequency K . They have had a delta wing experiencing cyclic motions, with $K=0.74$.

In the present, a hysteresis of the location of vortex breakdown flow with high rate of discrepancy relative to the stationary condition is developed similar to the work of Ozgoren and Sahin (2002). During the experiment of static delta wing with certain angles of attack, α a large amount of time was given to allow the flow structures to attain the equilibrium state. Red solid lines in all figures present the results of stationary delta wing as a function of angle of attack, α and blue solid line present the results of pitching delta wing based on mean angles of attack, α_m and dynamic angle of attack, $\alpha(t)$.

Also from the charts of hysteresis, it can be seen that there are time delays. For example, minimum and maximum distances, X_{vb}/C between the apex of delta wing and locations of vortex breakdown, correspond the amplitude is minimum and maximum for stationary wings. However, since the wing is in motion, vortex breakdowns occur at an angle between maximum and minimum dynamic angles of attack, $\alpha(t)$. Hysteresis presented in Figures 4.13 and 4.42 demonstrate the record of locations of vortex breakdown, X_{vb}/C , during pitching motion of delta wing in a closed loop. When the delta wing under perturbation with a high amplitude, α_m and time period, T_e a time delay takes place between the position of delta wing and locations of onset of vortex breakdown comparing to the stationary delta wing. During this pitching of delta wing dynamics of angles of attack changes from a higher angles of attack, α and lower angles of attack, α . In both extreme cases there is leading edge vortex bursting with time delay. If we think of this unstable effect as an advantage, high performance aircraft can make certain maneuvers faster and more efficiently (LeMay et al., 1990). Aerodynamic hysteresis mechanism of the sinusoidal pitching delta wing is also observed. The unstable model of the vortex system is developed to describe the phenomenon of the aerodynamic hysteresis in the case of sinusoidal pitching delta wing. Huang et al. (1994), have shown that the

split of the flow on the surface of the wing is related to dimensionless reduced frequency, K and the direction of the wing oscillation.

In this study, the pitching movement of delta wing is shown for the dimensionless reduced frequency, K from the geometrical center of the delta wing, $K=0.16, 0.25, 0.49, 1.96$ and $\alpha_o=\pm 5^\circ$ between the range of dynamic angles of attack, $\alpha(t) = (20^\circ-30^\circ), (25^\circ-35^\circ)$ and $(30^\circ-40^\circ)$. The reason for the inconsistency between the constant and oscillating hysteresis is the high dimensionless reduced frequency, K . As it is shown in Figure 4.13, when the mean angle of attack is, $\alpha_m=25^\circ$, amplitude of pitching motion is, $\alpha_o=\pm 5^\circ$ and yaw angle is, $\beta=0^\circ$, at the period of oscillation, $T_e = 5s$, there is a discrepancy between static and oscillating wing cases caused by the dimensionless reduced frequency, K . When period of oscillation, T_e , increases so the dimensionless reduced frequency, K , decreases, the large discrepancies between the locations of vortex breakdown, X_{vb}/C and dynamics angle of attack, $\alpha(t)$ disappear. Perturbing the delta wing for period of $T_e = 5s$ onset of vortex breakdown happens at a location of $X_{vb}/C=1.05$ for the dynamic angle of attack, $\alpha(t)=30^\circ$, on the other hand for the same angle of attack, α the onset of vortex breakdown take place at a location of $X_{vb}/C=0.75$ for stationary delta wing. When the period of time, T_e is taken as 60s and the dynamic angle of attack, $\alpha(t)$ is set to a value of 30° for the oscillating state, vortex breakdown occurs at $X_{vb}/C = 0.8$. In summary, the location of leading edge vortex breakdown of delta wing gets closer to the tip of the wing as angle of attack, α , increases. So the minimum value of X_{vb}/C , should take place at the maximum angle of attack, α . However during the pitching motion of delta wing at $T_e= 5s$, this situation didn't occur at maximum amplitude of pitching motion, $\alpha(t)=30^\circ$. The difference is because of the time delay. The minimum dimensionless length of X_{vb}/C can be seen at a dynamic attack angle of $\alpha(t)=20^\circ$. At $T_e=60s$, the minimum dimensionless length of X_{vb}/C occurs at the dynamic angle of attack of $\alpha(t)=27^\circ$. However, we can conclude that the time delay decreases as the period of oscillation, T_e increases.

In a similar way if we examine Figure 4.20, when the mean angle of attack is, $\alpha_m = 30^\circ$, amplitude of the pitching motions of delta wing is $\alpha_o = \pm 5^\circ$ and yaw angle is, $\beta = 8^\circ$, at the period of oscillation, $T_e = 5s$ with the dynamic angle of attack, $\alpha(t) = 35^\circ$ for the static delta wing case, the length of dimensionless X_{vb}/C is 0.22, but in the case of the oscillating delta wing the value of X_{vb}/C is 0.5 under similar conditions of pitching delta wing. When the period time, T_e is taken as 60s having dynamic angle of attack as $\alpha(t) = 35^\circ$ the value of dimensionless length of X_{vb}/C is 0.25 for the oscillating delta wing case. In additions, if we examine other cases of delta wing, for example, the time delay of occurrence of vortex breakdown, at a period of $T_e = 5s$, during the pitching motion of delta wing, the minimum dimensionless length of X_{vb}/C does not occur at the maximum amplitude, α_a . However, the minimum X_{vb}/C can be seen at a dynamic angle of $\alpha(t) = 25^\circ$. On the other hand, when the period of oscillation, T_e is expanded to a value of 60s, the minimum dimensionless length of X_{vb}/C occurs at the dynamic angle of $\alpha(t) = 33^\circ$.

If we analyze experimental results presented in Figure 4.27 we can see more or less similar time delay that happens in the other case examined above. For example, when the mean angle of attack, α_m is to a value of 35° , amplitude of the pitching motion, α_o is set to a value of $\pm 5^\circ$ and setting yaw angle, β as 16° , at the period of oscillation, $T_e = 5s$ with the dynamic angle of attack, $\alpha(t) = 40^\circ$, for the constant state of delta wing, the dimensionless of delta wing is taken as $X_{vb}/C = 0.03$, but, having identical conditions for the oscillating state of delta wing the dimensionless of delta wing is taken as X_{vb}/C is 0.28. When expanding the period oscillating, T_e to a value of 40s with the dynamic angle of attack, $\alpha(t) = 40^\circ$, for the of oscillating state of delta wing, the dimensionless of delta wing, X_{vb}/C increases to a value of 0.06. Furthermore, the time delay of occurrence of vortex breakdown in the oscillating and stationary delta wing case are needed to be examined. For instance, taking the period of oscillating delta wing T_e as 5s, during pitching motion of the delta wing, the minimum dimensionless length of X_{vb}/C does not

occur at a maximum dynamic angle of the delta wing such as $\alpha(t)=40^\circ$. But the minimum value of $X_{vb}/C = 0.19$, can be seen at the dynamic angle of $\alpha(t)=32^\circ$. In additions, at $T_e=40s$ the minimum length of X_{vb}/C is 0.03, for the dynamic angle of attack of $\alpha(t)=37^\circ$. As a result, the effect of the dimensionless reduced frequency, $K=\pi f_e C/U_{ref}$ is proven and it is shown that the effect of the time delay is related to the period of oscillation, T_e .

The hysteresis charts presented in Figures 4.28- 4.42, are constructed with the amplitude of the pitching motion of delta wing such as $\alpha_o=\pm 10^\circ$. An increase of the amplitude of the pitching motion delta wing, α_o , alters the locations of vortex breakdown. If the amplitude of the pitching motion of the delta wing is set at $\alpha_o=\pm 10^\circ$, the angular speed is higher than those cases with amplitude of the pitching motion of delta wing of $\alpha_o=\pm 5^\circ$. Since the delta wing scans more space at the same amount of time during the delta wing oscillation. These angular speed differences alter the hysteresis of locations of vortex breakdowns, X_{vb}/C .

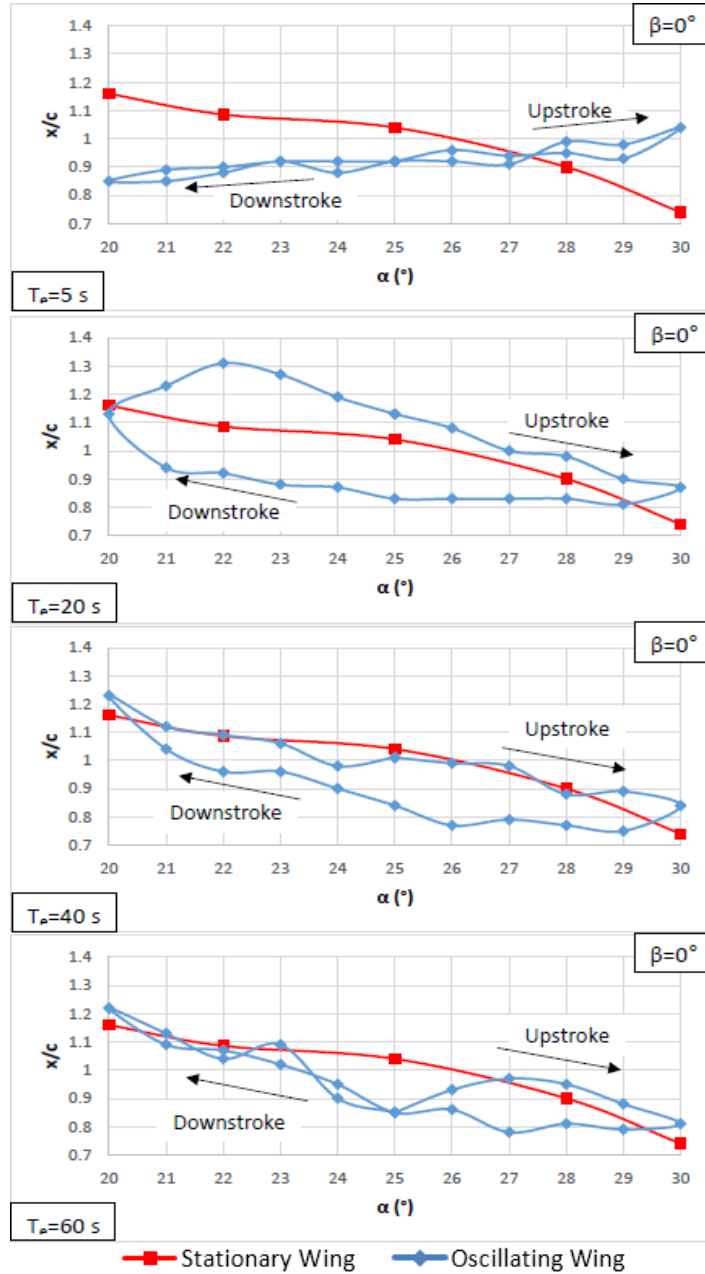


Figure 4.13. Comparisons of static and dynamic loops of vortex breakdown as a function of angle of attack, α . Mean angle of attack is $\alpha_m = 25^\circ$, amplitude of pitching motion is $\alpha_o = \pm 5^\circ$, yaw angle is $\beta = 0^\circ$, period of oscillation is $T_e = 5\text{ s}, 20\text{ s}, 40\text{ s}, 60\text{ s}$ and reduced frequency is $K = 0.16, 0.25, 0.49, 1.96$

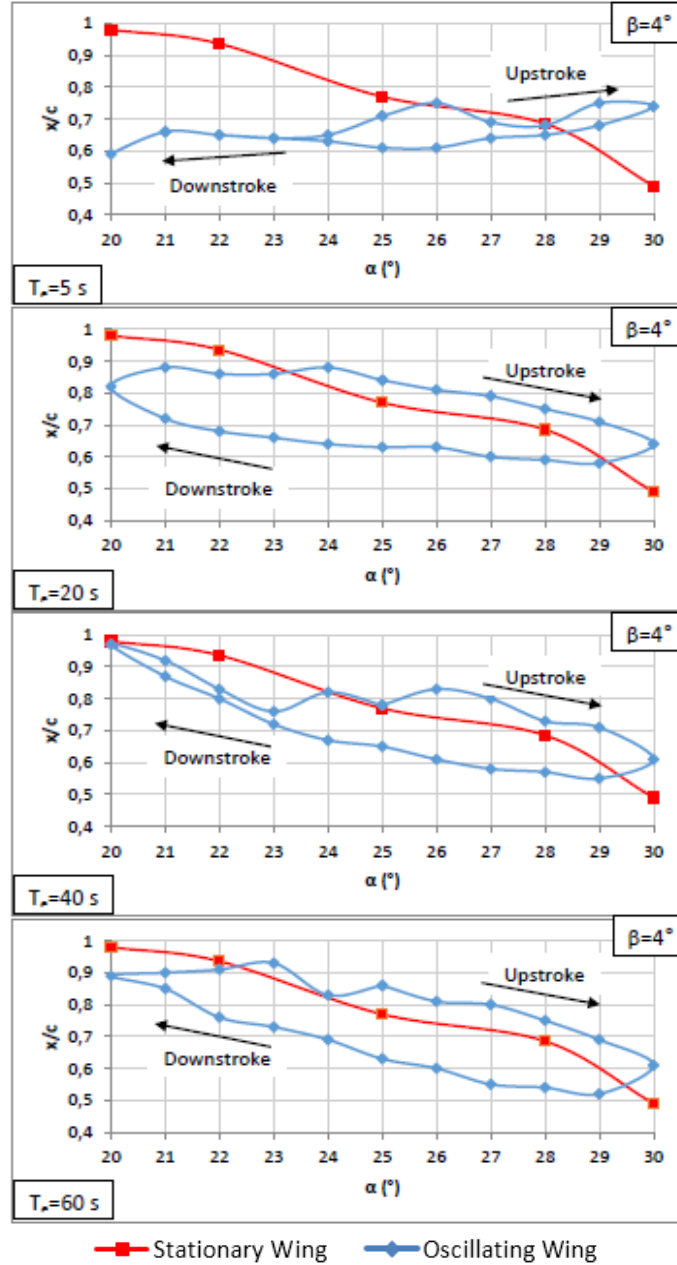


Figure 4.14. Comparisons of static and dynamic loops of vortex breakdown as a function of angle of attack, α . Mean angle of attack is $\alpha_m=25^\circ$, amplitude of pitching motion is $\alpha_o=\pm 5^\circ$, yaw angle is $\beta=4^\circ$, period of oscillation is $T_e=5s, 20s, 40s, 60s$ and reduced frequency is $K= 0.16, 0.25, 0.49, 1.96$

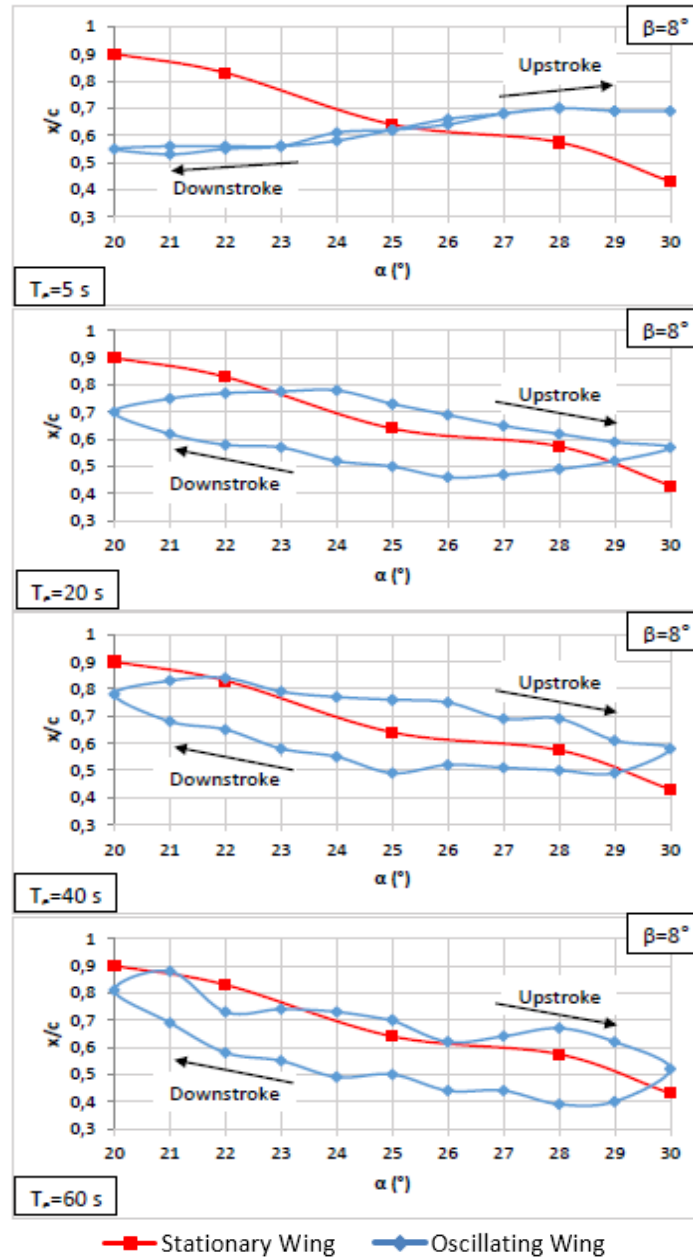


Figure 4.15. Comparisons of static and dynamic loops of vortex breakdown as a function of angle of attack, α . Mean angle of attack is $\alpha_m=25^\circ$, amplitude of pitching motion is $\alpha_o=\pm 5^\circ$, yaw angle is $\beta=8^\circ$, period of oscillation is $T_e=5s, 20s, 40s, 60s$ and reduced frequency is $K= 0.16, 0.25, 0.49, 1.96$

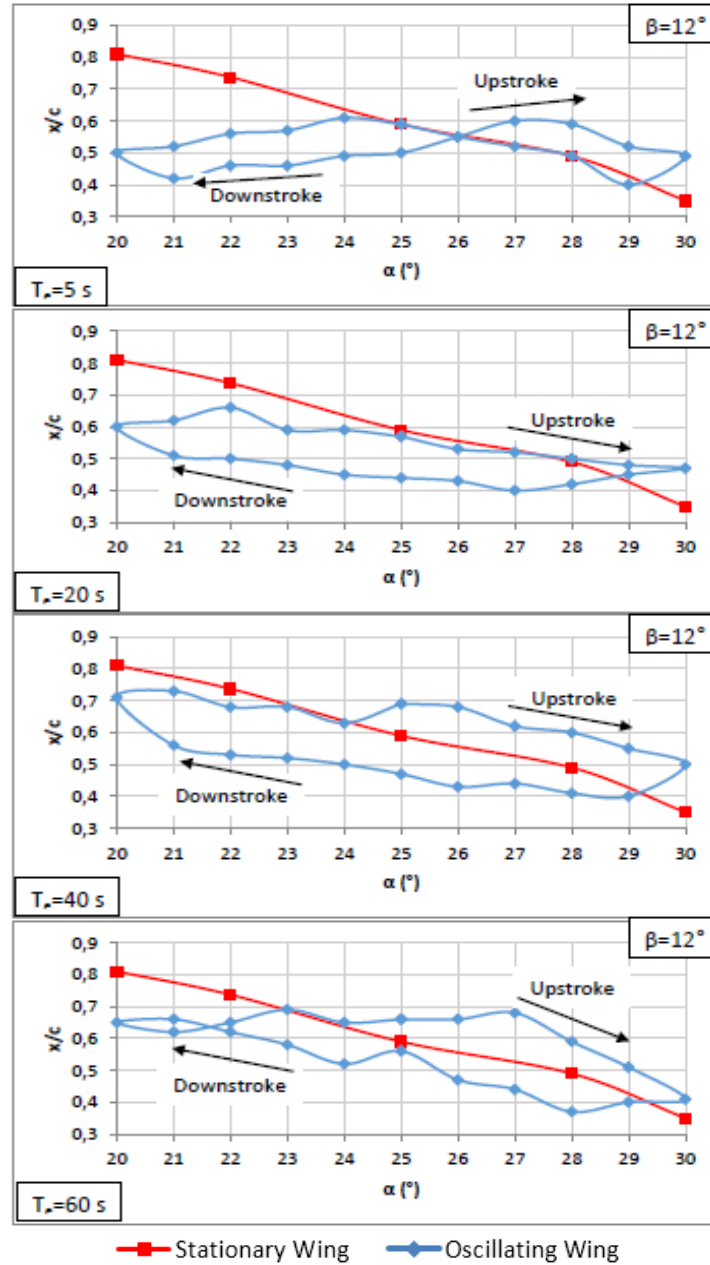


Figure 4.16. Comparisons of static and dynamic loops of vortex breakdown as a function of angle of attack, α . Mean angle of attack is $\alpha_m=25^\circ$, amplitude of pitching motion is $\alpha_0=\pm 5^\circ$, yaw angle is $\beta=12^\circ$, period of oscillation is $T_e=5s, 20s, 40s, 60s$ and reduced frequency is $K=0.16, 0.25, 0.49, 1.96$

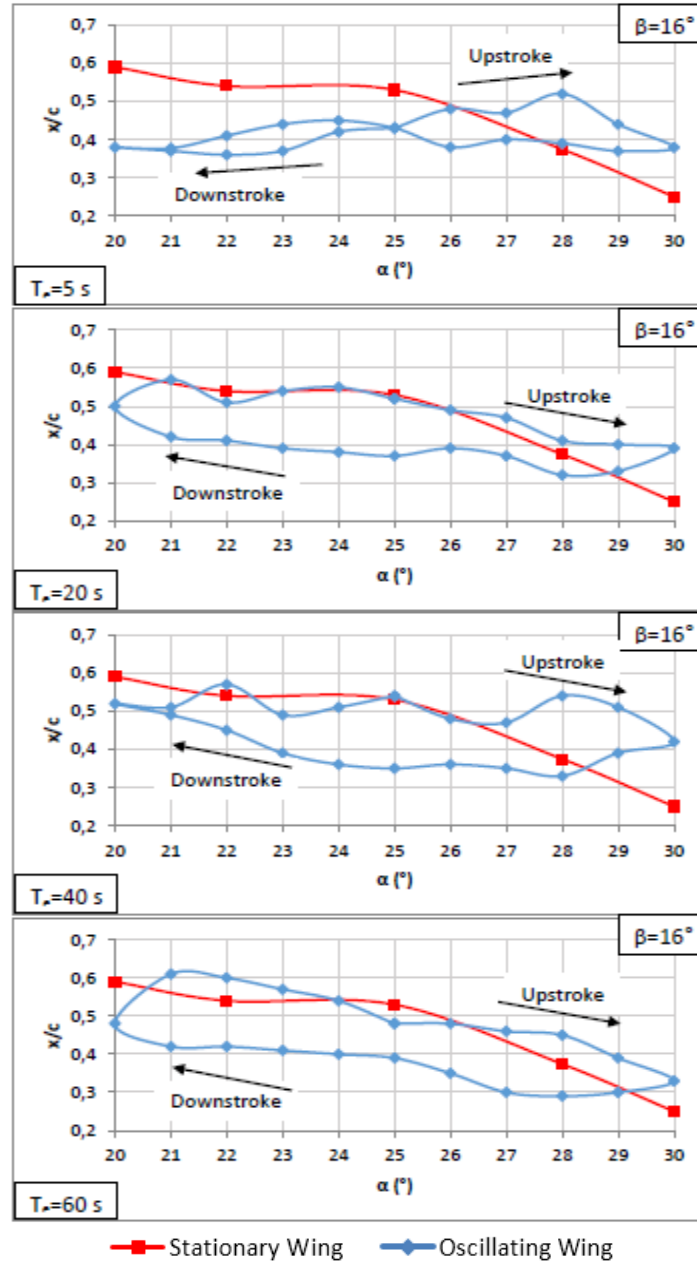


Figure 4.17. Comparisons of static and dynamic loops of vortex breakdown as a function of angle of attack, α . Mean angle of attack is $\alpha_m=25^\circ$, amplitude of pitching motion is $\alpha_0=\pm 5^\circ$, yaw angle is $\beta=16^\circ$, period of oscillation is $T_e=5s, 20s, 40s, 60s$ and reduced frequency is $K= 0.16, 0.25, 0.49, 1.96$

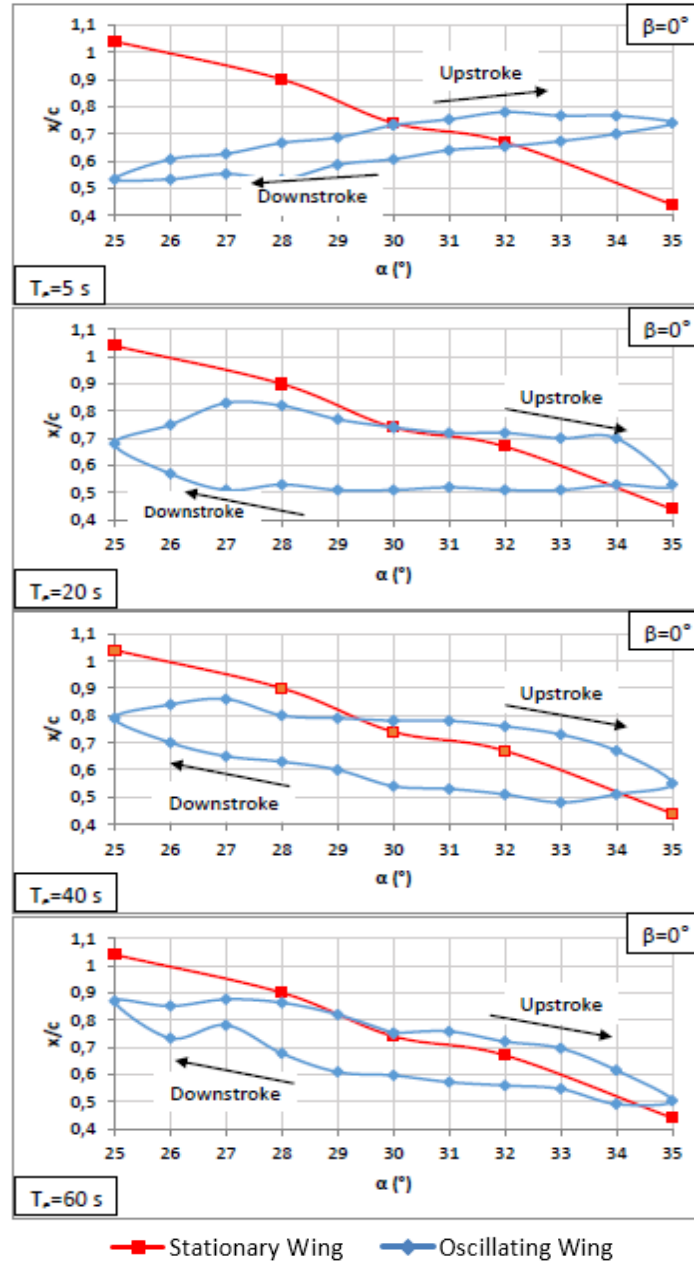


Figure 4.18. Comparisons of static and dynamic loops of vortex breakdown as a function of angle of attack, α . Mean angle of attack is $\alpha_m = 30^\circ$, amplitude of pitching motion is $\alpha_o = \pm 5^\circ$, yaw angle is $\beta = 0^\circ$, period of oscillation is $T_e = 5s, 20s, 40s, 60s$ and reduced frequency is $K = 0.16, 0.25, 0.49, 1.96$

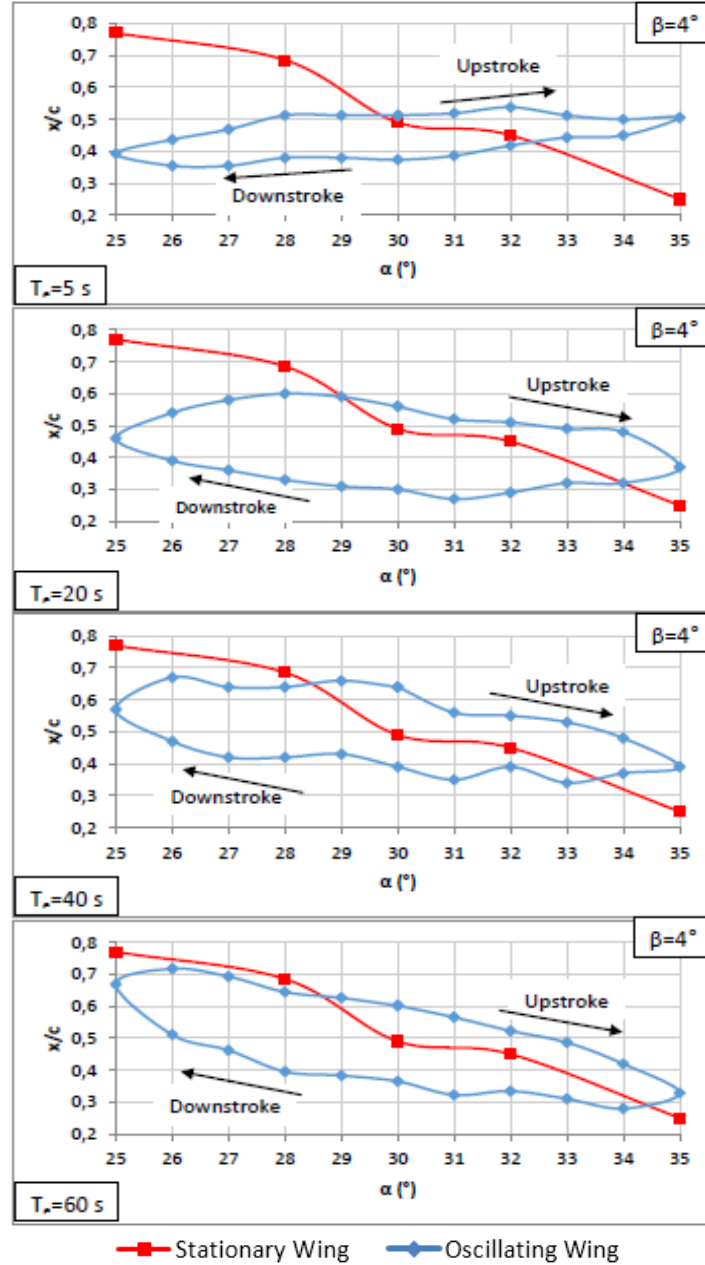


Figure 4.19. Comparisons of static and dynamic loops of vortex breakdown as a function of angle of attack, α . Mean angle of attack is $\alpha_m=30^\circ$, amplitude of pitching motion is $\alpha_o=\pm 5^\circ$, yaw angle is $\beta=4^\circ$, period of oscillation is $T_e=5s, 20s, 40s, 60s$ and reduced frequency is $K=0.16, 0.25, 0.49, 1.96$

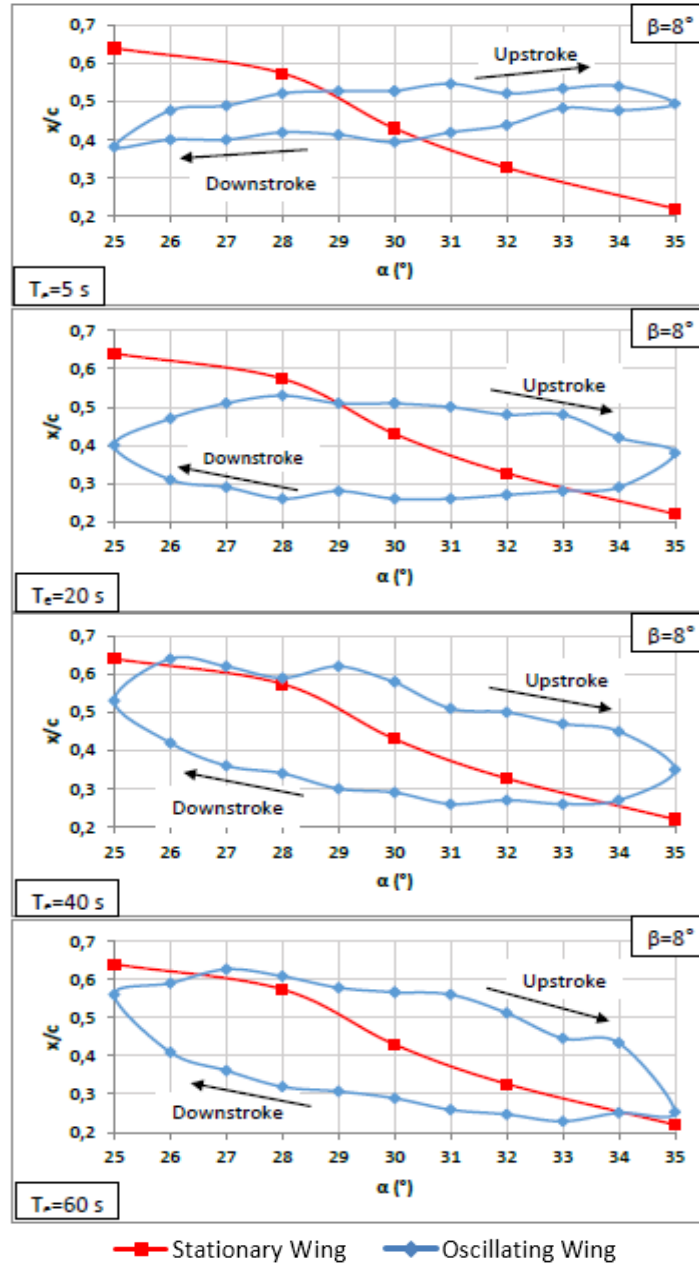


Figure 4.20. Comparisons of static and dynamic loops of vortex breakdown as a function of angle of attack, α . Mean angle of attack is $\alpha_m = 30^\circ$, amplitude of pitching motion is $\alpha_o = \pm 5^\circ$, yaw angle is $\beta = 8^\circ$, period of oscillation is $T_e = 5s, 20s, 40s, 60s$ and reduced frequency is $K = 0.16, 0.25, 0.49, 1.96$

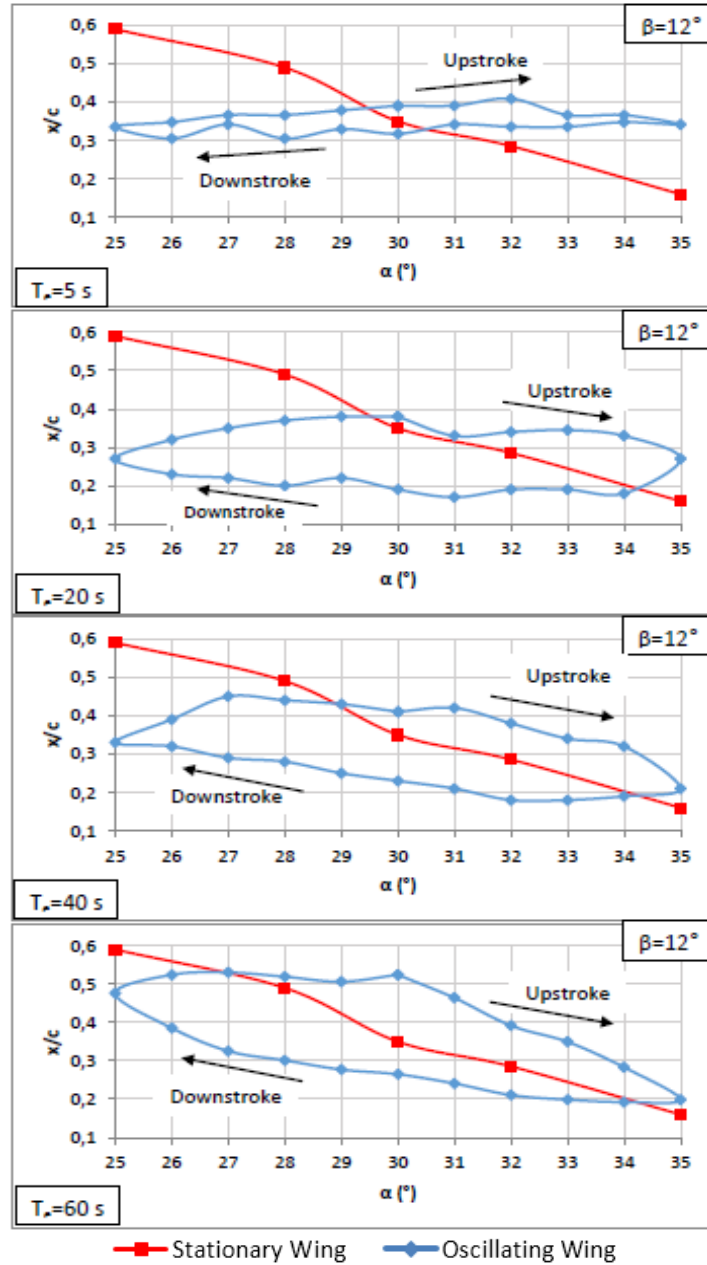


Figure 4.21. Comparisons of static and dynamic loops of vortex breakdown as a function of angle of attack, α . Mean angle of attack is $\alpha_m=30^\circ$, amplitude of pitching motion is $\alpha_0=\pm 5^\circ$, yaw angle is $\beta=12^\circ$, period of oscillation is $T_e=5s, 20s, 40s, 60s$ and reduced frequency is $K=0.16, 0.25, 0.49, 1.96$

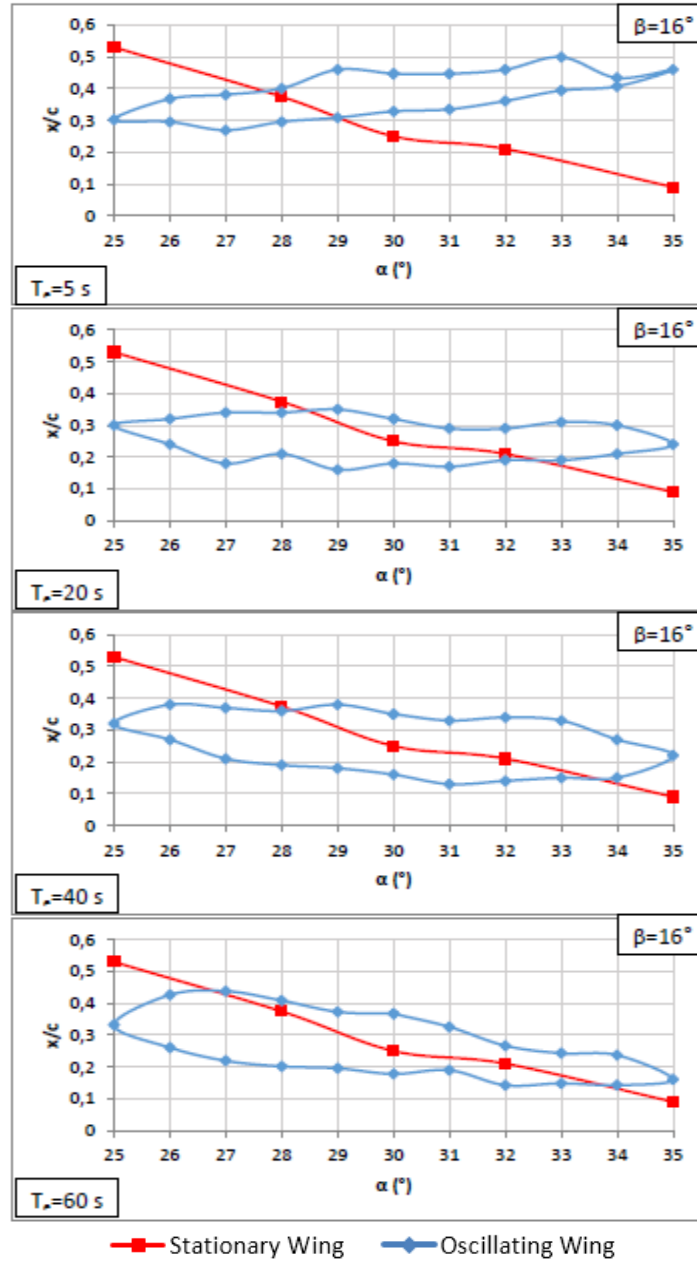


Figure 4.22. Comparisons of static and dynamic loops of vortex breakdown as a function of angle of attack, α . Mean angle of attack is $\alpha_m=30^\circ$, amplitude of pitching motion is $\alpha_0=\pm 5^\circ$, yaw angle is $\beta=16^\circ$, period of oscillation is $T_e=5s, 20s, 40s, 60s$ and reduced frequency is $K=0.16, 0.25, 0.49, 1.96$

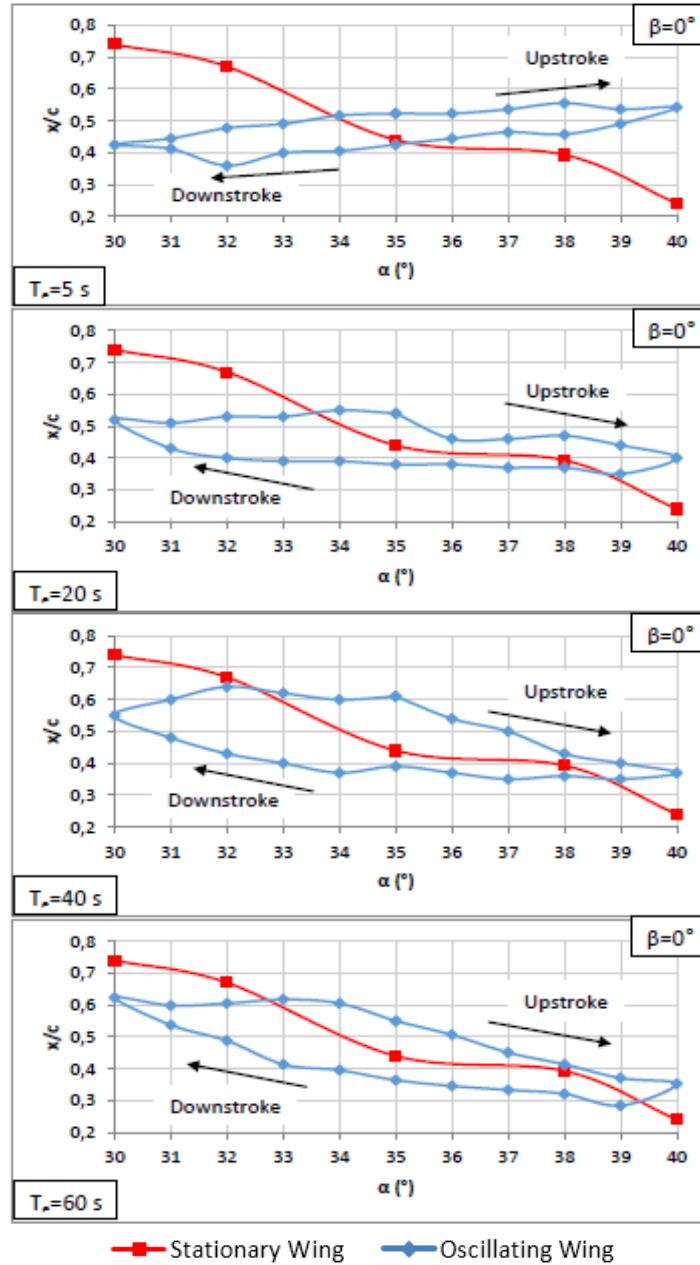


Figure 4.23. Comparisons of static and dynamic loops of vortex breakdown as a function of angle of attack, α . Mean angle of attack is $\alpha_m=35^\circ$, amplitude of pitching motion is $\alpha_o=\pm 5^\circ$, yaw angle is $\beta=0^\circ$, period of oscillation is $T_e=5s, 20s, 40s, 60s$ and reduced frequency is $K=0.16, 0.25, 0.49, 1.96$

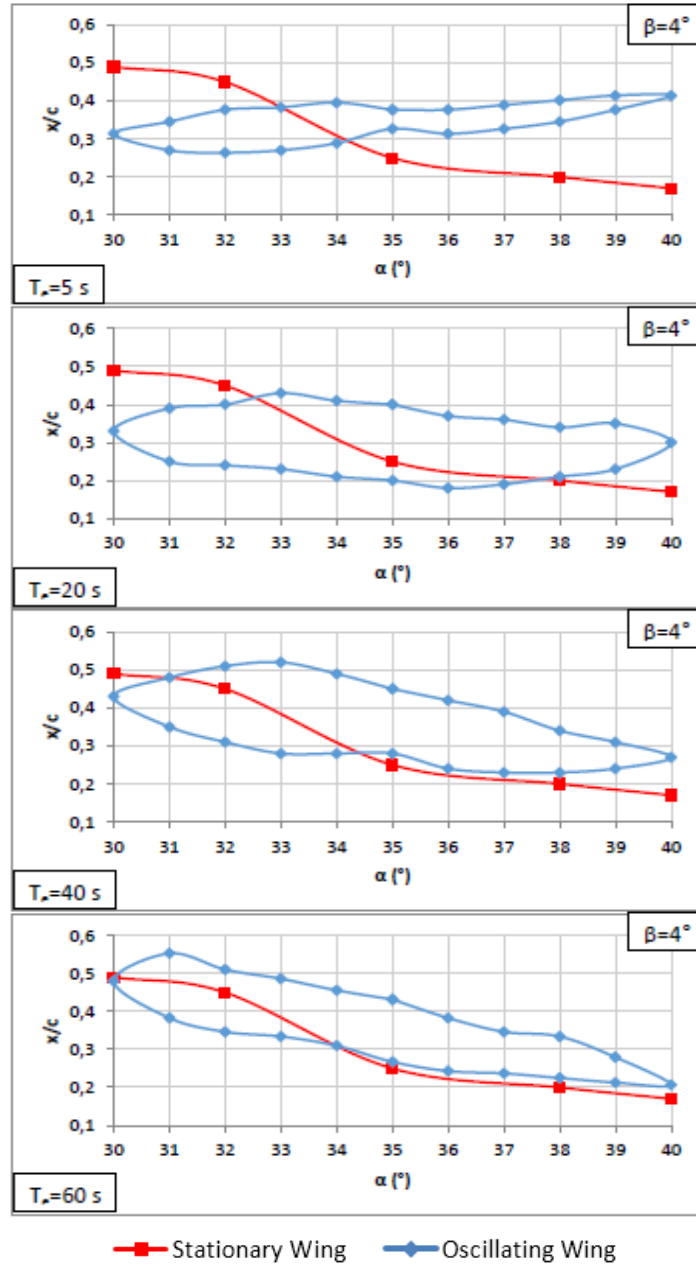


Figure 4.24. Comparisons of static and dynamic loops of vortex breakdown as a function of angle of attack, α . Mean angle of attack is $\alpha_m=35^\circ$, amplitude of pitching motion is $\alpha_o=\pm 5^\circ$, yaw angle is $\beta=4^\circ$, period of oscillation is $T_e=5s, 20s, 40s, 60s$ and reduced frequency is $K= 0.16, 0.25, 0.49, 1.96$

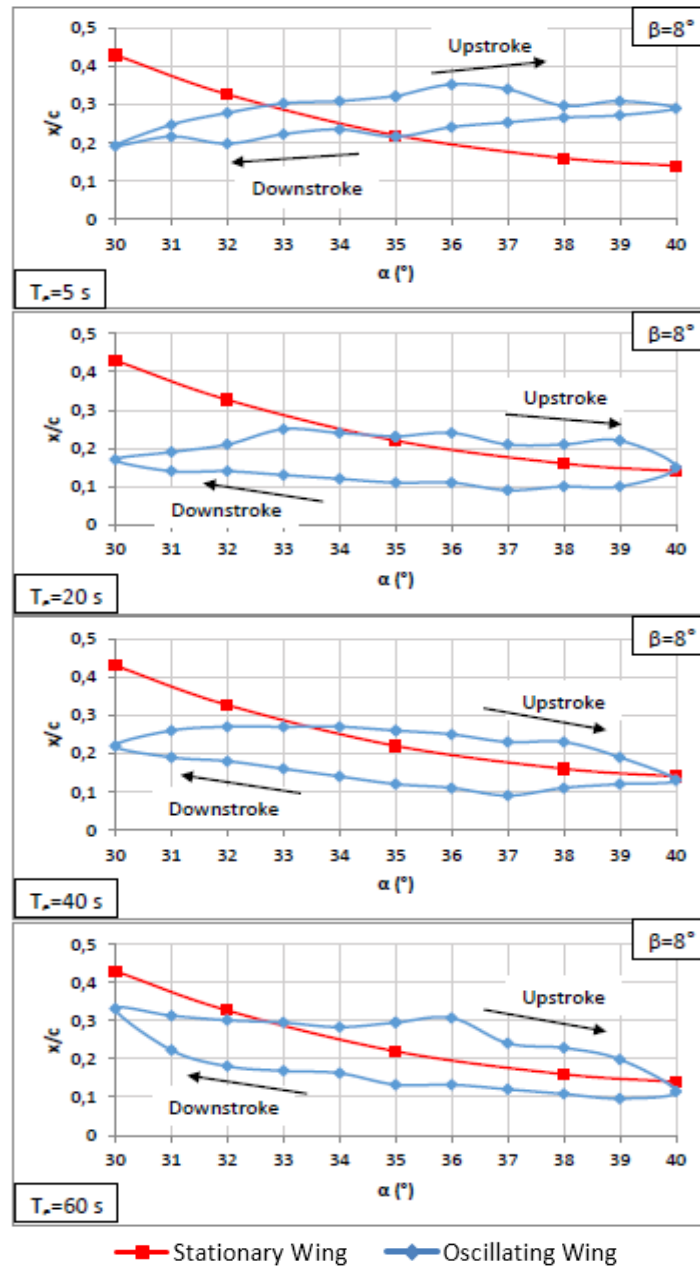


Figure 4.25. Comparisons of static and dynamic loops of vortex breakdown as a function of angle of attack, α . Mean angle of attack is $\alpha_m=35^\circ$, amplitude of pitching motion is $\alpha_o=\pm 5^\circ$, yaw angle is $\beta=8^\circ$, period of oscillation is $T_e=5s, 20s, 40s, 60s$ and reduced frequency is $K=0.16, 0.25, 0.49, 1.96$

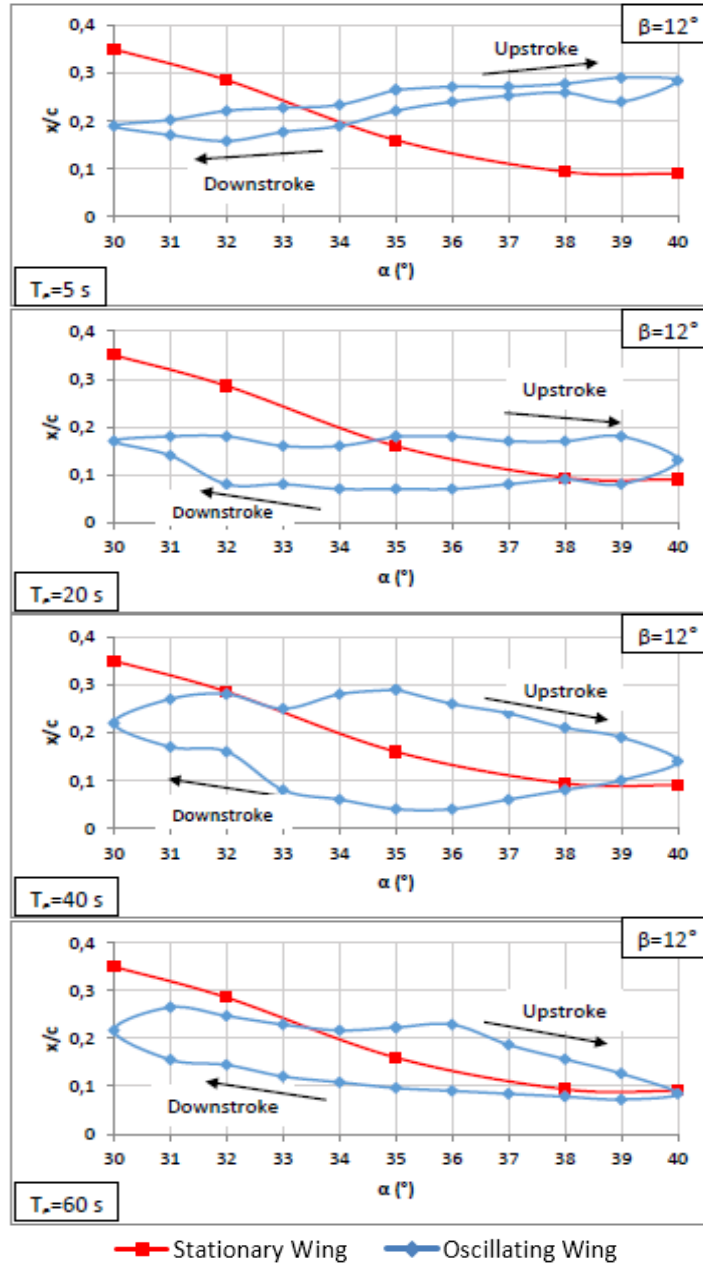


Figure 4.26. Comparisons of static and dynamic loops of vortex breakdown as a function of angle of attack, α . Mean angle of attack is $\alpha_m=35^\circ$, amplitude of pitching motion is $\alpha_0=\pm 5^\circ$, yaw angle is $\beta=12^\circ$, period of oscillation is $T_e=5s, 20s, 40s, 60s$ and reduced frequency is $K= 0.16, 0.25, 0.49, 1.96$

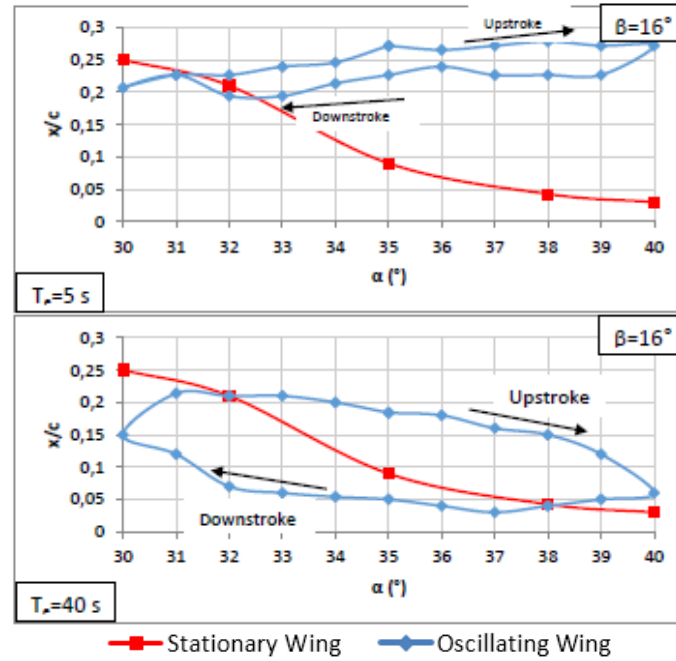


Figure 4.27. Comparisons of static and dynamic loops of vortex breakdown as a function of angle of attack, α . Mean angle of attack is $\alpha_m = 35^\circ$, amplitude of pitching motion is $\alpha_o = \pm 5^\circ$, yaw angle is $\beta = 16^\circ$, period of oscillation is $T_e = 5$ s, 20 s, 40 s, 60 s and reduced frequency is $K = 0.16, 0.25, 0.49, 1.96$

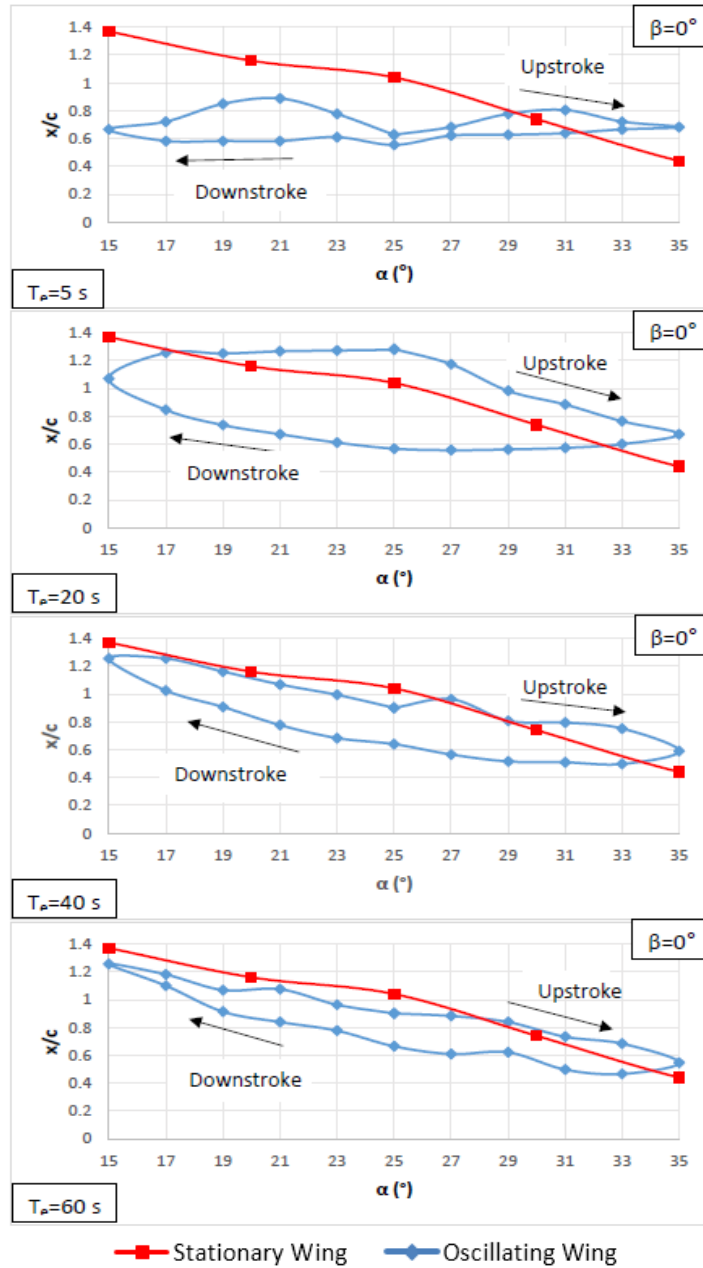


Figure 4.28. Comparisons of static and dynamic loops of vortex breakdown as a function of angle of attack, α . Mean angle of attack is $\alpha_m=25^\circ$, amplitude of pitching motion is $\alpha_0=\pm 10^\circ$, yaw angle is $\beta=0^\circ$, period of oscillation is $T_e=5s, 20s, 40s, 60s$ and reduced frequency is $K= 0.16, 0.25, 0.49, 1.96$

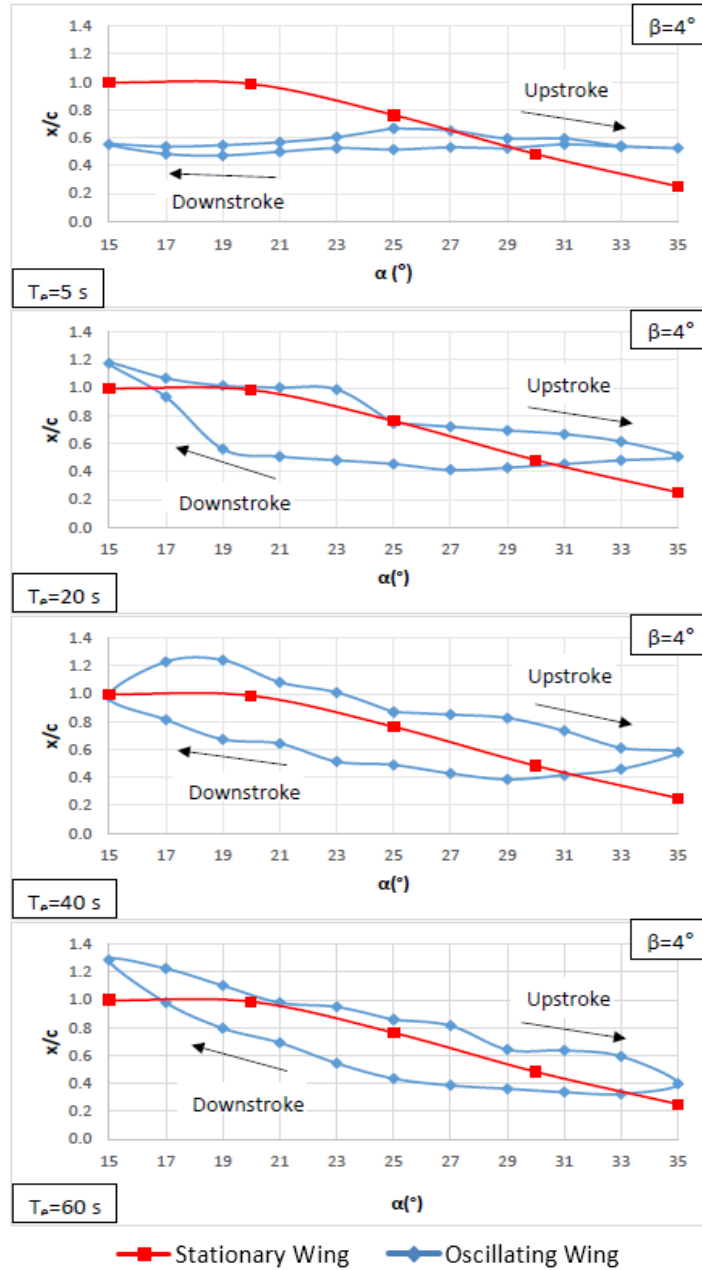


Figure 4.29. Comparisons of static and dynamic loops of vortex breakdown as a function of angle of attack, α . Mean angle of attack is $\alpha_m=25^{\circ}$, amplitude of pitching motion is $\alpha_0=\pm 10^{\circ}$, yaw angle is $\beta=4^{\circ}$, period of oscillation is $T_e=5s, 20s, 40s, 60s$ and reduced frequency is $K= 0.16, 0.25, 0.49, 1.96$

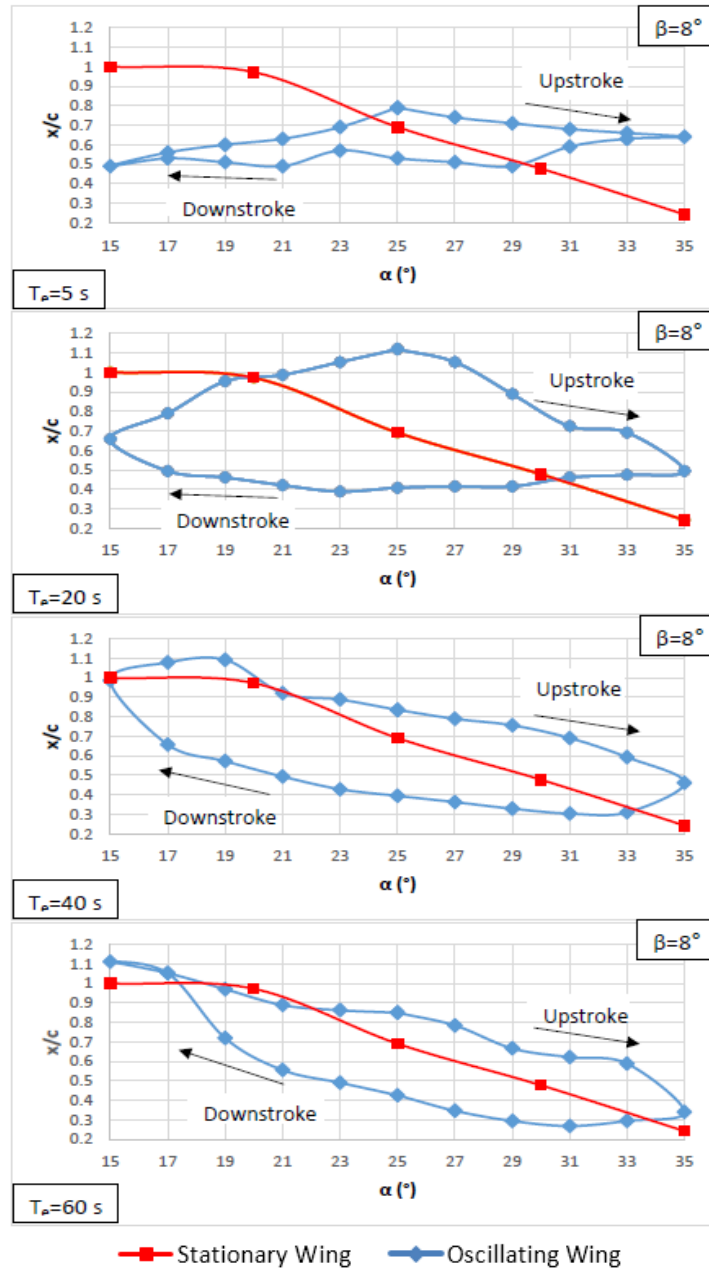


Figure 4.30. Comparisons of static and dynamic loops of vortex breakdown as a function of angle of attack, α . Mean angle of attack is $\alpha_m=25^\circ$, amplitude of pitching motion is $\alpha_0=\pm 10^\circ$, yaw angle is $\beta=8^\circ$, period of oscillation is $T_e=5s, 20s, 40s, 60s$ and reduced frequency is $K= 0.16, 0.25, 0.49, 1.96$

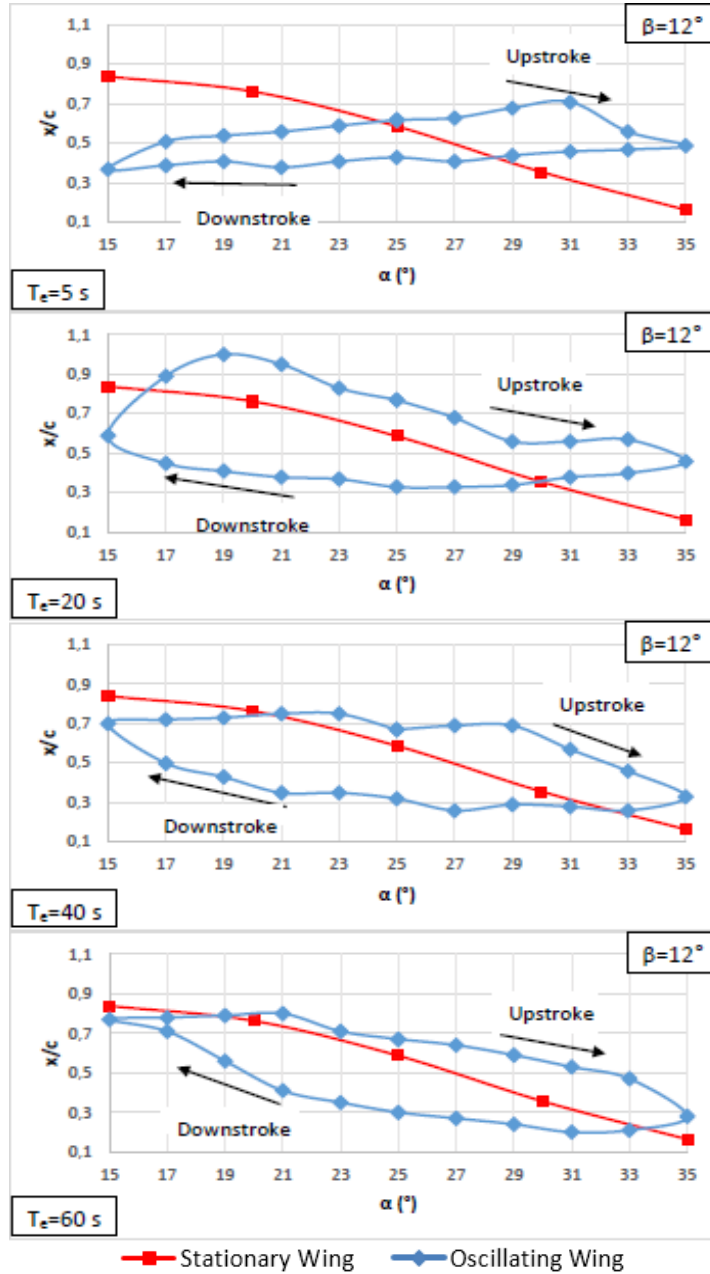


Figure 4.31. Comparisons of static and dynamic loops of vortex breakdown as a function of angle of attack, α . Mean angle of attack is $\alpha_m=25^\circ$, amplitude of pitching motion is $\alpha_o=\pm 10^\circ$, yaw angle is $\beta=12^\circ$, period of oscillation is $T_e=5s, 20s, 40s, 60s$ and reduced frequency is $K=0.16, 0.25, 0.49, 1.96$

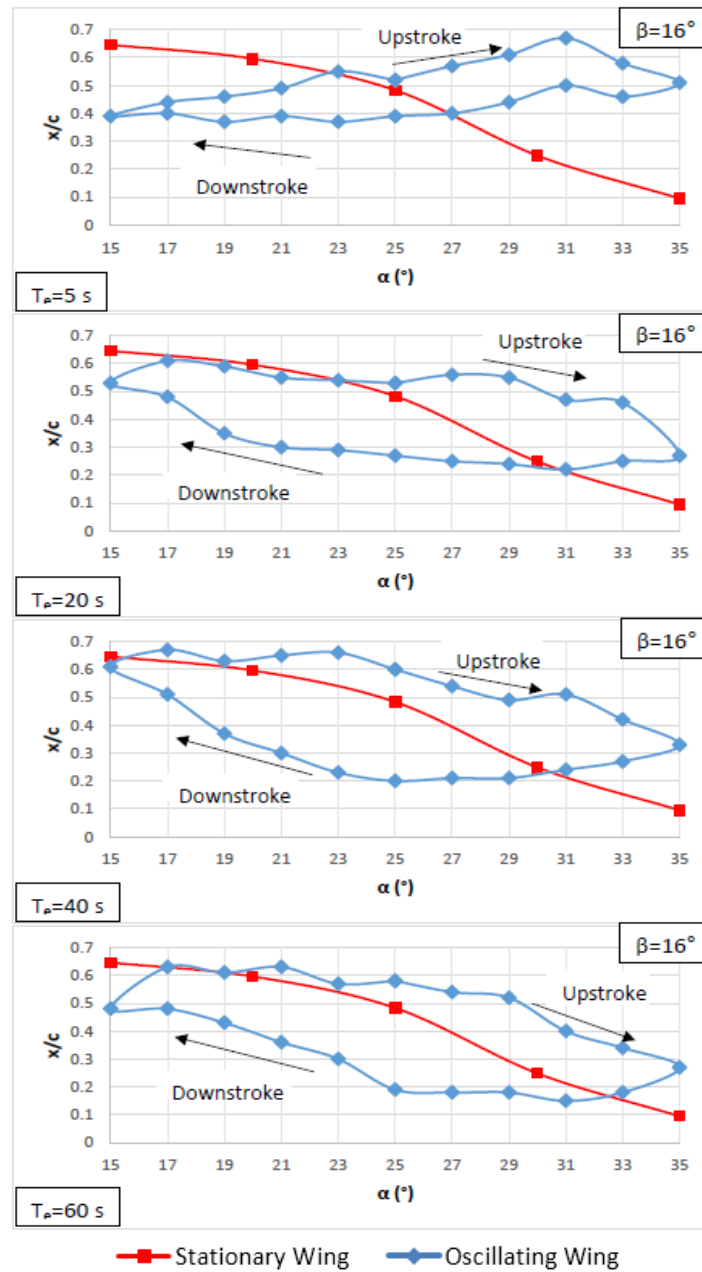


Figure 4.32. Comparisons of static and dynamic loops of vortex breakdown as a function of angle of attack, α . Mean angle of attack is $\alpha_m=25^\circ$, amplitude of pitching motion is $\alpha_o=\pm 10^\circ$, yaw angle is $\beta=16^\circ$, period of oscillation is $T_e=5s, 20s, 40s, 60s$ and reduced frequency is $K=0.16, 0.25, 0.49, 1.96$

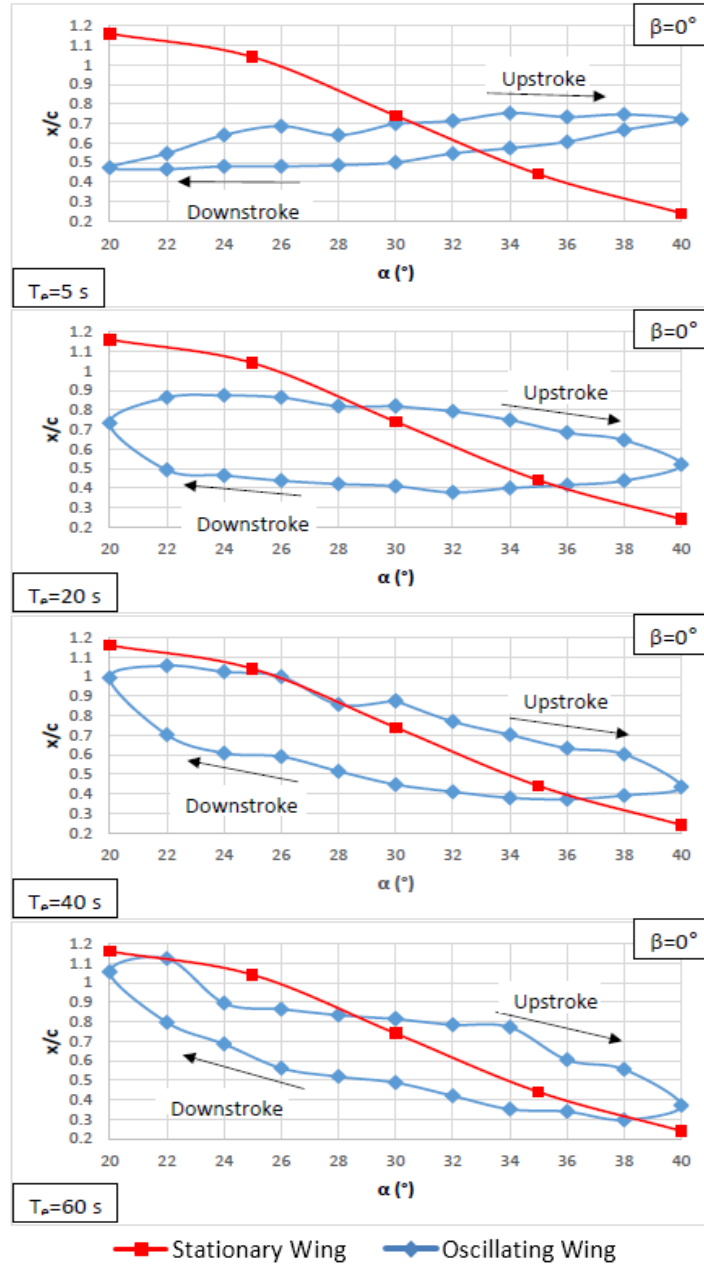


Figure 4.33. Comparisons of static and dynamic loops of vortex breakdown as a function of angle of attack, α . Mean angle of attack is $\alpha_m=30^\circ$, amplitude of pitching motion is $\alpha_0=\pm 10^\circ$, yaw angle is $\beta=0^\circ$, period of oscillation is $T_e=5s, 20s, 40s, 60s$ and reduced frequency is $K= 0.16, 0.25, 0.49, 1.96$

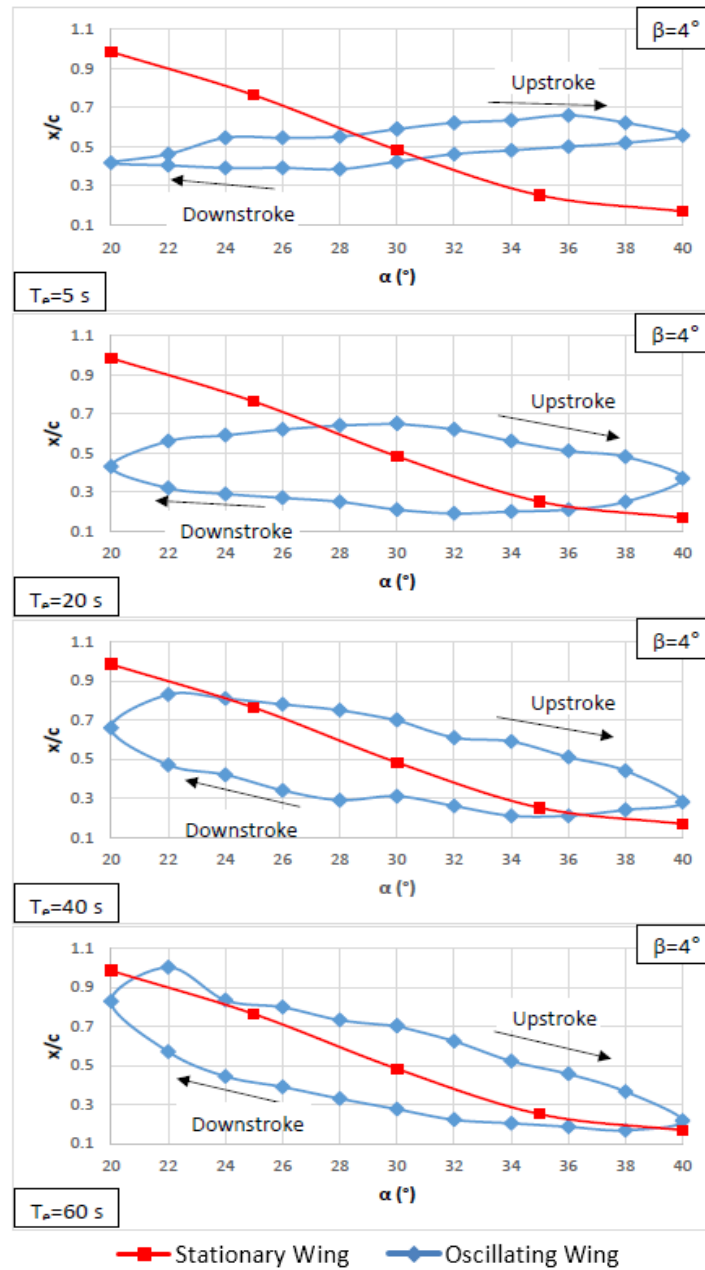


Figure 4.34. Comparisons of static and dynamic loops of vortex breakdown as a function of angle of attack, α . Mean angle of attack is $\alpha_m=30^\circ$, amplitude of pitching motion is $\alpha_0=\pm 10^\circ$, yaw angle is $\beta=4^\circ$, period of oscillation is $T_e=5s, 20s, 40s, 60s$ and reduced frequency is $K=0.16, 0.25, 0.49, 1.96$

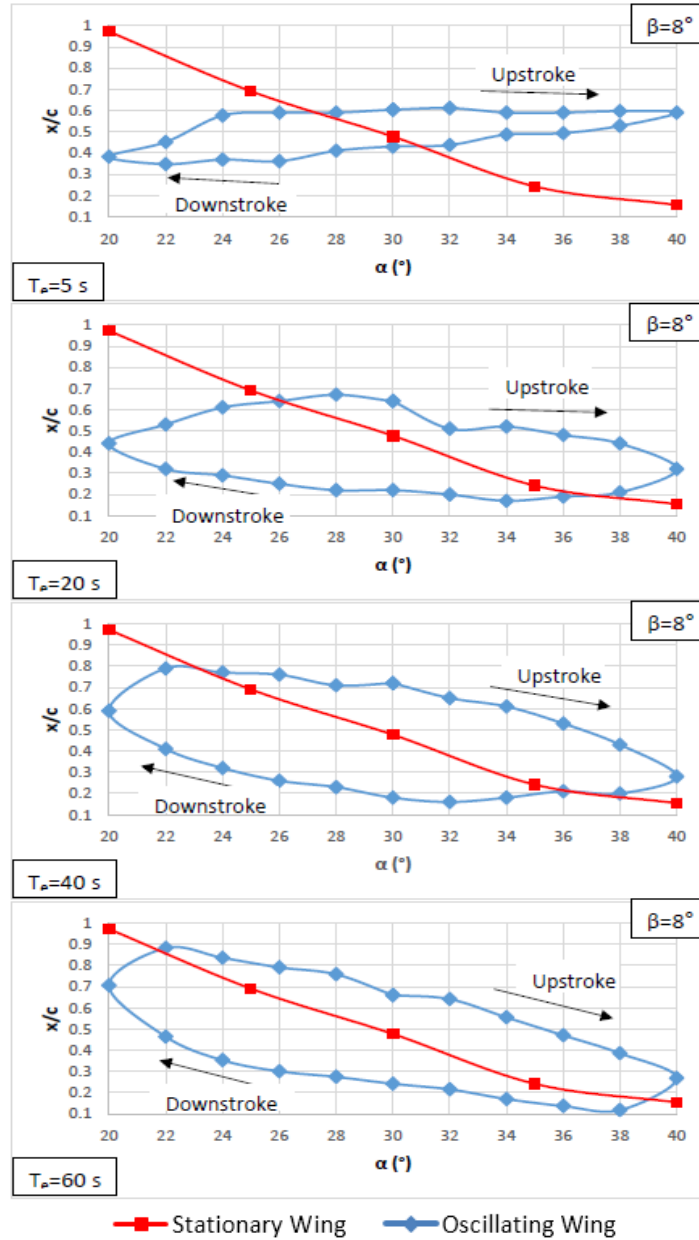


Figure 4.35. Comparisons of static and dynamic loops of vortex breakdown as a function of angle of attack, α . Mean angle of attack is $\alpha_m=30^\circ$, amplitude of pitching motion is $\alpha_o=\pm 10^\circ$, yaw angle is $\beta=8^\circ$, period of oscillation is $T_e=5s, 20s, 40s, 60s$ and reduced frequency is $K= 0.16, 0.25, 0.49, 1.96$

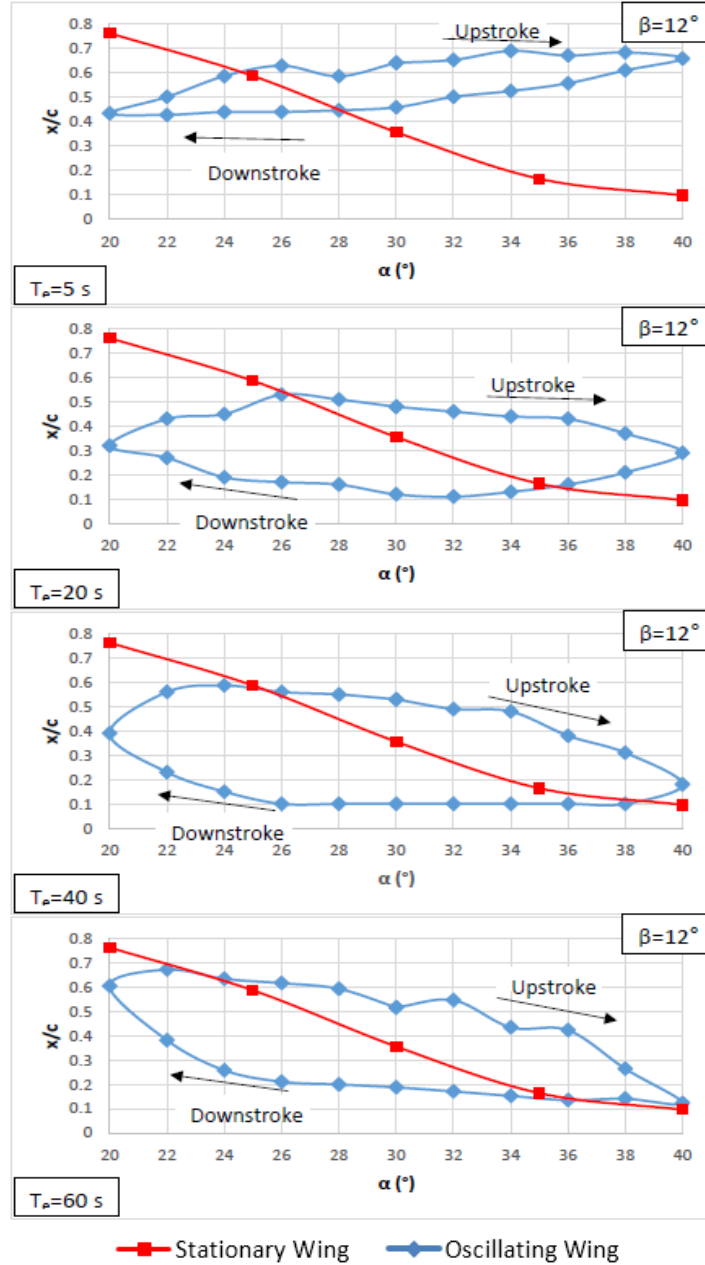


Figure 4.36. Comparisons of static and dynamic loops of vortex breakdown as a function of angle of attack, α . Mean angle of attack is $\alpha_m=30^\circ$, amplitude of pitching motion is $\alpha_o=\pm 10^\circ$, yaw angle is $\beta=12^\circ$, period of oscillation is $T_o=5s, 20s, 40s, 60s$ and reduced frequency is $K=0.16, 0.25, 0.49, 1.96$

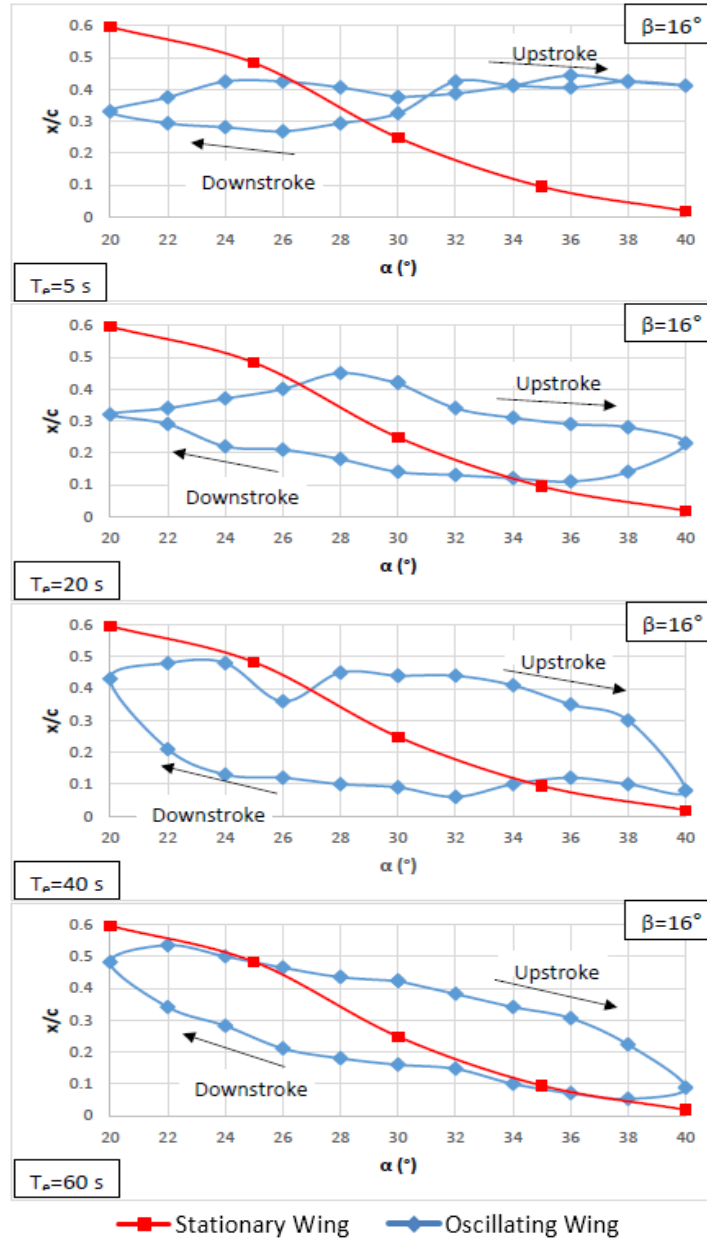


Figure 4.37. Comparisons of static and dynamic loops of vortex breakdown as a function of angle of attack, α . Mean angle of attack is $\alpha_m=30^\circ$, amplitude of pitching motion is $\alpha_o=\pm 10^\circ$, yaw angle is $\beta=16^\circ$, period of oscillation is $T_e=5s, 20s, 40s, 60s$ and reduced frequency is $K=0.16, 0.25, 0.49, 1.96$

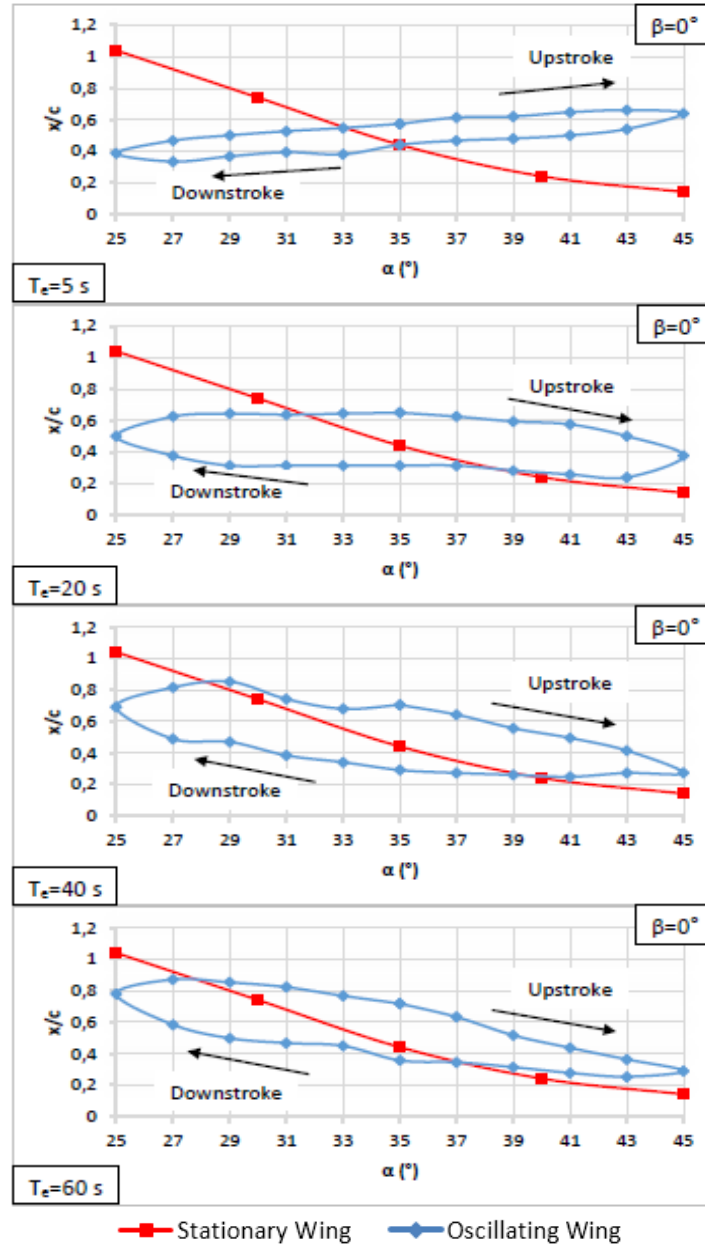


Figure 4.38. Comparisons of static and dynamic loops of vortex breakdown as a function of angle of attack, α . Mean angle of attack is $\alpha_m=35^\circ$, amplitude of pitching motion is $\alpha_o=\pm 10^\circ$, yaw angle is $\beta=0^\circ$, period of oscillation is $T_e=5s, 20s, 40s, 60s$ and reduced frequency is $K= 0.16, 0.25, 0.49, 1.96$

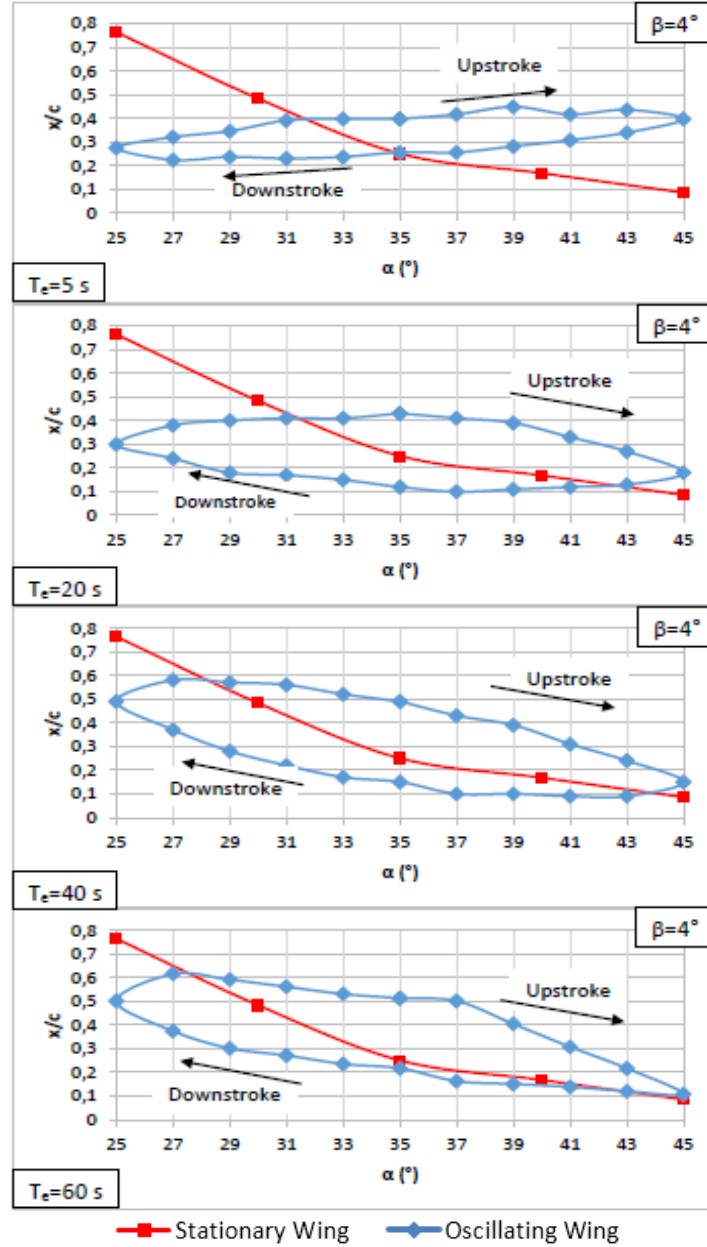


Figure 4.39. Comparisons of static and dynamic loops of vortex breakdown as a function of angle of attack, α . Mean angle of attack is $\alpha_m=35^\circ$, amplitude of pitching motion is $\alpha_o=\pm 10^\circ$, yaw angle is $\beta=4^\circ$, period of oscillation is $T_e=5s, 20s, 40s, 60s$ and reduced frequency is $K= 0.16, 0.25, 0.49, 1.96$

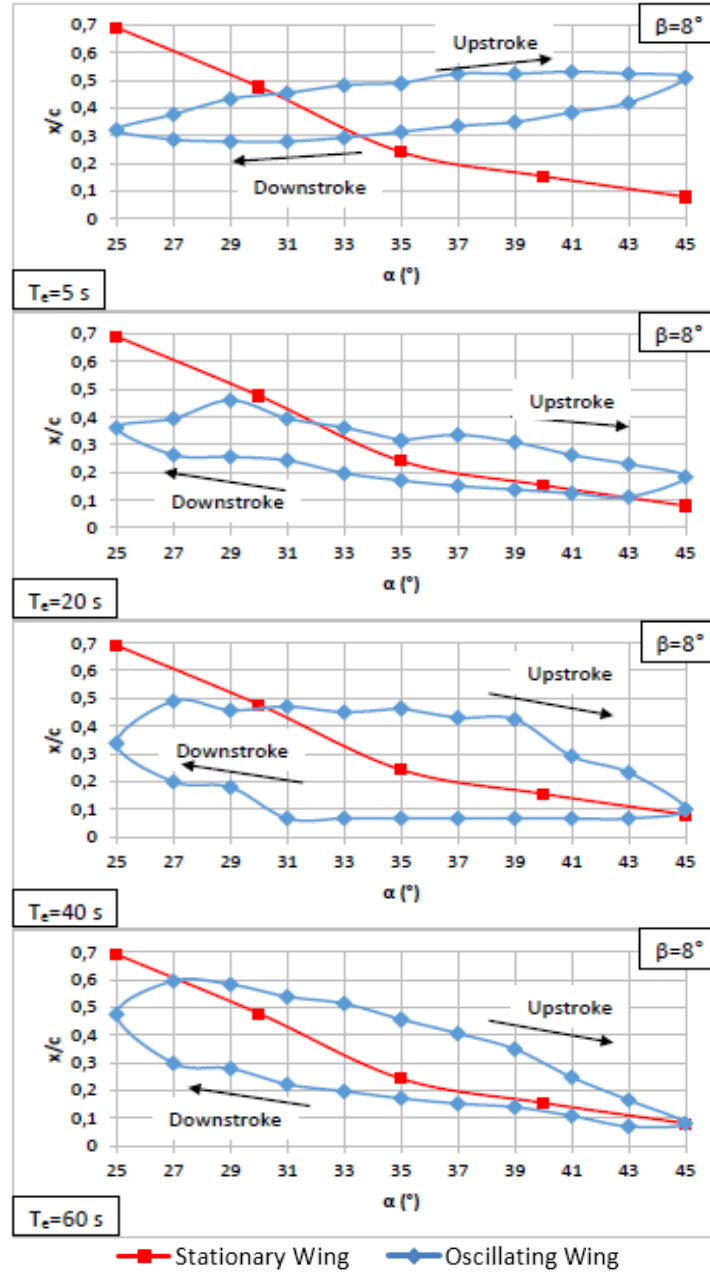


Figure 4.40. Comparisons of static and dynamic loops of vortex breakdown as a function of angle of attack, α . Mean angle of attack is $\alpha_m=35^\circ$, amplitude of pitching motion is $\alpha_0=\pm 10^\circ$, yaw angle is $\beta=8^\circ$, period of oscillation is $T_e=5s, 20s, 40s, 60s$ and reduced frequency is $K=0.16, 0.25, 0.49, 1.96$

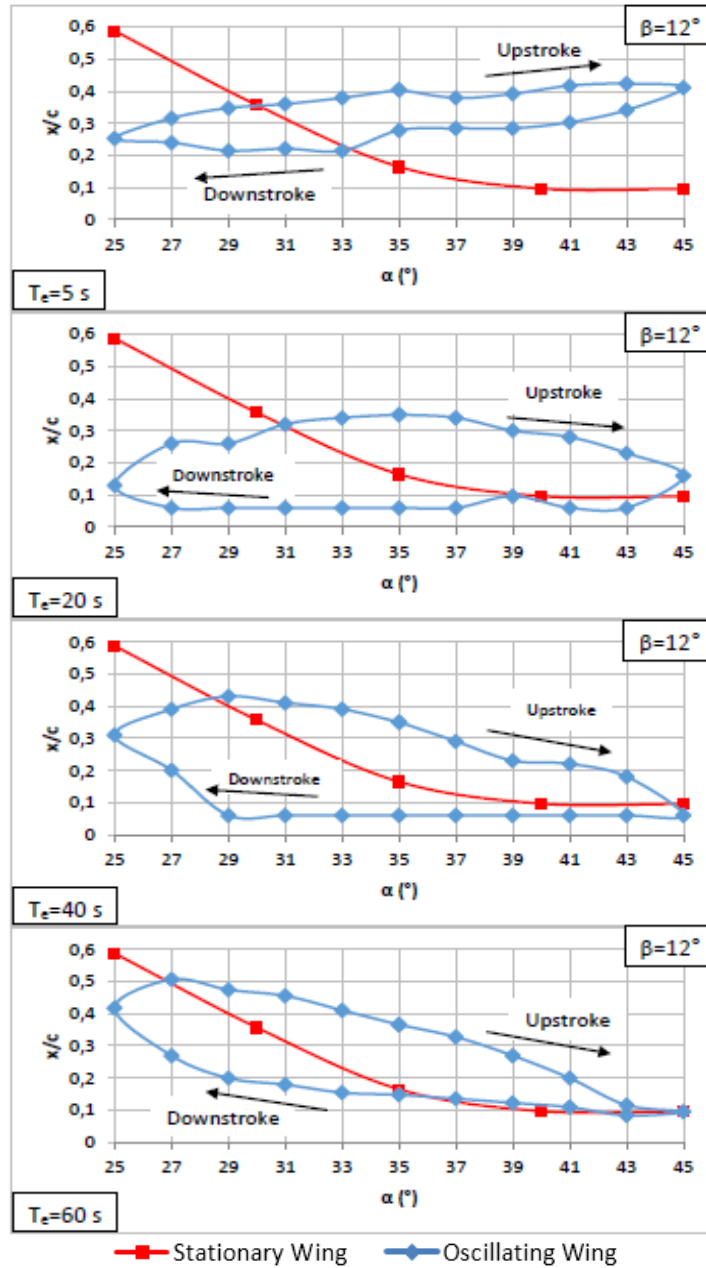


Figure 4.41. Comparisons of static and dynamic loops of vortex breakdown as a function of angle of attack, α . Mean angle of attack is $\alpha_m=35^\circ$, amplitude of pitching motion is $\alpha_o=\pm 10^\circ$, yaw angle is $\beta=12^\circ$, period of oscillation is $T_e=5s, 20s, 40s, 60s$ and reduced frequency is $K=0.16, 0.25, 0.49, 1.96$

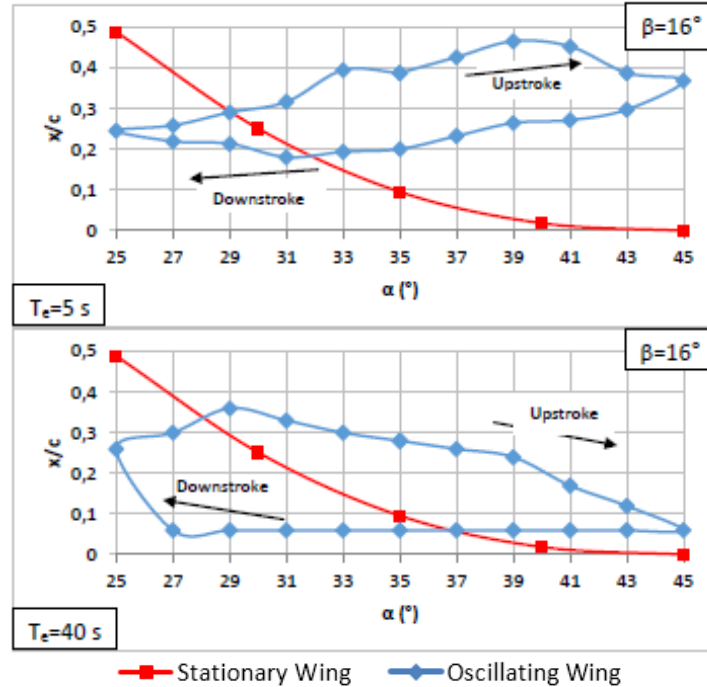


Figure 4.42. Comparisons of static and dynamic loops of vortex breakdown as a function of angle of attack, α . Mean angle of attack is $\alpha_m=35^\circ$, amplitude of pitching motion is $\alpha_o=\pm 10^\circ$, yaw angle is $\beta=16^\circ$, period of oscillation is $T_e=5s, 20s, 40s, 60s$ and reduced frequency is $K=0.16, 0.25, 0.49, 1.96$

A graphical representations indicated in Figures 4.43 and 4.44 present variations of vortex breakdown locations as a functions of yaw angles, β within the range of $0^\circ \leq \beta \leq 16^\circ$ compared with the case of stationary delta wing. During the experiment, three different mean angle of attack values, α_m and five different yaw angle values, β are taken. Amplitudes of the delta wing pitching motion, α_o are $+5^\circ$ (upstroke) presented in Figure 4.43 and $+10^\circ$ (upstroke) presented in Figure 4.44. Mean angle of attack of the delta wing are taken as $\alpha_m=25^\circ, 30^\circ, 35^\circ$ presented in similar figures. As clearly seen positions of vortex breakdown move towards the apex of the delta wing with increasing yaw angle, β from 0° to 16° . Also, when period of oscillation, T_e increases, flow characteristics get closer to the stationary delta wing case. As seen in Figures 4.43 and 4.44, due to experimental difficulties a record of flows were not obtained at some locations of the delta wing. Those points are shown with dashed lines. In summary, small yaw angle, β is more effective in altering the location of vortex breakdown in both cases either the stationary or oscillating delta wing.

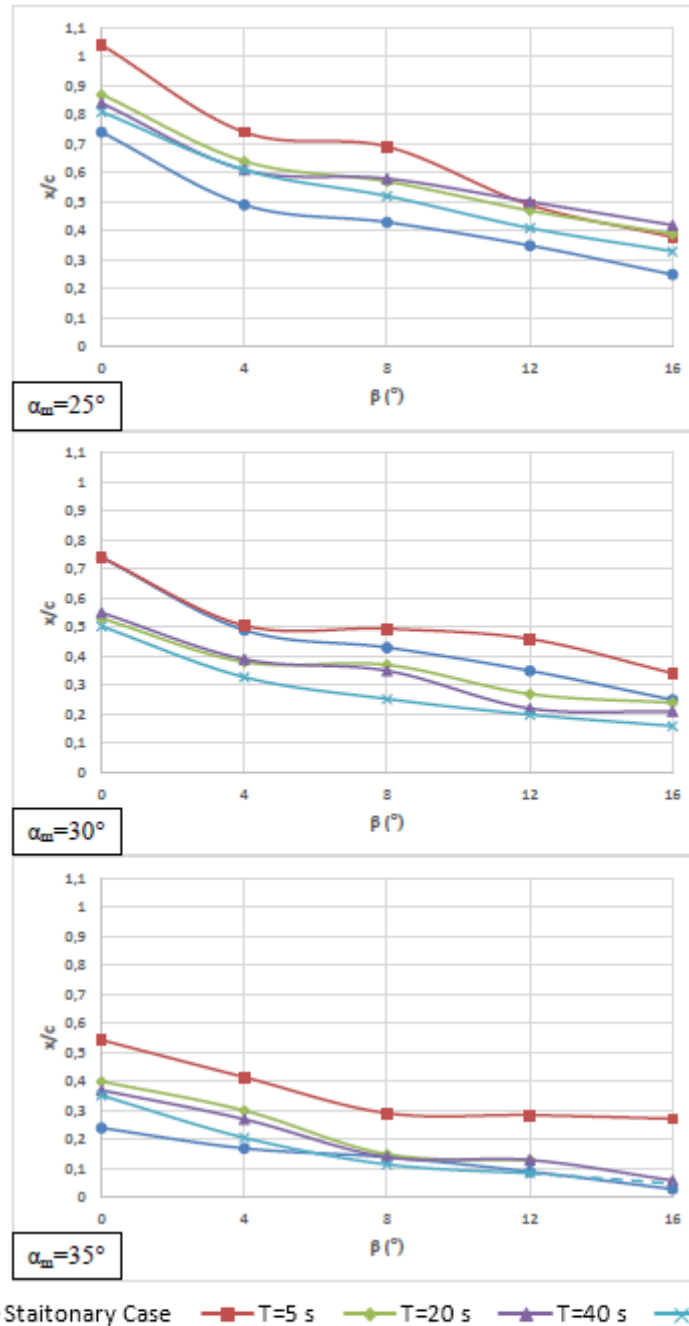


Figure 4.43. Comparisons of static and dynamic cases of vortex breakdown as a function of yaw angle, β . Amplitude of pitching motion is $\alpha_o=+5^\circ$ (upstroke), reduced frequency is $K= 0.16, 0.25, 0.49, 1.96$

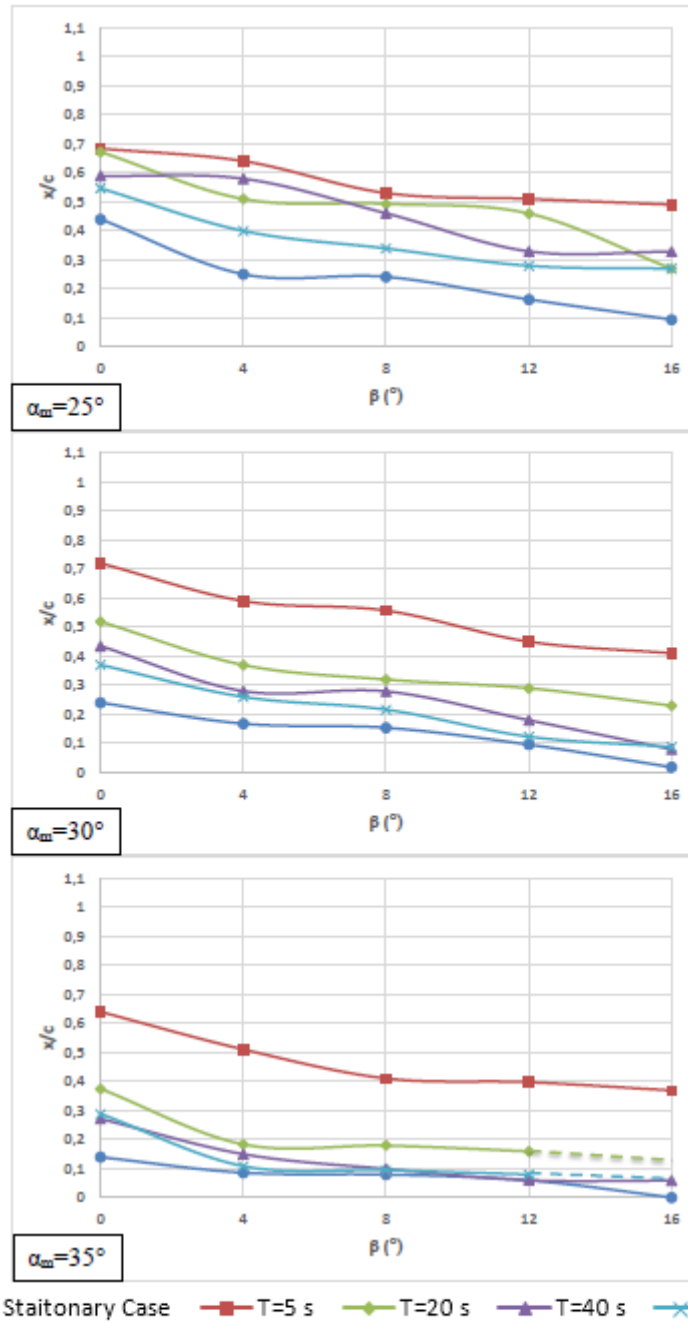


Figure 4.44. Comparisons of static and dynamic cases of vortex breakdown as a function of yaw angle, β . Amplitude of pitching motion is $\alpha_0 = +10^\circ$ (upstroke), reduced frequency is $K = 0.16, 0.25, 0.49, 1.96$

4.3. Instantaneous Velocity Measurements Using PIV

Effects of pitching motion on the windward side leading edge vortex are presented quantitatively by capturing instantaneous velocities over side-view planes by The PIV technique. During the experiment, mean angle of attack, α_m was selected as 30° and yaw angles, β was set as 0° . Amplitude of pitching motion, α_o was chosen as 10° and period of oscillation, T_e was varied over the range of $0s \leq T_e \leq 40s$. Laser reflection region near the apex and trailing edge of the delta wing was masked in order to avoid misreading. Data in first images shown in Figures 4.45-4.47 are averaged using 1000 images of instantaneous velocity vectors. Since the delta wing is under perturbation or moving continuously, it not possible to take average data from 1000 instantaneous images. Only ten instantaneous images are averaged for the rest of other images presented in Figures 4.45-4.47.

4.3.1. Time-Averaged and Instantaneous Vectors, Streamlines and Vorticity Patterns

Figure 4.43 presents time-averaged velocity vectors $\langle V \rangle$. Patterns of streamlines, $\langle \Psi \rangle$ indicated i Figure 4.44 and lastly vorticity contours $\langle \omega \rangle$ are presented in figures 4.45. It is worth to mention that a large numbers of experiment were performed using the PIV technique. But, only a selective experimental results are presented in the text of thesis. As can be seen in figures, streamlines with varying period of oscillation, T_e , flow characteristics changes in this side-view plane. Moreover, interactions of leading edge vortex with the delta wing can be seen in the cinema of instantaneous flow data. In this side-view plane vortex breakdown takes place where positive and negative vorticity interchange the locations. When a mean angle of attack α_m was arranged as 30° , dynamic angle of attack, $\alpha(t)$ becomes 40° in upstroke direction at yaw angle β equal to 0° for stationary wing, a divergent bifurcation line, Li and a saddle point, S occur in the observed flow region. At a period of oscillation, $T_e=5s$, a divergent bifurcation line, Li and a saddle point, S also occur. Enlarging this period of oscillation to a value of

$T_e=20s$, a saddle point, S and focus F, but, at a period of oscillation, $T_e=40s$, a bifurcation line, a saddle point S and two foci points F take place in the measuring flow region.

Although we have only used ten images of instantaneous velocity vectors to determine vorticity, $[\langle\omega\rangle]$, the onset of vortex breakdown is clearly evident. Here, a solid line indicates positive vorticity and dashed lines indicate a negative vorticity. Locations of vortex breakdown indicated by the PIV results agree well with the results of dye visualizations.

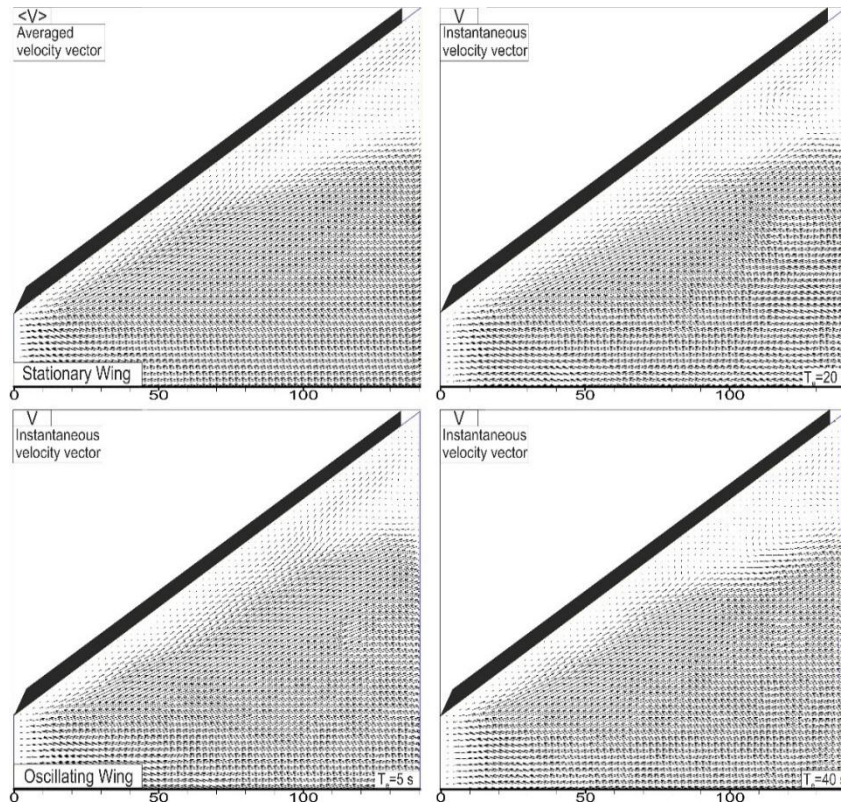


Figure. 4.45. Patterns of time-averaged velocity vectors, $\langle V \rangle$ and instantaneous velocity vectors, V for the stationary and oscillating wing under yaw angle, β of 0° , period of oscillation, T_e ranging from 5s to 40s at mean angle of attack, α_m of 30° , amplitude of delta wing pitching motion, α_0 of $\pm 10^\circ$ and dynamic angles of attack, $\alpha(t)$ of 40° in side view plane

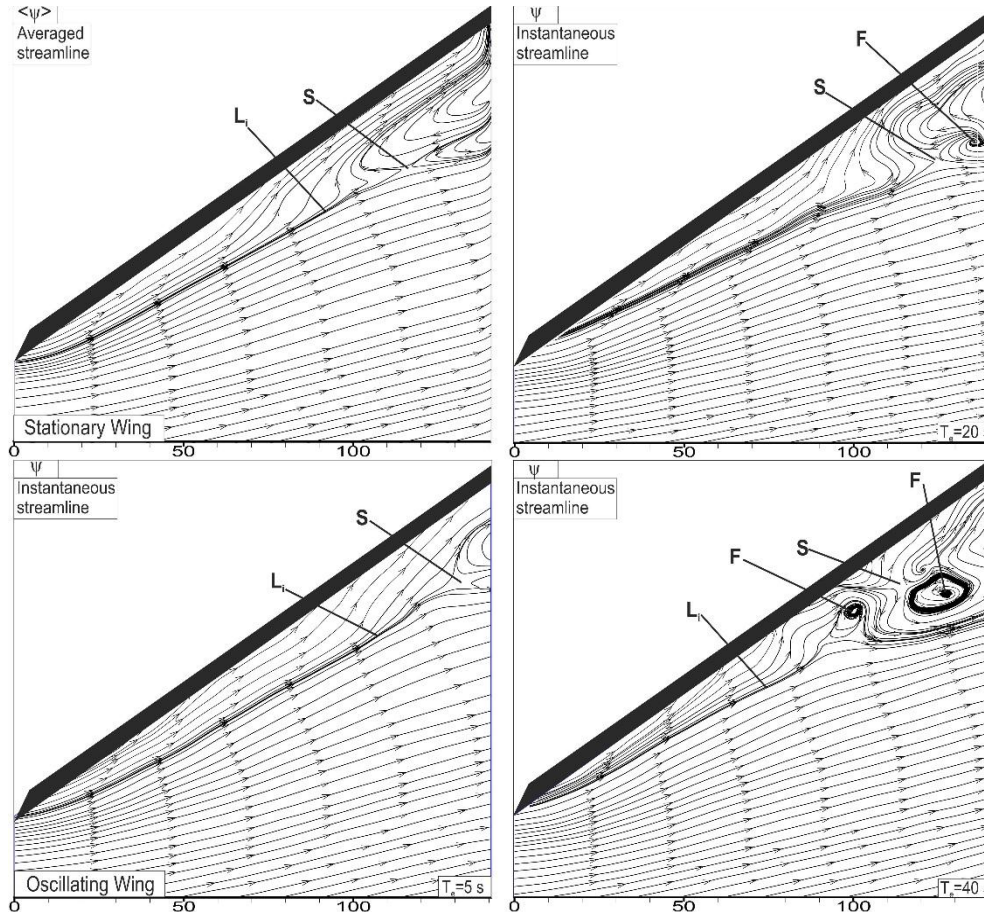


Figure. 4.46. Patterns of time-averaged streamline, $\langle \psi \rangle$ and instantaneous streamline, ψ for the stationary and oscillating wing under yaw angle, β of 0° , period of oscillation, T_e ranging from 5s to 40s at mean angle of attack, α_m of 30° , amplitude of delta wing pitching motion, α_o of $\pm 10^\circ$ and dynamic angles of attack, $\alpha(t)$ of 40° in side view plane

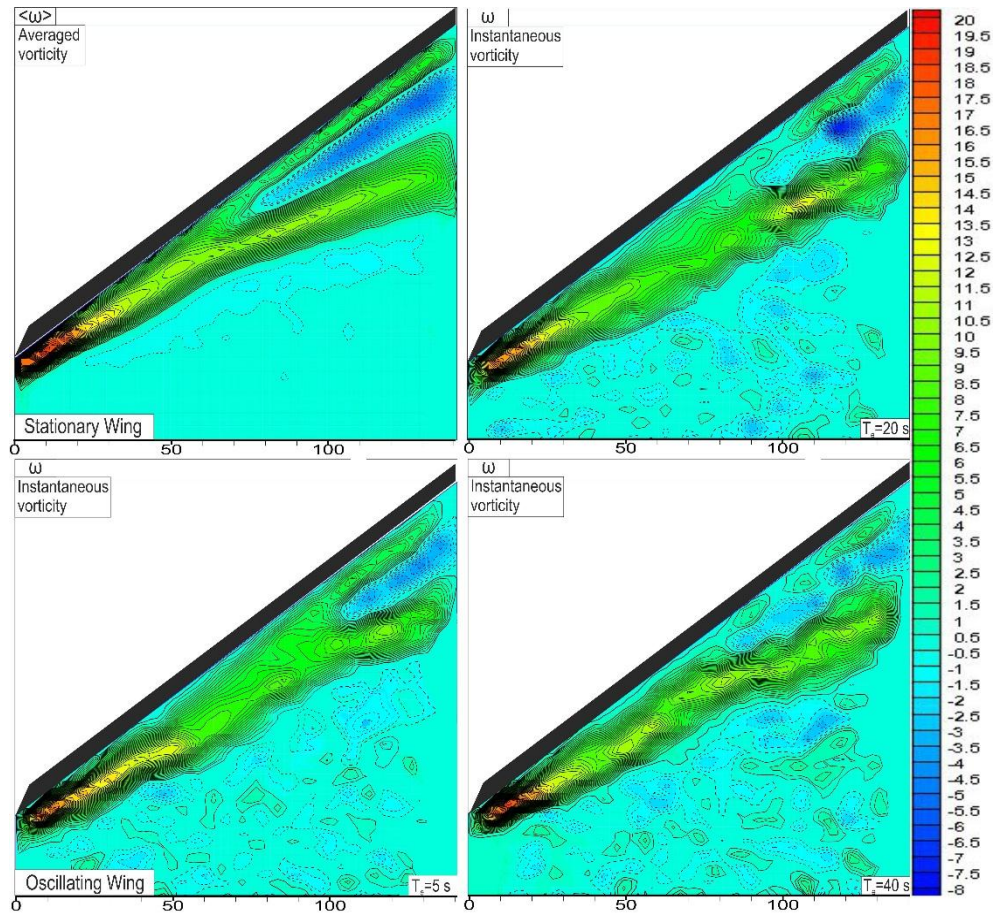


Figure. 4.47. Patterns of time-averaged vorticity, $\langle \omega \rangle$ and instantaneous vorticity, ω for the stationary and oscillating wing under yaw angle, β of 0° , period of oscillation, T_e ranging from 5s to 40s at mean angle of attack, α_m of 30° , amplitude of delta wing pitching motion, α_o of $\pm 10^\circ$ and dynamic angles of attack, $\alpha(t)$ of 40° in side view plane. Minimum and incremental values of vorticity, ω are $\omega_{\min} = \pm 0.5 \text{ sec}^{-1}$ and $\Delta\omega = 0.5 \text{ sec}^{-1}$

5. CONCLUSION AND FUTURE STUDIES

In the present investigation, a delta wing which has 70° sweep angle, Λ was oscillated on its midcord according to the equation of $\alpha(t)=\alpha_m+\alpha_o\sin(\omega_e t)$. This study focused on understanding effect of pitching and characterize the interaction of vortex breakdown with oscillating leading edges under different yaw angles, β over a slender delta wing.

The values of mean angle of attack, α_m was taken as 25° , 30° and 35° . The yaw angle, β was varied the interval of 4° over the range of $0^\circ \leq \beta \leq 16^\circ$. The delta wing was sinusoidally pitched within the range of period of time $5 \leq T_e \leq 60$ s or reduced frequency was set as $K=0.16, 0.25, 0.49, 1.96$ and lastly amplitude of pitching motion was arranged as $\alpha_o = \pm 5^\circ$ and $\pm 10^\circ$. Formations and locations of vortex breakdown were investigated by using the dye visualization technique in side view plane.

The following conclusions can be derived:

1. Structure of vortex breakdown by changing angle of attack, α under different yaw angle, β

Breakdown position of leading edge vortex on the windward side moves towards to the apex of the delta wing and vorticity concentrations spreads over majority of the delta wing surface. But the other side of leading edge vortex moves in forward direction without bursting underneath the delta wing for a higher yaw angle, β . Dye visualizations show that with increasing angle of attack, α and yaw angle, β , a strong Kelvin-Helmholtz instabilities form and leading edge vortices breakdown earlier causing a large scale vorticity concentrations and these vorticity concentrations interact with the surface of the delta wing leading to unsteady loading or buffeting the delta wing surface on the windward side of the wing.

2. Hysteresis effect

Pitching delta wing in upstroke or downstroke motion causes hysteresis loop onset of vortex breakdown locations. There is a time lag between movement of location of vortex breakdown and dynamics angles of attack, $\alpha(t)$ during oscillation of the wing cycle comparing to the case of stationary delta wing. This period of time lag gets shorter by increasing oscillation period, T_e or decreasing reduced frequency, K . It is seen from the experimental data that patterns of flow characteristics does not normally behaves in equilibrium position of the pitching delta wing. Aerodynamics of these perturbing delta wings with a oscillation period of $T_e=5$ s and at $T_e=60$ s resembling with flow characteristics of the static delta wing case. As a result, the effect of the dimensionless reduced frequency, K is proven and it is shown that the effect of the time delay is related to the period of oscillation, T_e . Formation of vortex breakdown towards wake region, losses energy and also pressure decreases at the rare side the delta wing.

3. Effect of amplitude of pitching motion

Increasing the amplitude of the delta wing pitching motion, α_o causes alterations in locations of vortex breakdowns for angles of attack, α . The area of flow separations expands in size with the amplitude of $\alpha_o=+10^\circ$ and the locations of vortex breakdown travels towards the apex of the delta wing more closer compared with the amplitude of $\alpha_o=+5^\circ$. Similarly, when the amplitude of the pitching delta wing is taken $\alpha_o=-10^\circ$, the location of vortex breakdown moves further down in the flow direction comparing to the case of $\alpha_o=-5^\circ$. The angular speed of the delta wing at an amplitude of the pitching delta wing, $\alpha_o=\pm 10^\circ$ is higher than the case of of $\alpha_o=\pm 5^\circ$. This differences causes alteration in the hysteresis of location of vortex breakdown at the same dynamic angles of attack, $\alpha(t)$.

When the delta wing is under pitching motion in upstroke or downstroke directions, a time delay between dynamic angles of attack, $\alpha(t)$ and dimensionless length of X_{vb}/C , that is to say, a delay of vortex breakdown formation occurs in both high and low dynamic angles of attack, $\alpha(t)$. In summary, small yaw angle, β is more effective in altering the location of vortex breakdown in both cases either the stationary or oscillating delta wing. Leading edge vortex breakdown can be controlled partially using active or passive control techniques in order to delay onset of vortex breakdown to improve aerodynamic performance and decline unsteady loading effects on the surface of delta wing. In conclusions, an experimental work should be performed to control the windward side of leading edge vortex breakdown either to delay leading edge vortex bursting process or to induce onset of leading edge vortex breakdown at an earlier stage.

REFERENCES

- Akilli, H., Sahin, B., & Rockwell, D. (2001). Control of vortex breakdown by a transversely oriented wire. *Physics of Fluids*, 13(2), 452-463. doi:10.1063/1.1336809
- Akilli, H., Sahin, B., & Rockwell, D. (2003). Control of vortex breakdown by a coaxial wire. *Physics of Fluids*, 15(1), 123-133. doi:10.1063/1.1519261
- Anderson, J.D. (2001). *Fundamentals of aerodynamics*. McGraw-Hill Higher Education, ISBN 0-07-118146-6.
- Breitsamter, C. (2008). Unsteady flow phenomena associated with leading-edge vortices. *Progress in Aerospace Sciences*, 44(1), 48-65. doi:10.1016/j.paerosci.2007.10.002
- Canpolat, C., Yayla, S., Sahin, B., & Akilli, H. (2009). Dye visualization of the flow structure over a yawed nonslender delta wing. *Journal of Aircraft*, 46(5), 1818-1821. doi:10.2514/1.45274
- Canpolat, C., Sahin, B., Yayla, S., & Akilli, H. (2015). Effects of perturbation on the flow over nonslender delta wings. 45th AIAA Fluid Dynamics Conference, 1-10.
- Clancy, L. (1975). *Aerodynamics*, Halsted, 293.
- DANTEC DAYNAMICS, (2013). Particle Image Velocimetry <http://www.dantecdynamics.com/docs/support-and-download/research-and-education/piv.pdf>
- DORR, R. F. (1985). *Modern Combat Aircraft 21 – Saab Viggen*, Shepperton, Surrey, ENG, UK: Ian Allan, ISBN 0-7110-1484-1
- Elkhoury, M., & Rockwell, D. (2004). Visualized vortices on unmanned combat air vehicle planform: Effect of Reynolds number. *Journal of Aircraft*, 41(5), 1244-1247. doi: 10.2514/1.6290

- Elkhoury, M., Yavuz, M. M., & Rockwell, D. (2005). Near-surface topology of unmanned combat air vehicle planform: Reynolds number dependence. *Journal of Aircraft*, 42(5), 1318-1330.
- Ericsson, L. E. (1999). Vortex characteristics of pitching double-delta wings. *Journal of Aircraft*, 36(2), 349-356. doi: 10.2514/2.2464
- Gad-El-Hak, M., & Blackwelder, R. F. (1985). The discrete vortices from a delta wing. *AIAA Journal*, 23(6), 961-962. doi:10.2514/3.9016
- Gad-El-Hak, M., & Ho, C.M. (1985). The pitching delta wing. *AIAA Journal*, 23(11), 1660-1665. doi:10.2514/3.9147
- Gilliam, F., Robinson, M., Walker, J. & Wissler, J., (1987). Visualization of unsteady separated flow about a pitching delta wing. *AIAA 25th Aerospace Sciences Meeting*. doi: 10.2514/6.1987-240
- Grismer, D. S., & Nelson, R. C. (1995). Double-delta-wing aerodynamics for pitching motions with and without sideslip. *Journal of Aircraft*, 32(6), 1303-1311. doi:10.2514/3.46879
- Gursul, I. (2005). Review of unsteady vortex flows over slender delta wings. *Journal of Aircraft*, 42(2), 299-319. doi:10.2514/1.5269
- Gursul, I., Allan, M. R., & Badcock, K. J. (2005). Opportunities for the integrated use of measurements and computations for the understanding of delta wing aerodynamics. *Aerospace Science and Technology*, 9(3), 181-189. doi:10.1016/j.ast.2004.08.007
- Heron, I., & Myose, R. Y. (2004). On the impingement of a von Kármán vortex street on a delta wing. *Collection of Technical Papers - AIAA 22nd Applied Aerodynamics Conference*, , 1 178-188.
- Huang, G. H., Wang, Y. M. & Cao, G. X. (1994). The mechanism of aerodynamic hysteresis for sinusoidally oscillating delta wings. *Science in China, Series A*, 37(11), 1337-1346.

- Karasu, I. (2015). Effect of yaw angle on vortex formation over a slender delta wing. Çukurova University Institute of Natural and Applied Sciences, Ph. D. Thesis, Adana, 159p.
- Lambourne, N.C., Bryer, D.W., & Maybrey, J.F.M. (1969). The behavior of the leading-edge vortices over a delta wing following a sudden change of incidence. Aeronautical Research Council, Research and Memorandum No.3645.
- LeMay, S. P., Batill, S. M., & Nelson, R. C. (1988). Leading edge vortex dynamics on a pitching delta wing. AIAA 6th Applied Aerodynamics Conference, 1988, 312-320. doi: 10.2514/6.1988-2559
- Lemay, S. P., Batill, S. M., & Nelson, R. C. (1990). Vortex dynamics on a pitching delta wing. *Journal of Aircraft*, 27(2), 131-138. doi:10.2514/3.45908
- Lin, H. (1998). Vortex breakdown over delta wings in an unsteady free-stream. University of Southern California, Ph.D. Thesis, California.
- Magness, C., Robinson, O., & Rockwell, D. (1993). Instantaneous topology of the unsteady leading-edge vortex at high angle of attack. *AIAA Journal*, 31(8), 1384-1391. doi:10.2514/3.11786
- Maltby, R. L., Engler, P. B., & Keating, R. F. A. (1963). Some exploratory measurements of leading-edge vortex positions on a delta wing oscillating in heave. Aeronautical Research Council, Research and Memorandum No. 3410.
- Miau, J. J., Chang, R. C., Chou, J. H., & Lin, C. K. (1992). Nonuniform motion of leading-edge vortex breakdown on ramp pitching delta wings. *AIAA Journal*, 30(7), 1691-1702. doi:10.2514/3.11125
- NASA, (2015) The F-16XL's double delta wing. <https://www.nasa.gov/centers/armstrong/news/FactSheets/FS-023-DFRC.html>
- NASA, (2016). Jet Exit Facility-Bubble Type Vortex Breakdown and Spiral Type Vortex Breakdown. https://crgis.ndc.nasa.gov/historic/Jet_Exit_Facility

- Nelson, R. C., & Pelletier, A. (2003). The unsteady aerodynamics of slender wings and aircraft undergoing large amplitude maneuvers. *Progress in Aerospace Sciences*, 39(2-3), 185-248. doi:10.1016/S0376-0421(02)00088-X
- Ozgoren, M., Sahin, B., Kahraman, A. & Akilli, H. (2005). Instantaneous flow structure and circulation of vorticity concentrations due to wing perturbation. Conference proceedings : ULIBTK'05 15th National Journal of Thermal Science and Technology, Trabzon.
- Ozgoren, M. (2000) Impingement of Vortex Breakdown upon an Edge: Flow Structure and Origin of Loading. Çukurova University Institute of Natural and Applied Sciences, Ph. D. Thesis, Adana, 215p.
- Ozgoren, M., & Sahin, B. (2002). Effect of pitching delta wing on vortex structures with and without impingement plate. *Turkish J. Eng. Env. Sci.*, 26, 325-343.
- Ozgoren, M., Sahin, B., & Rockwell, D. (2002). Vortex structure on a delta wing at high angle of attack. *AIAA Journal*, 40(2), 285-292.
- Ozgoren, M., Sahin, B., & Rockwell, D. (2001). Perturbations of a delta wing: Control of vortex breakdown and buffeting. *Journal of Aircraft*, 38(6), 1040-1050.
- PAKISTAN DEFENCE, (2012). Design characteristics of canard and non-canard fighters. <http://defence.pk/threads/design-characteristics-of-canard-non-canard-fighters.178592/page-2>
- Payne, F. M., & Nelson, R. C. (1986). Experimental investigation of vortex breakdown on a delta wing. *NASA Conference Publication*, 135-161.
- Rediniotis, O. K., Stapountzis, H., & Telionis, D. P. (1993). Periodic vortex shedding over delta wings. *AIAA Journal*, 31(9), 1555-1562. doi:10.2514/3.11814
- Reynolds, G. A. & Abtahi, A. A. (1987). Instabilities in Leading-Edge Vortex Development. AIAA-87-2424, Applied Aerodynamics and Atmospheric Flight Mechanics Conference.

- Rockwell, D., Atta, R., Kuo, C. -H., Hefele, C., Magness, C. & Utsch, T. (1987). On Unsteady Flow Structure from Sweep Eddies Subjected to Controlled Motion. AFOSR Workshop on Unsteady Separated Flows, USAF Academy, CO.
- Sahin, B., Akilli, H., Lin, J.-C., & Rockwell, D. (2001). Vortex breakdown-edge interaction: Consequence of edge oscillations. *AIAA Journal*, 39(5), 865-876.
- Sahin, B., Yayla, S., Canpolat, C., & Akilli, H. (2012). Flow structure over the yawed nonslender diamond wing. *Aerospace Science and Technology*, 23(1), 108-119. doi:10.1016/j.ast.2011.06.008
- Sarpkaya, T. (1971). On stationary and travelling vortex breakdowns. *Journal of Fluid Mechanics*, 45(3), 545-559. doi:10.1017/S0022112071000181
- Shih, C., & Ding, Z. (1996). Unsteady structure of leading-edge vortex flow over a delta wing. Paper presented at the 34th Aerospace Sciences Meeting and Exhibit, Reno, NV, USA.
- Su, W., Liu, M., & Liu, Z. (1990). Topological structures of separated flows about a series of sharp-edged delta wings at angles of attack up to 90°. *Topological Fluid Mechanics*, edited by H. K. Moffatt, and A. Tsinober, Cambridge Univ. Press, New York.
- WIKIPEDIA, (2016). Canard Saab AJS-37 Viggen. https://en.wikipedia.org/wiki/Saab_37_Viggen#cite_note-bomber_247-1
- WIKIPEDIA, (2016). Jet-powered tailless delta wing. https://en.wikipedia.org/wiki/Delta_wing
- Woodiga, S., Liu, T., Ramasamy, R. S. V., & Kode, S. K. (2016). Effects of pitch, yaw, and roll on delta wing skin friction topology. *Proceedings of the Institution of Mechanical Engineers, Part G: Journal of Aerospace Engineering*, 230(4), 639-652. doi:10.1177/0954410015594823
- Yaniktepe, B., & Rockwell, D. (2004). Flow structure on a delta wing of low sweep angle. *AIAA Journal*, 42(3), 513-523.

- Yayla, S., Canpolat, C., Sahin, B., & Akilli, H. (2010). Yaw angle effect on flow structure over the nonslender diamond wing. *AIAA Journal*, 48(10), 2457-2461. doi:10.2514/1.J050380
- Yayla, S., Canpolat, C., Şahin, B., & Akilli, H. (2010). Effect of yaw angle on the formation of vortex breakdown over the diamond wing. *Journal of Thermal Science and Technology*, 30(1), 79-89.
- Yayla, S., Canpolat, C., Sahin, B., & Akilli, H. (2013). The effect of angle of attack on the flow structure over the nonslender lambda wing. *Aerospace Science and Technology*, 28(1), 417-430. doi:10.1016/j.ast.2012.12.007
- Yilmaz, T. O., & Rockwell, D. (2012). Flow structure on finite-span wings due to pitch-up motion. *Journal of Fluid Mechanics*, 691, 518-545. doi:10.1017/jfm.2011.490

CURRICULUM VITAE

Mehmet Can PEKTAŞ graduated in 2009 from Adana Collage High School in Adana. He enrolled in Mechanical Engineering Department of Çukurova University in Adana in 2009 and also enrolled in Industrial Engineering Department of Çukurova University in 2011. He graduated from the department of Mechanical Engineering and Industrial Engineering in 2014 and began his Master of Science in Mechanical Engineering Department in 2015. Presently, he takes part in a project supported by The Scientific and Technological Research Council of Turkey (TÜBİTAK) as a project assistant.